Università degli Studi della Tuscia di Viterbo

Dipartimento di Scienze Ecologiche e Biologiche

Corso di Dottorato di Ricerca in

Ecologia e Gestione Sostenibile delle Risorse Ambientali - XXXVI Ciclo

BLACK FUNGI FOR SPACE RESEARCH AND GENETIC ENGINEERING TO UNRAVEL MELANIN'S IMPACT ON STRESS TOLERANCE

(s.s.d. BIO/03)

Tesi di Dottorato di:

Dott.ssa Ilaria Catanzaro

Ilaria Catanzaro

Coordinatore del Corso

Prof. Claudio Carere

Tutore

Prof. Silvano Onofri

Co-Tutore

Prof.ssa Laura Zucconi Galli Fonseca

A.A. 2023/24 (A.Y. 2023/24)

To Grandma Rosa,
to Serena and Hesam

Summary

Abstract

The rich diversity of extreme habitats and associated organisms on Earth serves as reference for astrobiological research. This diversity sheds light on potential habitable environments on other planetary bodies, potential adaptive mechanisms that life may have evolved in extraterrestrial contexts, and the search for traces of life and its former presence. Microcolonial and melanised fungi, a polyphyletic and extremophilic group capable of thriving under a broad spectrum of extreme conditions, are particularly promising eukaryotic organisms. Previous studies have demonstrated their remarkable survival capabilities – especially of one cryptoendolithic representative, *Cryomyces antarcticus* – even under space conditions, attributed in part to the protective functions of melanin pigments in their cell walls. However, fundamental questions persist regarding the role of fungal melanins in the polyextremotolerance of this group, as well as the genetic and physiological factors underlying this group adaptation. In this study, we focus on the common melanogenic trait of black fungi to delineate their potential as astrobiological models for studying life adaptations in extreme environments. To achieve this, we introduce a preliminary study on fungal biomolecules of *C. antarcticus* to assess their biosignature stability in a Mars scenario, with melanin emerging as a promising candidate. Subsequently, we develop efficient transformation tools using *Knufia petricola* as a reference system, resulting in a genetically tractable *C. antarcticus*. While targeted gene editing of this polyextremotolerant fungus necessitate an extended timeframe, this milestone validates the feasibility of genetic manipulation on extremotolerant, recalcitrant fungi. Finally, we propose a first comparative study on the protective role of DHN melanin in UV-B tolerance capabilities of two microcolonial black fungi. Our findings suggest that they may not rely on pigment protecting against harmful UV radiation, but rather employ different strategies to cope with the same stress factor. These novel insights into the adaptive mechanisms of polyextremotolerant fungi underscore the importance of enriching the pool of model organisms with alternative experimental models, as traditional ones may not comprehensively capture all the adaptive mechanisms and real limits of life.

Chapter 1

Introduction

1.1 Exploring life's limits and traces in the quest for extraterrestrial life

The interdisciplinary field of astrobiology seeks to unravel the origin, evolution, and future of life across the cosmos (Cockell, 2020). Within this context, Earth serves as a primary focal point due to its status as the only currently known inhabited planet. Notably, our planet hosts a wide spectrum of environments characterised by severe physical and chemical conditions prohibitive in supporting human life, thus earning the title of 'extreme environments' (Martins et al., 2017). Many of these environments exhibit geological and/or environmental features similar to those observed on other planetary bodies within the Solar System (**Figure 1**). For instance, the Antarctic continent serves as a representative repository for surface and subsurface environments (i.e., 'planetary field analogues', PFAs) that resemble current or past environmental parameters of Mars and the icy moons of Jupiter and Saturn (Cassaro et al., 2021a).

Traditionally considered aseptic due to their inhospitable conditions, extreme environments have emerged as effective ecosystems harbouring mostly microbial life forms capable of enduring such conditions (Shu and Huang, 2022). Continuous exploration efforts have revealed a richer microbial diversity than expected, spanning among prokaryotic and eukaryotic representatives. These organisms have evolved various molecular and physiological mechanisms, including antiporters' efflux pumps, membrane fluidity and cytoplasmic pH regulation, to thrive under extreme conditions (Salwan and Sharma, 2020). Based on their degree of adaptation to a diverse range of abiotic stress factors, these organisms are identified as (poly-)extremophilic or (poly-) extremotolerant species (Gostinčar et al., 2023). Therefore, investigations on extreme environments and the adaptive strategies of associated organisms not only can provide insights into the origin and evolution of life on Earth (Rappaport and Oliverio, 2023), but also contribute to the enduring quest to discover potential life forms in other planetary environments (Merino et al., 2019).

Given the lack of evidence for life beyond Earth, planetary exploration for signs of life is

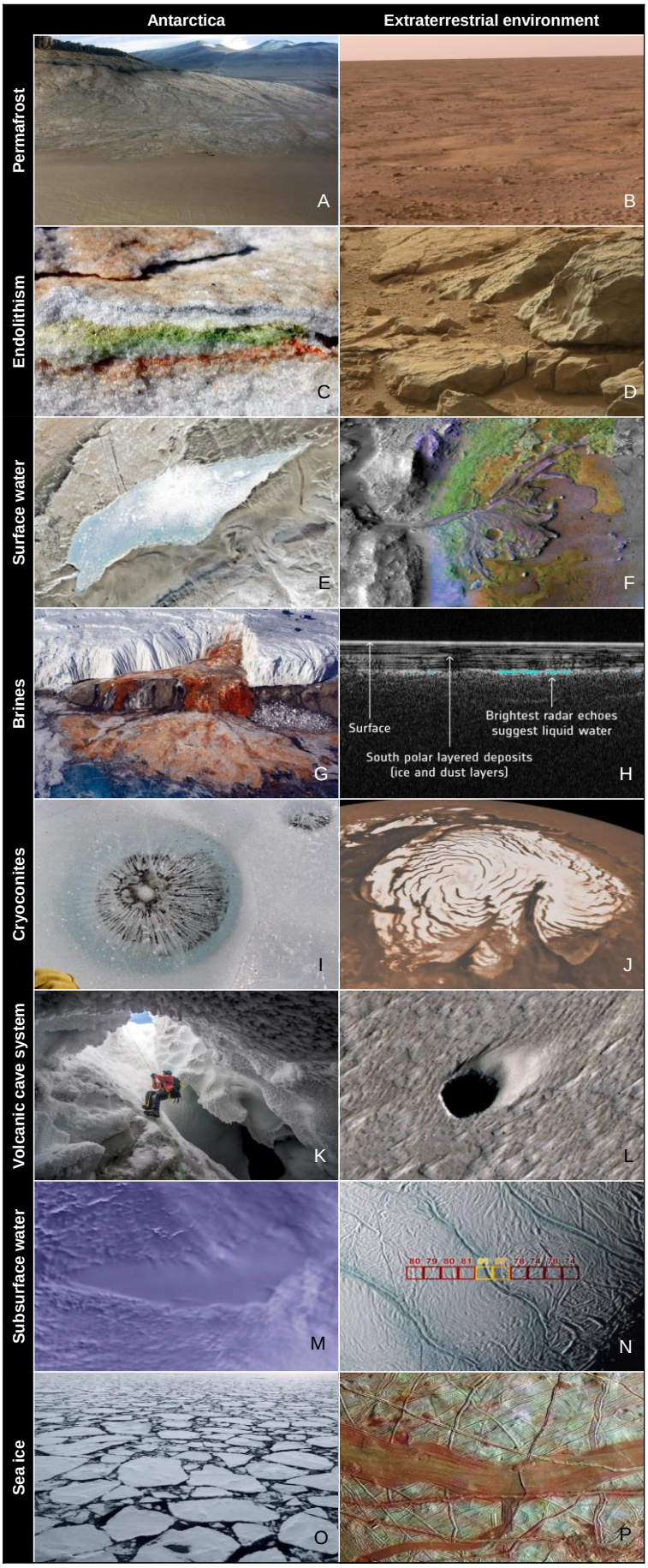

Figure 1. Illustrative comparison of known habitats in Antarctica (left column) and potentially habitable extraterrestrial environments (right column).
A. Ice-wedge polygon soil typical of permafrost in the Wright Valley, South Victoria Land (image credit: Nate Biletnikoff/NSF). **B. Polygonal soil** possibly from periodic contraction and expansion of surface ice in north polar regions, Mars (image credit: NASA/JPL-Caltech/University of Arizona). **C. Cryptoendolithic communities within sandstone** at Linnaeus Terrace, South Victoria Land (image credit: Onofri et al. (2007)). **D. Surface barren rocks**, Mars (image credit: NASA/JPL-Caltech/MSSS). **E. Ice-covered Lake Vida** in Victoria Valley, South Victoria Land (image credit: Google Earth/Maxar Tecnologies/CNES/ Airbus). **F. Orbital view of Jezero Crater paleolake**, Mars (satellite image credit: NASA/JPL-Caltech/MSSS/JHU-APL). **G. Blood Falls outflowing from Taylor Glacier** and resulting from iron-rich, saline liquid from an upstream subglacial pond, South Victoria Land (image credit: Peter Rejcek/NSF). **H. Radar image of subsurface ice deposits** with probable liquid saltwater (bright blue) in south polar regions, Mars (image credit: Orosei et al. (2018)). **I. Cryoconite holes** on the surface of Canada Glacier, South Victoria Land (image credit: Zamora (2018)). **J. Orbital view of the ice-rich north pole**, Mars (image credit: NASA/JPL-Caltech/ MSSS). **K. Ice caves** in Mount Erebus volcano, Ross Island (image credit: Alasdair Turner/National Geographic Traveler Photo Contest). **L. Pit crater after ceiling collapse of lava tubes** in Arsia Mons volcano, Mars (image credit: NASA/JPL-Caltech/University of Arizona). **M. Radar image of subglacial Lake Vostok**, East Antarctic Ice Sheet (image credit: NASA/Goddard Space Flight Centre Scientific Visualization Studio/Canadian Space Agency/RADARSAT International Inc.). **N. Orbital view of ice surface fractures** with internal heat release in south polar regions, Saturn's moon Enceladus (image credit: NASA/JPL/GSFC/Space Science Institute). **O. Floating ice** in the Ross Sea (image credit: John B. Weller/The Pew Charitable Trusts). **P. Orbital view of pure water ice (white areas) and mixed with salts (brown areas)** on the surface of Jupiter's moon Europa (image credit: NASA/JPL-Caltech/SETI Institute).

recommended to proceed alongside a comprehensive understanding of the habitability concept (Cockell et al., 2016). However, the mere presence of candidate habitats does not imply their current or past inhabitation. As for Mars, which is the primary target planet in life detection missions, current surface conditions are not compatible with life as we know it, featuring high radiation and oxidising environments with extremely low water activity (Catling, 2014). Yet, the search for potential life has been driven by repeated evidence of stable liquid water – essential for habitability – on Mars during its geological history (Cockell, 2014). If early Mars did host milder conditions conducive to emergence of putative life (Sasselov et al., 2020), it is possible that any existing life remained in a very primitive stage of evolution due to the relatively short period of favourable conditions (pre-Noachian to Noachian era) and the rapidly changing scenario on the Martian surface (Westall et al., 2015). However, the planet's subsurface might better preserve traces of microorganisms, as suggested by the possibility of an early microbial scenario.

Considering the evolutionary history of Earth, it is possible to use the terrestrial fossil records as a reference for the type of evidence we might expect to find on Mars as indicators of the past presence of life. In fact, life traces on Earth range from morphological fossils to organic materials with compositional profiles, complexities and/or stereoisomerisms, as well as isotopic, geochemical or mineralogical patterns in the geological record (Malaterre et al., 2023). All these 'biosignatures' suggest a biosynthetic origin and have provided detailed evidence of ancient terrestrial life, but their preservation potentials are highly influenced by both biotic and abiotic stress factors (Bosak et al., 2021). Nonetheless, under certain conditions, some traces can persist for billions of years, thus serving as reliable indicators for the search for extinct life on Earth and Mars. The search for Martian life is, however, challenging due to the hostile environmental conditions that compromise the stability and detectability of potential biosignatures (Hays et al., 2017). Ultraviolet (UV) and ionising radiation as well as oxidising regolith compounds can destroy potential life traces on the Martian surface and up to the near subsurface. Furthermore, the biogenicity of life-similar geological records remains an open question within the astrobiological community (McMahon and Cosmidis, 2022). Hence, future life detection efforts will need to focus on the systematic identification of traces from extinct or extant life by implementation of robust sets of all biosignatures we can find on Earth (Baqué et al., 2022).

1.2 A multi-stage investigative approach for astrobiological research

Recurrent findings of habitats previously deemed inhospitable have boosted the search for life beyond our planet, while investigations concerning extremophiles have reshaped our understanding on the limits of life and the concept of planetary habitability. Moreover, extreme environments can be used by researchers to gain knowledge on the long-term potential for preservation of life traces, guiding the selection of targeted biosignatures and the most appropriate analytical methods for their detection in analogous extraterrestrial environments (Warren-Rhodes et al., 2023). In the context of 'life in space' investigations, the identification of hypothetical biosignatures in extraterrestrial environments is one of the major challenges of the current space age (Onofri et al., 2020b). For instance, the ongoing exploration of Mars by the NASA Perseverance rover (Mars 2020 mission) is aimed at retrieving Martian rock samples for studying their structure and the possible traces of extinct life forms by advanced laboratory tools on Earth. Due to the complex circumstances of these research topics – no *in situ* human exploration available at the current time – an investigative approach combining field work in PFAs, experimental work using laboratory simulation facilities, replication of experimental work in real space, and design of life detection missions has been outlined to comprehensively support astrobiological research. By addressing the challenge of replicating extraterrestrial conditions on Earth, this systematic approach can better assess the impact of space environments on life, and advance dedicated libraries and diagnostic tools for biosignature detection (Cassaro et al., 2021b).

As Earth is the only planet known to support life, it is reasonable to use terrestrial environments as PFAs to study the ability of life to persist in hostile extraterrestrial environments and how to detect it there. Field research is the first step in an astrobiological investigation (Step 1 in **Figure 2**). It involves the exploration of an extreme environment, both terrestrial (e.g., hot and cold deserts, rivers) and marine (e.g., hydrothermal vents, oceanic clathrates, submarine hydrothermal regions) habitats on Earth, and the selection of the best inhabiting microorganism (usually an extremophile) to be used as a test organism in simulated space and Low Earth Orbit (LEO) exposure experiments. It is also necessary to validate the experimental procedures and tools to be used for biosignature analysis, which can be carried out both *in situ* by rovers and in laboratory by researchers. As extreme terrestrial environments cannot exhibit all the physico-chemical parameters described on other planetary bodies, a complementary approach involving experimental work through laboratory simulations of extraterrestrial environments is then required . Planetary simulation facilities are designed for ground-based experiments (Step 2 in **Figure 2**) to determine whether both material and biological samples could persist in the extreme

conditions found in deep space and celestial bodies. These investigations are carried out by analysing the resistance, stability or survivability of the exposed samples (Martins et al., 2017).

However, no laboratory is equipped with simulation facilities that can simultaneously test all the conditions that samples might experience in real space environments. To study the different responses of samples in a range of conditions as close as possible to those typical of extraterrestrial environments, exposure to real space conditions is subsequently necessary (Step 3 in **Figure 2**). Whenever possible, this following investigation step is usually performed in LEO and supported by exposure facilities outside the ISS. It involves exposure of samples to hostile space conditions such as vacuum, intense radiation flux from both solar and galactic sources, extreme temperatures and microgravity. The choice of the appropriate exposure facility may depend on the duration of the experiment. For example, the BIOPAN facility has been designed for short-term space experiments (two weeks), allowing the exposure of both biological and non-biological payloads to a wide range of space conditions. Conversely, all EXPOSE facilities (EXPOSE-E/-R/-R2) have been used for long-term interdisciplinary experiments, where biological samples for different astrobiological experiments can be housed together, despite the limited space for samples (Cottin et al., 2017).

Once back on Earth, the exposed samples must be analysed according to the sample-type and by comparing the results with those from previous ground-based experiments. All the results from both ground-based simulation and real space exposure will be combined for the ultimate goal, i.e. to support space exploration missions to search for life beyond Earth. Eventually, the multi-step investigation approach can benefit astrobiological research by providing a broader and more realistic view of what traces of extinct life might look like and how to detect them on extraterrestrial environments (Step 4 in **Figure 2**) (Carrier et al., 2020).

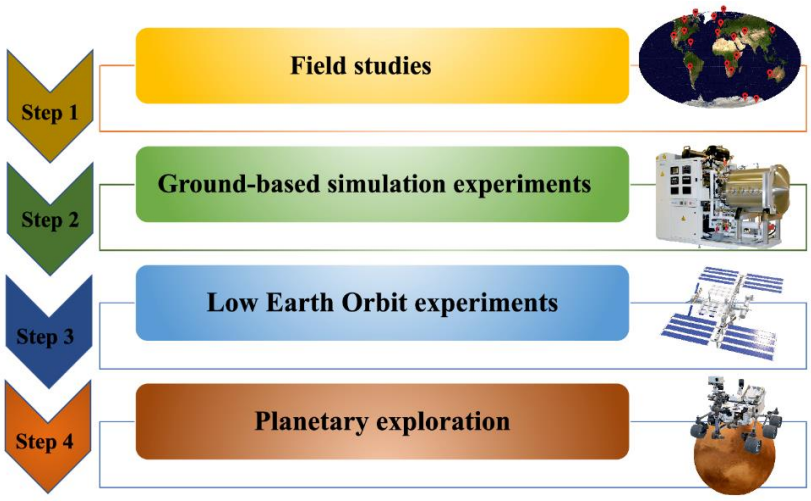

Figure 2. Schematic representation of the proposed multi-step approach for astrobiological research.

1.3 Lithic habitats are home to extreme microbial diversity

The Earth is home to a broad spectrum of extreme environments that can be chosen for PFA studies. For instance, desert environments are characterised by high solar radiation, severe temperature fluctuations, hyperosmolarity, and limited nutrient/water availability (Alsharif et al., 2020). As these conditions are not exclusive of warm climates, deserts come under many shades of temperatures, leading to both – quoting a top hit from early 2000[1] – 'hot and cold' examples. As previously shown, Antarctica contains many habitats with potential extraterrestrial relevance (**Figure 1**). In terms of severe low temperature and desiccating conditions, the McMurdo Dry Valleys (MDVs) are the coldest and hyperarid desert known on Earth. They are the largest ice-free region in the Antarctic continent, featuring high levels of UV-B radiation, low precipitation, oligotrophic conditions, high salt content, and steep geochemical gradients. Because their environmental profile mirrors current surface conditions on Mars, the MDVs have long been studied and used as Martian field analogues for space exploration [see Salvatore and Levy (2021) for details]. However, a significant environmental factor not naturally reproducible on Earth is the ionising radiation from solar and cosmic rays. Since Mars lacks a thick atmosphere and a global dipolar magnetic field, its surface is vulnerable to these energetic primary particles, which trigger secondary cascades that penetrate in the near subsurface (Zhang et al., 2022). Thus, the ionising radiation represents a major hazard to any putative Martian life, and biological radioresistance is another adaptive mechanism to be extensively investigated in terrestrial extremophiles (Romano et al., 2022; Aureli et al., 2023). Despite the absence of ionising radiation, the MDVs provide the closest field analogues known for simulating either the survival or extinction scenarios of hypothetical life on the surface and near subsurface of Mars, e.g., with fossilised microbial traces in well-preserved Antarctic rocks (Westall et al., 2015).

Deserts may seem exotic, but their defining conditions are widespread on Earth. Looking at a micro-scale, arid and nutrient-poor conditions are ubiquitous in both natural and anthropogenic settings, such as on barren rocks or on monuments and solar panels (Knabe and Gorbushina, 2018). Yet some microorganisms have specialised to thrive in niches provided by these exposed solid surfaces (Coleine et al., 2022b; De Leo et al., 2022). In fact, throughout Earth's history, rocks have served as a primordial terrestrial niche for pioneering life as well as a last shelter for microbial colonisation before extinction (Gorbushina and Krumbein, 2000; Coleine et al., 2021). The biodiversity of lithic niches is intrinsically linked to the surrounding climatic conditions.

[1] Perry, K. (2008) Hot N Cold. In *One of the Boys*. Capitol Records

Initially comprised of free-living and symbiotic fungi, algae and bacteria, microbial associations colonise exposed rock surfaces, succeeded by macroscopic vegetation in temperate climates (Gorbushina, 2007). When harsh climatic conditions persist – as in deserts or at high altitudes – colonisation remains limited to the microbial level and gradually shifts further into the rock matrix (Nienow, 2017). Microbial communities within rocks have been originally discovered in the MDVs (Friedmann et al., 1988). Among all the lithic lifestyles, the cryptoendolithic niche provides the most buffered conditions for microbial communities, offering advantages such as water retention and protection against abiotic stresses (Chan et al., 2012). This ultimate adaptation improves the survival prospects of microbial life in extreme environments (Selbmann et al., 2015).

In the Antarctic Dry Valleys, the most complex and successful rock-colonising community is the one dominated by cryptoendolithic lichens (Friedmann et al., 1988). The spatial organisation of these communities mirrors the specific physiological needs of each associated microorganism, as it displays coloured and biologically distinct stratifications at few millimetres below the rock surface (**Figure 3**). Particularly, endemic chlorophyte algae and cyanobacteria form a deep green band, where they are efficiently shielded from the solar radiation. Directly above, lichenised fungi and algae form a white band through loose but obligate symbiotic associations. Lastly, the upper presence of a black speckled band with meristematic, dark pigmented fungi is supposedly acting as a protective layer from the excessive solar radiation (Onofri et al., 2007).

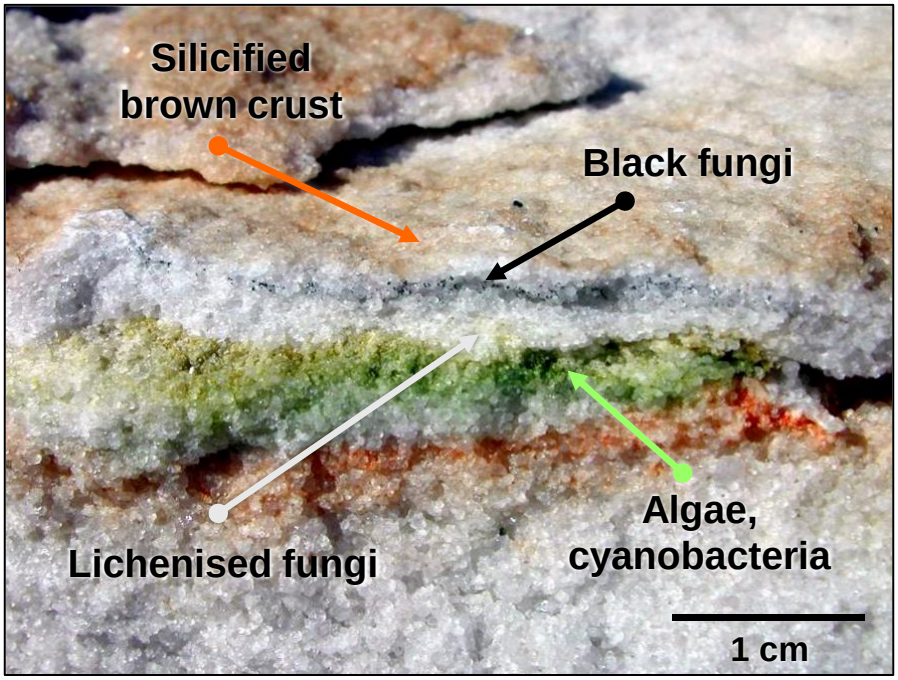

Figure 3. The biological organisation of a lichen-dominated community in Antarctic sandstone.
Porous rocks can be colonised up to 10 mm deep, acting as ultimate refuges for microbial life in extreme environments. Image modified from Onofri et al. (2007).

Due to the evolved high tolerance to extreme terrestrial conditions, the survival ability of selected cryptoendolithic microorganisms was eventually explored in both space and planetary conditions, with the aim of addressing astrobiological questions such as the theory of Lithopanspermia (Scalzi et al., 2012; Onofri et al., 2015). Furthermore, cryptoendolithic fossil remnants were proposed as diagnostic indicators for putative extinct life preserved within Martian rocks (Cassaro et al., 2021a).

1.4 Black rock fungi as diagnostic tools in astrobiological research

The kingdom of Fungi comprises species that can inhabit nearly all ecosystems. Fungi exist as both free-living and symbiotic unicellular and multicellular organisms with different morphologies. As heterotrophic organisms, they obtain nutrients from external sources. Filamentous fungi are the most abundant and studied representatives due to their prominence in litter decomposition and biogeochemical cycles. Their ability to take up large amounts of nutrients and translocate them through an extensive hyphal network, even over long distances, is one of the characteristic strategies of these organisms (Klein and Paschke, 2004). A variety of biological associations are found throughout the fungal kingdom. Ectomycorrhizal and arbuscular mycorrhizal fungi form mutualistic associations with plants, exchanging plant-produced carbohydrates for inorganic nitrogen, phosphorus, and other minerals. Other mutualistic associations include lichenised fungi, which live in symbiosis with one or more green algae or cyanobacteria. Lichen associations usually form compact structures known as thalli. Different from the other fungi, which usually reside beneath the surface of their substrates, the lichen thallus is typically at the surface and exposed to the atmospheric conditions, playing a pivotal role in mediating fundamental functions of terrestrial ecosystems (Grube and Wedin, 2016).

Some fungi can thrive in extreme environments as well. Meristematic, dark pigmented fungi are recurrent inhabitants of lithic environments and thus conventionally known as rock-inhabiting fungi (Knabe and Gorbushina, 2018). These ascomycetes are among the most stress-tolerant organisms on Earth due to characteristic traits that enable thriving across a broad spectrum of abiotic stress factors, including an oligotrophic regime, slow radial growth, subspherical cells with an optimal thermodynamic surface (‘meristematic form’), and multilayered melanised cell walls (Tesei, 2022). According to alternative perspectives on their ecological and morpho-physiological characteristics, these fungi may also be referred to as microcolonial fungi or black yeasts,

distinguishing them from the typical filamentous or lichenised counterparts. While the latter can reproduce both sexually and asexually, many rock-inhabiting fungi have lost the ability to cell differentiate and produce spores or fruiting bodies, so they are known as yeast-like organisms due to vegetative reproduction by budding or fission (Liu et al., 2021).

Although black fungi are prominently associated with rocky environments, they are found in other habitats as well (Ametrano et al., 2019). They thrive in all climatic zones on a wide range of solid surfaces – even on plastics and concrete – and in acidic or heavily contaminated sites. Additionally, they include opportunistic and pathogenic strains that affect plants (e.g., *Alternaria alternata*, *Botrytis cinerea*) and warm-blooded animals, humans included (e.g., *Aspergillus niger*, *Exophiala dermatitidis*). Black fungi form an ecological group specialised in poly-extremotolerance yet containing an impressive phylogenetic diversity. Although they share a common set of adaptations, these have independently emerged multiple times during evolution in response to harsh environmental conditions (Gueidan et al., 2008; Gueidan et al., 2011). As a result, black fungi are distributed across the classes of Dothideomycetes and Eurotiomycetes, featuring an assorted pool of representatives.

Research on black rock fungi began within the field of cultural heritage conservation, where they were first identified as primary contributors to the biodeterioration of lithic materials (De Leo et al., 2022). Initially treated as foes, these fungi have been eventually investigated for their potentials in bioremediation of polluted sites (Isola et al., 2013; Blasi et al., 2016). In this context, the black *Knufia petricola* (syn. *Sarcinomyces petricola*) has long served as model system for elucidating the lifestyle and physiology of rock-inhabiting fungi (Tonon et al., 2021; Breitenbach et al., 2022). Originally isolated from a marble surface in Athens (Greece) (Wollenzien et al., 1997; Gorbushina et al., 2008), the strain A95 belongs to the pathogen-rich order Chaetothyriales (Eurotiomycetes) as a non-pathogenic, relatively fast-growing representative (Gueidan et al., 2008). Over the past two decades, *K. petricola* has been extensively studied first as part of subaerial biofilms causing mineral weathering, to the point of defining a complete profile of the single organism over a thousand physicochemical conditions (Gorbushina et al., 2008; Nai et al., 2013). Later, *K. petricola* has emerged as a reliable model system, with its genome annotated (Heeger et al., unpublished) and an efficient toolkit for genetic engineering implemented (Voigt et al., 2020; Erdmann et al., 2022).

The discovery of cryptoendolithic microbial communities redirected attention towards black fungi in the astrobiological field, because of their peculiar lifestyle challenging conventional understandings on the limits of life (Friedmann and Ocampo-Friedmann, 1984; Onofri et al., 2004). Within this context, the black *Cryomyces antarcticus* (Dothideomycetes *incertae sedis*), a

cryptoendolithic representative endemic to Antarctica (Selbmann et al., 2013), holds particular significance. Isolated from sandstone collected at Linnaeus Terrace (MDVs, Southern Victoria Land) (Selbmann et al., 2005), this psychrophilic species presents multilayered, strongly melanised cell walls coupled with extremely slow growth– a constitutive trait of Antarctic fungi even under optimal incubation conditions (Gostinčar et al., 2022). Research efforts have focused intensively on *C. antarcticus* to understand its adaptive lifestyle to extreme conditions. Studies carried out for over two decades have led to the progressive exposure of fungal samples to a range of extreme conditions, starting from the local ones found in Antarctic habitats (e.g., wide thermal fluctuations, intense UV radiation) to the exotic ones found in space or planetary contexts (e.g., vacuum, ionising radiation, perchlorate media) (Onofri et al., 2020a; Cassaro et al., 2022; Aureli et al., 2023). Eventually, *C. antarcticus* MNA-CCFEE 515 emerged as the most appropriate test strain for astrobiological investigations due its remarkable survival limits even under real space conditions (Simões et al., 2023).

As a response to stressful environmental conditions, fungi demonstrate the capacity to synthetise various metabolites, including melanin pigments (Cordero and Casadevall, 2017). These pigments integrate in the cell wall, thus imparting the typical brownish to blackish appearance of these fungi. They are negatively charged and hydrophobic macromolecules with complex structures, derived from the oxidative polymerisation of different phenolic precursors (Butler and Day, 1998). Fungi can employ three distinct strategies for melanin synthesis (**Figure 4**): via 1,8-dihydroxynaphthalene (DHN), via 3,4 dihydroxyphenylalanine (DOPA), or via L-tyrosine degradation (Cao et al., 2021). Despite their different origins, melanins possess a combination of physicochemical and structural characteristics, such as free radical, antioxidant, metal chelating and semiconductor-like properties, not replicated by any other biomolecule. This led to numerous investigations on the role of melanins in eukaryotic systems and possible biotechnological applications (Singh et al., 2021).

The widespread distribution of melanogenic fungi suggests that melanins confer environmental advantages to these organisms, such as improved survival and fitness under stress conditions. Despite the challenges in studying their multifunctional potential, fungal melanins have long been linked to biological functions such as photoprotection, energy harvest, thermoregulation against heat and cold stress, resistance to mechanical and chemical stress, protection against desiccation, cell development, and host virulence (Gessler et al., 2014). Fungi inhabiting rocky environments endure a broad spectrum of abiotic stresses, primarily solar UV irradiation (Coleine et al., 2022a). Exposure to harmful UV radiation can induce various chemical alterations in a biological system, most notably helix-distorting damages in the DNA (Jones and Baxter, 2017). UV radiation may

also leads to the accumulation of reactive oxygen species (ROS), which can indirectly damage the DNA and proteins, while triggering the oxidation of lipids (Kebbi et al., 2020). In this scenario, the accumulation of dark melanins in the fungal cell wall may act as a first line of defence against UV irradiation. Due to their broad-spectrum absorption, especially in the UV range, and antioxidant properties, melanin pigments are deemed to serve as photoprotective compounds by preventing UV-induced damage before it occurs (Wong et al., 2019). For example, the high tolerance to UV and ionising radiation observed in *C. antarcticus* has always been attributed to the presence of melanised fungal cell walls rather than other protective mechanisms, e.g. DNA repair systems (Pacelli et al., 2017; Selbmann et al., 2018).

Due to the inherently complex nature of melanin polymers, it remains a challenge to elucidate the higher-order structure of these biomolecules and thus to understand their functions under stress conditions (Solano, 2016; Berthelot et al., 2020; Gaber et al., 2020; Vasileiou and Summerer, 2020). However, the integration of advanced experimental techniques and computational analyses holds promise to elucidate the enigmatic nature of melanins e.g., by providing a means to understand the polyextremotolerant adaptations of black fungi and their ecology.

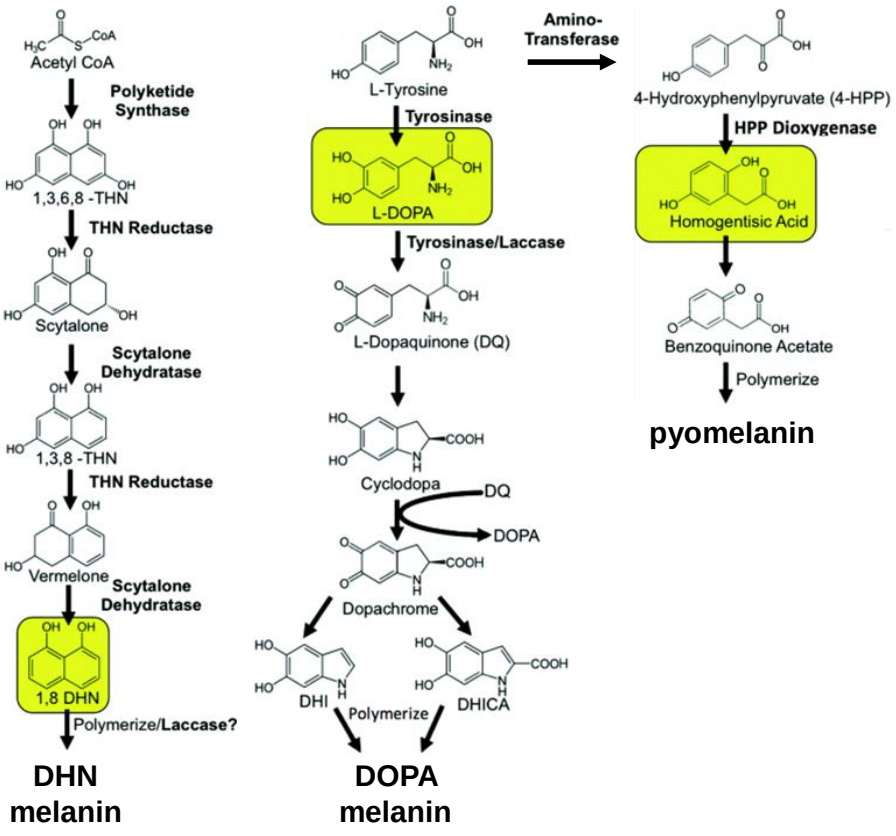

Figure 4. The three biosynthetic pathways employed by fungi for melanogenesis.

DHN melanin uses 1,8 DHN as immediate precursor to the final polymer, while DOPA melanin and pyomelanin use L-DOPA and HGA as precursors, respectively [highlighted in green].

1.5 Extreme challenges, synthetic solutions: tractable black fungi for astrobiological applications

In recent years, there has been a boost in research focused on black fungi, largely due to the increasing availability of high-throughput methodologies such as 'omics' technologies (Moreno et al., 2018). These techniques have allowed extensive exploration of the genome, transcriptome, and proteome of black rock fungi, even though they are 'non-traditional organisms' (Gostinčar et al., 2012). In parallel, the integration of metagenomics and metabolomics approaches (Blachowicz et al., 2019) has emerged as useful strategy to explore the diversity within these extremotolerant fungi.

While unravelling the molecular mechanisms underlying the extreme adaptations of black fungi remains a challenge, omics approaches have provided valuable insights. However, the adoption of these methods entails both the generation and mining of substantial computational data (Moreno et al., 2018). To sustain the momentum of these projects e.g., Selbmann et al. (2020), the development of dedicated libraries is required to ensure easy data access for comparative analyses. Furthermore, while these approaches are powerful, they are not exhaustive and cannot fully substitute for *in vivo* studies (Coker, 2019). Especially when addressing astrobiological questions concerning the interaction between extremophiles and their habitats (Haqq-Misra et al., 2024), diversifying the repertoire of model organisms by including (poly-)extremophilic/(poly-) extremotolerant representatives is crucial. However, given the methodological challenges associated with experimental studies involving such extremophilic organisms (Schultz et al., 2023), the integration of alternative models with reliable and efficient molecular tools for genetic manipulation offer a promising approach to ensure the reproducibility and temporal resolution of these studies (Knabe and Gorbushina, 2018).

Advanced engineering methods, such as the CRISPR (Clustered Regularly Interspaced Short Palindromic Repeats)/nuclease system, may overcome these issues and unlock the full research potential of (poly-)extremotolerant fungi (Spasskaya et al., 2021; Erdmann et al., 2022; Li et al., 2023). Indeed, advanced molecular tools were effectively established for genetic manipulation of filamentous fungi, including various saprophytic, phyto- and human-pathogenic representatives (Perez-Nadales et al., 2014; Lichius et al., 2020), whereas they have only recently expanded to encompass microcolonial, rock-inhabiting fungi as well (Voigt et al., 2020; Erdmann et al., 2022). This advancement suggests that genetic manipulation is now potentially applicable to the most recalcitrant, non-model fungus. In particular, the CRISPR/Cas9-based genome editing approach facilitates precise mutagenesis through gene knockout and knock-in (Ye et al., 2023).

Implementing both gene strategies can support the study of the gene functions and the manipulation of metabolic pathways. In turn, engineered (poly-)extremotolerant fungi may contribute to both understanding the evolved fungal mechanisms and regulatory networks in response to stress conditions, and eventually enhance the metabolic production of specific compounds with biotechnological relevance.

Some extremophiles are known to produce valuable biochemicals with biotechnological and industrial applications. For instance, DNA polymerases from thermophilic bacteria are essential components of modern polymerase chain reaction (PCR) technologies (Coker, 2019). Consequently, genetic engineering of suitable candidates among (poly-)extremotolerant fungi could bolster the use of unconventional biological chassis to produce biocompounds for different industrial applications like pharmaceuticals and biofuels (Garg et al., 2023; Ye et al., 2023).

Beyond terrestrial applications, other possibilities have been proposed for space exploration, industry, and science. Space synthetic biology, an emerging branch of biotechnology, aims to design robust and reliable organisms capable of supporting long-lasting astronaut missions (Menezes et al., 2015). As the future planetary exploration missions plan to establish permanent human settlements on exotic destinations such as the Moon and Mars, minimal reliance on Earth-based resupplies as well as optimisation of payloads and life-support resources become a priority. The integration of engineered microbial candidates can be advantageous in the context of human resource exploitation in extraterrestrial scenarios. One illustrative approach would involve the genetic manipulation of suitable microorganisms by introducing genes that are known to confer stress tolerance in extremophiles, enhancing the overall microbial fitness in extraterrestrial conditions (Verseux et al., 2016). The end goal is to engineer useful organisms that can endure space and planetary conditions while simultaneously producing life-supporting resources from local resources, paving the way for the sustainable human exploration of deep space and candidate planetary bodies.

1.6 Aims of the thesis and chapters description

The exceptional stress tolerance of black rock-inhabiting fungi to a broad spectrum of extreme conditions makes them attractive eukaryotic organisms for exploring the limits of life in an astrobiological context. Specifically, the study of fungal melanins has garnered attention for their potential applications in various biotechnological areas. However, within the astrobiological

community, research efforts have predominantly focused on experimentally assessing the extreme stress tolerance of few black representatives without a systematic investigation thus far. Indeed, biological experiments under space conditions pose challenges in terms of cost demands and methodological constraints, thus limiting the reproducibility of such experiments (Cottin et al., 2017). Although similar investigations are still fundamental, they may not comprehensively represent the genetic and molecular adaptations of black fungi in extreme environments. Moreover, due to the phylogenetic heterogeneity, studies on different black representatives with no reference system may yield inconsistent results, leading to speculative interpretations on the adaptive mechanisms involved in these polyextremotolerant fungi.

This study aims to comprehensively investigate the potential of black rock-inhabiting fungi for multiple astrobiological applications, focusing on the melanin production as a key life adaptation. First, it seeks to identify reliable biosignatures to support the detection of extinct or extant life on the Martian surface, by advancing dedicated libraries with stable fungal biomolecules. In addition, the study proposes the use of genetically tractable black rock fungi as reference systems for studying the adaptive mechanisms underlying the polyextremotolerance of this group. Detailed exploration of these points is presented in the following chapters of this thesis.

Chapter 2, entitled 'The ground-based BIOMEX Experiment Verification Tests for life detection on Mars', offers a preliminary view on ground-based simulation experiments in the framework of astrobiological investigations through a multi-stage approach. Focusing on DNA and melanin pigments from the black *C. antarcticus* MNA-CCFEE 515, this chapter explores the stability and detectability of these fungal biomolecules as possible biosignatures in a Martian scenario. The molecular characterisation of dehydrated fungal colonies previously cultured on Martian regolith analogues and exposed to polychromatic UV irradiation, was conducted through both destructive and non-destructive analytical techniques. While DNA serves as an unequivocal indicator of life, even in trace amounts (0.018 ng/µL), its low preservation potential and susceptibility to cross-contamination may limit its utility in life detection missions on Mars. In contrast, melanins exhibited higher molecular stability and significant detectability, thus supporting their potential biosignature reliability despite possible background interference with the Martian environment.

Subsequent chapters illustrate the complementary application of black rock fungi for the study of the genetic and molecular mechanisms involved in fungal stress tolerance to extreme conditions. As suggested by the title ('Deletion of the polyketide synthase-encoding gene *pks1* prevents melanisation in the extremophilic fungus *Cryomyces antarcticus*'), **Chapter 3** focuses on the application of genome manipulation techniques on the polyextremotolerant *C. antarcticus*.

For the first time ever among Antarctic fungi, gene knockouts were successful delivered to silence the production of two fungal pigments. Employing the black model *K. petricola* A95 as genetic reference, transformation procedures and CRISPR/Cas9-based approach were established for *C. antarcticus*, resulting in the generation of pigment-free mutants lacking either the DHN-melanin or carotenoid content. Despite the successful realisation of the whole transformation process requiring a lengthy timeframe, these results demonstrate the feasibility of gene manipulation in non-model fungi, paving the way for further engineering of extremophilic candidates.

Once non-melanised strains were available for both *C. antarcticus* and *K. petricola*, a comparative study was performed for the first time involving the two engineered systems, to investigate the adaptive mechanisms involved in the stress tolerance strategies of black fungi. Specifically, **Chapter 4** ('1,8-dihydroxynaphthalene (DHN) melanin plays a different role in protection against UV-B in the black fungi *Knufia petricola* and *Cryomyces antarcticus*') presents a comparative study between *C. antarcticus* and *K. petricola* for elucidating whether the ubiquitous presence of DHN-melanins confers protection against UV-B radiation. In this regard, viable melanised wild type and non-melanised mutants of both fungi were subjected to UV-B irradiation and incubated either in complete darkness or under a diurnal cycle. Findings revealed a divergent role of DHN-melanin in the two species: while melanin significantly contributed to the survival of *C. antarcticus* to UV-B radiation, it held no protective role in *K. petricola*. Conversely, *K. petricola* preserved an efficient photorepair system for UV-damaged DNA, whereas *C. antarcticus* adapted to rely on the damage avoidance strategy of melanin. Ultimately, this study demonstrates that black fungi do not use melanins only as protective biomolecules against harmful UV conditions; instead, they may employ diverse strategies to cope with the same stress condition.

1.7 References

Alsharif, W., Saad, M.M., and Hirt, H. (2020) Desert microbes for boosting sustainable agriculture in extreme environments. *Front Microbiol* **11**.

Ametrano, C.G., Muggia, L., and Grube, M. (2019) Extremotolerant black fungi from rocks and lichens. In *Fungi in extreme environments: Ecological role and biotechnological significance*. Tiquia-Arashiro, S.M., and Grube, M. (eds). Cham: Springer International Publishing, pp. 119-143.

Aureli, L., Coleine, C., Delgado-Baquerizo, M., Ahren, D., Cemmi, A., Di Sarcina, I. et al. (2023) Geography and environmental pressure are predictive of class-specific radioresistance in black fungi. *Environ Microbiol* **25**: 2931-2942.

Baqué, M., Backhaus, T., Meessen, J., Hanke, F., Bottger, U., Ramkissoon, N. et al. (2022) Biosignature stability in space enables their use for life detection on Mars. *Sci Adv* **8**.

Berthelot, C., Zegeye, A., Gaber, D.A., Chalot, M., Franken, P., Kovács, G.M. et al. (2020) Unravelling the role of melanin in Cd and Zn tolerance and accumulation of three dark septate endophytic species. *Microorganisms* **8**.

Blachowicz, A., Chiang, A.J., Elsaesser, A., Kalkum, M., Ehrenfreund, P., Stajich, J.E. et al. (2019) Proteomic and metabolomic characteristics of extremophilic fungi under simulated Mars conditions. *Front Microbiol* **10**.

Blasi, B., Poyntner, C., Rudavsky, T., Prenafeta-Boldú, F.X., de Hoog, S., Tafer, H., and Sterflinger, K. (2016) Pathogenic yet environmentally friendly? Black fungal candidates for bioremediation of pollutants. *Geomicrobiol J* **33**: 308-317.

Bosak, T., Moore, K.R., Gong, J., and Grotzinger, J.P. (2021) Searching for biosignatures in sedimentary rocks from early Earth and Mars. *Nat Rev Earth Environ* **2**: 490-506.

Breitenbach, R., Gerrits, R., Dementyeva, P., Knabe, N., Schumacher, J., Feldmann, I. et al. (2022) The role of extracellular polymeric substances of fungal biofilms in mineral attachment and weathering. *NPJ Mater Degrad* **6**: 42.

Butler, M.J., and Day, A.W. (1998) Fungal melanins: a review. *Can J Microbiol* **44**: 1115-1136.

Cao, W., Zhou, X., McCallum, N.C., Hu, Z., Ni, Q.Z., Kapoor, U. et al. (2021) Unraveling the structure and function of melanin through synthesis. *J Am Chem Soc* **143**: 2622-2637.

Carrier, B.L., Beaty, D.W., Meyer, M.A., Blank, J.G., Chou, L., DasSarma, S. et al. (2020) Mars extant life: what's next? Conference report. *Astrobiology* **20**: 785-814.

Cassaro, A., Pacelli, C., and Onofri, S. (2022) Survival, metabolic activity, and ultrastructural damages of Antarctic black fungus in perchlorates media. *Front Microbiol* **13**: 992077.

Cassaro, A., Pacelli, C., Aureli, L., Catanzaro, I., Leo, P., and Onofri, S. (2021a) Antarctica as a reservoir of planetary analogue environments. *Extremophiles* **25**: 437-458.

Cassaro, A., Pacelli, C., Aureli, L., Leo, P., Catanzaro, I., de Vera, J.P., and Onofri, S. (2021b) A multi-step astrobiological approach for supporting life-detection. *J Ital Astron Soc* **92**: 103-106.

Catling, D.C. (2014) Mars atmosphere: history and surface interactions. In *Encyclopedia of the Solar System*. Spohn, T., Breuer, D., and Johnson, T.V. (eds). Boston: Elsevier, pp. 343-357.

Chan, Y., Lacap, D.C., Lau, M.C.Y., Ha, K.Y., Warren-Rhodes, K.A., Cockell, C.S. et al. (2012) Hypolithic microbial communities: between a rock and a hard place. *Environ Microbiol* **14**: 2272-2282.

Cockell, C.S. (2014) Trajectories of Martian Habitability. *Astrobiology* **14**: 182-203.

Cockell, C.S. (2020) *Astrobiology: understanding life in the universe*. Hoboken: John Wiley & Sons.

Cockell, C.S., Bush, T., Bryce, C., Direito, S., Fox-Powell, M., Harrison, J.P. et al. (2016) Habitability: a review. *Astrobiology* **16**: 89-117.

Coker, J.A. (2019) Recent advances in understanding extremophiles. *F1000Res* **8**: 1917.

Coleine, C., Stajich, J.E., de Los Rios, A., and Selbmann, L. (2021) Beyond the extremes: Rocks as ultimate refuge for fungi in drylands. *Mycologia* **113**: 108-133.

Coleine, C., Selbmann, L., Singh, B.K., and Delgado-Baquerizo, M. (2022a) The poly-extreme tolerant black yeasts are prevalent under high ultraviolet light and climatic seasonality across soils of global biomes. *Environ Microbiol* **24**: 1988-1999.

Coleine, C., Delgado-Baquerizo, M., Albanese, D., Singh, B.K., Stajich, J.E., Selbmann, L., and Egidi, E. (2022b) Rocks support a distinctive and consistent mycobiome across contrasting dry regions of Earth. *FEMS Microbiol Ecol* **98**.

Cordero, R.J.B., and Casadevall, A. (2017) Functions of fungal melanin beyond virulence. *Fungal Biol Rev* **31**: 99-112.

Cottin, H., Kotler, J.M., Billi, D., Cockell, C.S., Demets, R., Ehrenfreund, P. et al. (2017) Space as a tool for astrobiology: Review and recommendations for experimentations in Earth orbit and beyond. *Space Sci Rev* **209**: 83-181.

De Leo, F., Marchetta, A., and Urzì, C. (2022) Black fungi on stone-built heritage: Current knowledge and future outlook. *Appl Sci* **12**: 3969.

Erdmann, E.A., Nitsche, S., Gorbushina, A.A., and Schumacher, J. (2022) Genetic engineering of the rock inhabitant *Knufia petricola* provides insight into the biology of extremotolerant black fungi. *Front Fungal Biol* **3**: 862429.

Friedmann, E.I., and Ocampo-Friedmann, R. (1984) The Antarctic cryptoendolithic ecosystem: Relevance to exobiology. *Origins Life Evol Biosphere* **14**: 771-776.

Friedmann, E.I., Hua, M., and Ocampo-Friedmann, R. (1988) Cryptoendolithic lichen and cyanobacterial communities of the Ross Desert, Antarctica. *Polarforschung* **58**: 251-259.

Gaber, D.A., Berthelot, C., Camehl, I., Kovács, G.M., Blaudez, D., and Franken, P. (2020) Salt stress tolerance of dark septate endophytes is independent of melanin accumulation. *Front Microbiol* **11**: 562931.

Garg, D., Samota, M.K., Kontis, N., Patel, N., Bala, S., and Rosado, A.S. (2023) Revolutionizing biofuel generation: Unleashing the power of CRISPR-Cas mediated gene editing of extremophiles. *Microbiol Res* **274**: 127443.

Gessler, N.N., Egorova, A.S., and Belozerskaya, T.A. (2014) Melanin pigments of fungi under extreme environmental conditions. *Appl Biochem Microbiol* **50**: 105-113.

Gorbushina, A.A. (2007) Life on the rocks. *Environ Microbiol* **9**: 1613-1631.

Gorbushina, A.A., and Krumbein, W.E. (2000) Rock dwelling fungal communities: Diversity of life styles and colony structure. In *Journey to diverse microbial worlds: Adaptation to exotic environments*. Seckbach, J. (ed). Dordrecht: Springer Netherlands, pp. 317-334.

Gorbushina, A.A., Kotlova, E.R., and Sherstneva, O.A. (2008) Cellular responses of microcolonial rock fungi to long-term desiccation and subsequent rehydration. *Stud Mycol* **61**: 91-97.

Gostinčar, C., Muggia, L., and Grube, M. (2012) Polyextremotolerant black fungi: oligotrophism, adaptive potential, and a link to lichen symbioses. *Front Microbiol* **3**: 390.

Gostinčar, C., Zalar, P., and Gunde-Cimerman, N. (2022) No need for speed: slow development of fungi in extreme environments. *Fungal Biol Rev* **39**: 1-14.

Gostinčar, C., Stajich, J.E., and Gunde-Cimerman, N. (2023) Extremophilic and extremotolerant fungi. *Curr Biol* **33**: R752-R756.

Grube, M., and Wedin, M. (2016) Lichenized fungi and the evolution of symbiotic organization. *Microbiol Spectr* **4**: 10-1128.

Gueidan, C., Ruibal, C., de Hoog, G.S., and Schneider, H. (2011) Rock-inhabiting fungi originated during periods of dry climate in the late Devonian and middle Triassic. *Fungal Biol* **115**: 987-996.

Gueidan, C., Villasenor, C.R., de Hoog, G.S., Gorbushina, A.A., Untereiner, W.A., and Lutzoni, F. (2008) A rock-inhabiting ancestor for mutualistic and pathogen-rich fungal lineages. *Stud Mycol* **61**: 111-119.

Haqq-Misra, J., Mendonça, M.d.S., and Meurer, J.C. (2024) Astroecology: bridging the gap between ecology and astrobiology. *Int J Astrobiology* **23**: e3.

Hays, L.E., Graham, H.V., Des Marais, D.J., Hausrath, E.M., Horgan, B., McCollom, T.M. et al. (2017) Biosignature preservation and detection in Mars analog environments. *Astrobiology* **17**: 363-400.

Isola, D., Selbmann, L., de Hoog, G.S., Fenice, M., Onofri, S., Prenafeta-Boldú, F.X., and Zucconi, L. (2013) Isolation and screening of black fungi as degraders of volatile aromatic hydrocarbons. *Mycopathologia* **175**: 369-379.

Jones, D.L., and Baxter, B.K. (2017) DNA repair and photoprotection: mechanisms of overcoming environmental ultraviolet radiation exposure in halophilic Archaea. *Front Microbiol* **8**.

Kebbi, Y., Muhammad, A.I., Sant'Ana, A.S., do Prado-Silva, L., Liu, D., and Ding, T. (2020) Recent advances on the application of UV-LED technology for microbial inactivation: Progress and mechanism. *Rev Food Sci Food Saf* **19**: 3501-3527.

Klein, D.A., and Paschke, M.W. (2004) Filamentous fungi: the indeterminate lifestyle and microbial ecology. *Microb Ecol* **47**: 224-235.

Knabe, N., and Gorbushina, A.A. (2018) Territories of rock-inhabiting fungi: survival on and alteration of solid air-exposed surfaces. In *Methods in Microbiology*. Gurtler, V., and Trevors, J.T. (eds): Elsevier Ltd, pp. 145-169.

Li, J., Wang, X., Zou, J., Yang, K., Wang, X., Wang, Y. et al. (2023) Identification and characterization of the determinants of copper resistance in the acidophilic fungus *Acidomyces richmondensis* MEY-1 using the CRISPR/Cas9 system. *Appl Environ Microbiol* **89**: e02107-e02122.

Lichius, A., Ruiz, D.M., and Zeilinger, S. (2020) Genetic transformation of filamentous fungi: Achievements and challenges. In *Grand challenges in fungal biotechnology*. Nevalainen, H. (ed). Cham: Springer, pp. 123-164.

Liu, B., Fu, R., Wu, B., Liu, X., and Xiang, M. (2021) Rock-inhabiting fungi: terminology, diversity, evolution and adaptation mechanisms. *Mycology* **13**: 1-31.

Malaterre, C., ten Kate, I.L., Baqué, M., Debaille, V., Grenfell, J.L., Javaux, E.J. et al. (2023) Is there such a thing as a biosignature? *Astrobiology* **23**: 1213-1227.

Martins, Z., Cottin, H., Kotler, J.M., Carrasco, N., Cockell, C.S., de la Torre Noetzel, R. et al. (2017) Earth as a tool for astrobiology—A European perspective. *Space Sci Rev* **209**: 43-81.

McMahon, S., and Cosmidis, J. (2022) False biosignatures on Mars: anticipating ambiguity. *J Geol Soc London* **179**: jgs2021-2050.

Menezes, A.A., Montague, M.G., Cumbers, J., Hogan, J.A., and Arkin, A.P. (2015) Grand challenges in space synthetic biology. *J R Soc Interface* **12**: 2015/2008/2003.

Merino, N., Aronson, H.S., Bojanova, D.P., Feyhl-Buska, J., Wong, M.L., Zhang, S., and Giovannelli, D. (2019) Living at the extremes: Extremophiles and the limits of life in a planetary context. *Front Microbiol* **10**: 780.

Moreno, L.F., Vicente, V.A., and de Hoog, S. (2018) Black yeasts in the omics era: achievements and challenges. *Med Mycol* **56**: S32-S41.

Nai, C., Wong, H.Y., Pannenbecker, A., Broughton, W.J., Benoit, I., de Vries, R.P. et al. (2013) Nutritional physiology of a rock-inhabiting, model microcolonial fungus from an ancestral lineage of the Chaetothyriales (Ascomycetes). *Fungal Genet Biol* **56**: 54-66.

Nienow, J.A. (2017) Extremophiles: dry environments (including cryptoendoliths). In *Encyclopedia of microbiology*. Schmidt, T.M. (ed). Oxford: Academic Press, pp. 239-262.

Onofri, S., Selbmann, L., Zucconi, L., and Pagano, S. (2004) Antarctic microfungi as models for exobiology. *Planet Space Sci* **52**: 229-237.

Onofri, S., Pacelli, C., Selbmann, L., and Zucconi, L. (2020a) The amazing journey of *Cryomyces antarcticus* from Antarctica to space. In *Extremophiles as astrobiological models*. Seckbach, J., and Stan-Lotter, H. (eds): Scrivener Publishing LLC, pp. 237-254.

Onofri, S., Zucconi, L., Selbmann, L., de Hoog, S., de los Ríos, A., Ruisi, S., and Grube, M. (2007) Fungal associations at the cold edge of life. In *Algae and cyanobacteria in extreme environments*. Seckbach, J. (ed). Dordrecht: Springer, pp. 735-757.

Onofri, S., de Vera, J.P., Zucconi, L., Selbmann, L., Scalzi, G., Venkateswaran, K.J. et al. (2015) Survival of Antarctic cryptoendolithic fungi in simulated Martian conditions on board the International Space Station. *Astrobiology* **15**: 1052-1059.

Onofri, S., Balucani, N., Barone, V., Benedetti, P., Billi, D., Balbi, A. et al. (2020b) The Italian national project of astrobiology-Life in Space-Origin, presence, persistence of life in space, from molecules to extremophiles. *Astrobiology* **20**: 580-582.

Orosei, R., Lauro, S.E., Pettinelli, E., Cicchetti, A., Coradini, M., Cosciotti, B. et al. (2018) Radar evidence of subglacial liquid water on Mars. *Science* **361**: 490-493.

Pacelli, C., Bryan, R.A., Onofri, S., Selbmann, L., Shuryak, I., and Dadachova, E. (2017) Melanin is effective in protecting fast and slow growing fungi from various types of ionizing radiation. *Environ Microbiol* **19**: 1612-1624.

Perez-Nadales, E., Almeida Nogueira, M.F., Baldin, C., Castanheira, S., El Ghalid, M., Grund, E. et al. (2014) Fungal model systems and the elucidation of pathogenicity determinants. *Fungal Genet Biol* **70**: 42-67.

Rappaport, H.B., and Oliverio, A.M. (2023) Extreme environments offer an unprecedented opportunity to understand microbial eukaryotic ecology, evolution, and genome biology. *Nat Commun* **14**: 4959.

Romano, I., Camerlingo, C., Vaccari, L., Birarda, G., Poli, A., Fujimori, A. et al. (2022) Effects of ionizing radiation and long-term storage on hydrated vs. dried cell samples of extremophilic microorganisms. *Microorganisms* **10**: 190.

Salvatore, M.R., and Levy, J.S. (2021) The McMurdo Dry Valleys of Antarctica: a geological, environmental, and ecological analog to the Martian surface and near surface. In *Mars Geological Enigmas*. Soare, R.J., Conway, S.J., Williams, J.-P., and Oehler, D.Z. (eds): Elsevier, pp. 291-332.

Salwan, R., and Sharma, V. (2020) Physiology of extremophiles. In *Physiological and biotechnological aspects of extremophiles*. Salwan, R., and Sharma, V. (eds): Academic Press, pp. 13-22.

Sasselov, D.D., Grotzinger, J.P., and Sutherland, J.D. (2020) The origin of life as a planetary phenomenon. *Sci Adv* **6**: eaax3419.

Scalzi, G., Selbmann, L., Zucconi, L., Rabbow, E., Horneck, G., Albertano, P., and Onofri, S. (2012) LIFE experiment: isolation of cryptoendolithic organisms from Antarctic colonized sandstone exposed to space and simulated Mars conditions on the International Space Station. *Orig Life Evol Biosph* **42**: 253-262.

Schultz, J., Modolon, F., Peixoto, R.S., and Rosado, A.S. (2023) Shedding light on the composition of extreme microbial dark matter: alternative approaches for culturing extremophiles. *Front Microbiol* **14**.

Selbmann, L., Zucconi, L., Isola, D., and Onofri, S. (2015) Rock black fungi: excellence in the extremes, from the Antarctic to space. *Curr Genet* **61**: 335-345.

Selbmann, L., de Hoog, G.S., Mazzaglia, A., Friedmann, E.I., and Onofri, S. (2005) Fungi at the edge of life: cryptoendolithic black fungi from Antarctic desert. *Stud Mycol* **51**: 1-32.

Selbmann, L., Grube, M., Onofri, S., Isola, D., and Zucconi, L. (2013) Antarctic epilithic lichens as niches for black meristematic fungi. *Biology* **2**: 784-797.

Selbmann, L., Pacelli, C., Zucconi, L., Dadachova, E., Moeller, R., de Vera, J.P., and Onofri, S. (2018) Resistance of an Antarctic cryptoendolithic black fungus to radiation gives new insights of astrobiological relevance. *Fungal Biol* **122**: 546-554.

Selbmann, L., Benko, Z., Coleine, C., de Hoog, S., Donati, C., Druzhinina, I. et al. (2020) Shed light in The daRk LineagES of the fungal tree of life-STRES. *Life* **10**: 362.

Shu, W., and Huang, L. (2022) Microbial diversity in extreme environments. *Nat Rev Microbiol* **20**: 219-235.

Simões, M.F., Cortesão, M., Azua-Bustos, A., Bai, F., Canini, F., Casadevall, A. et al. (2023) The relevance of fungi in astrobiology research – Astromycology. *Mycosphere* **14**: 1190-1253.

Singh, S., Nimse, S.B., Mathew, D.E., Dhimmar, A., Sahastrabudhe, H., Gajjar, A. et al. (2021) Microbial melanin: Recent advances in biosynthesis, extraction, characterization, and applications. *Biotechnol Adv* **53**: 107773.

Solano, F. (2016) Photoprotection versus photodamage: updating an old but still unsolved controversy about melanin. *Polym Int* **65**: 1276-1287.

Spasskaya, D.S., Kotlov, M.I., Lekanov, D.S., Tutyaeva, V.V., Snezhkina, A.V., Kudryavtseva, A.V. et al. (2021) CRISPR/Cas9-mediated genome engineering reveals the contribution of the 26S proteasome to the extremophilic nature of the yeast *Debaryomyces hansenii*. *ACS Synt Biol* **10**: 297-308.

Tesei, D. (2022) Black fungi research: Out-of-this-world implications. *Encyclopedia* **2**: 212-229.

Tonon, C., Breitenbach, R., Voigt, O., Turci, F., Gorbushina, A.A., and Favero-Longo, S.E. (2021) Hyphal morphology and substrate porosity-rather than melanization-drive penetration of black fungi into carbonate substrates. *J Cult Herit* **48**: 244-253.

Vasileiou, T., and Summerer, L. (2020) A biomimetic approach to shielding from ionizing radiation: the case of melanized fungi. *PLoS One* **15**: e0229921.

Verseux, C.N., Paulino-Lima, I.G., Baqué, M., Billi, D., and Rothschild, L.J. (2016) Synthetic biology for space exploration: promises and societal implications. In *Ambivalences of creating life: societal and philosophical dimensions of synthetic biology*. Hagen, K., Engelhard, M., and Toepfer, G. (eds). Cham: Springer International Publishing, pp. 73-100.

Voigt, O., Knabe, N., Nitsche, S., Erdmann, E.A., Schumacher, J., and Gorbushina, A.A. (2020) An advanced genetic toolkit for exploring the biology of the rock-inhabiting black fungus *Knufia petricola*. *Sci Rep* **10**: 22021.

Warren-Rhodes, K., Cabrol, N.A., Phillips, M., Tebes-Cayo, C., Kalaitzis, F., Ayma, D. et al. (2023) Orbit-to-ground framework to decode and predict biosignature patterns in terrestrial analogues. *Nat Astron* **7**: 406-422.

Westall, F., Foucher, F., Bost, N., Bertrand, M., Loizeau, D., Vago, J.L. et al. (2015) Biosignatures on Mars: what, where, and how? Implications for the search for Martian life. *Astrobiology* **15**: 998-1029.

Wollenzien, U., de Hoog, G.S., Krumbein, W., and Uijthof, J.M. (1997) *Sarcinomyces petricola*, a new microcolonial fungus from marble in the Mediterranean basin. *Antonie van Leeuwenhoek* **71**: 281-288.

Wong, H.J., Mohamad-Fauzi, N., Rizman-Idid, M., Convey, P., and Alias, S.A. (2019) Protective mechanisms and responses of micro-fungi towards ultraviolet-induced cellular damage. *Polar Sci* **20**: 19-34.

Ye, J.-W., Lin, Y.-N., Yi, X.-Q., Yu, Z.-X., Liu, X., and Chen, G.-Q. (2023) Synthetic biology of extremophiles: a new wave of biomanufacturing. *Trends Biotechnol* **41**: 342-357.

Zamora, F.J. (2018). Measuring and modeling evolution of cryoconite holes in the McMurdo Dry Valleys, Antarctica [Master's thesis]. Portland State University.

Zhang, J., Guo, J., Dobynde, M.I., Wang, Y., and Wimmer-Schweingruber, R.F. (2022) From the top of Martian Olympus to deep craters and beneath: Mars radiation environment under different atmospheric and regolith depths. *J Geophys Res Planets* **127**: e2021JE007157.

Chapter 2

The ground-based BIOMEX experiment verification tests for life detection on Mars

Claudia Pacelli [1,2], Alessia Cassaro [2,*], Ilaria Catanzaro [2], Mickael Baqué [3], Alessandro Maturilli [3], Ute Böttger [4], Elke Rabbow [5], Jean-Pierre P. de Vera [6], and Silvano Onofri [2]

[1] Italian Space Agency, via del Politecnico snc, 00133 Rome, Italy

[2] Department of Ecological and Biological Sciences, University of Tuscia, largo dell'Università snc, 01100 Viterbo, Italy

[3] Research Group Astrobiological Laboratories, Institute of Planetary Research, Management and Infrastructure, German Aerospace Centre (DLR), Rutherfordstraße 2, 12489 Berlin, Germany

[4] Institute of Optical Sensor Systems, German Aerospace Centre (DLR), Rutherfordstraße 2, 12489 Berlin, Germany

[5] Institute of Aerospace Medicine, Radiation Biology, German Aerospace Centre (DLR), Linder Höhe, 51147 Cologne, Germany

[6] Space Operations and Astronaut Training, MUSC, German Aerospace Centre (DLR), Linder Höhe, 51147 Cologne, Germany

Published on *Life*, 2021, 11(11), 1212. DOI: 10.3390/life11111212

2.1 Author contributions

Conceptualization: E.R., J.-P.P.d.V., S.O.; Methodology: C.P, A.C., M.B., A.M., U.B.; Validation: C.P., A.C., M.B.; Formal analysis: A.C., **I.C.**, M.B.; Investigation: C.P., A.C., **I.C.**, M.B.; Resources: S.O.; Writing – original draft preparation: C.P., A.C., **I.C.**; Writing – review and editing: C.P., A.C., **I.C.**, M.B., A.M., U.B., E.R., J.-P.P.d.V., S.O.; Visualization: C.P., A.C., **I.C.**; Supervision: S.O.; Project administration: J.-P.P.d.V., S.O.; Funding acquisition: S.O.

2.2 Abstract

The success of an astrobiological search for life campaign on Mars, or other planetary bodies in the Solar System, relies on the detectability of past or present microbial life traces, namely, biosignatures. Spectroscopic methods require little or no sample preparation, can be repeated almost endlessly, and can be performed in contact or even remotely. Such methods are therefore ideally suited to use for the detection of biosignatures, which can be confirmed with supporting instrumentation. Here, we discuss the use of Raman and Fourier Transform Infrared (FT-IR) spectroscopies for the detection and characterisation of biosignatures from colonies of the fungus *Cryomyces antarcticus*, grown on Martian analogues and exposed to increasing doses of UV irradiation under dried conditions. The results report significant UV-induced DNA damage, but the non-exceeding of thresholds for allowing DNA amplification and detection, while the spectral properties of the fungal melanin remained unaltered, and pigment detection and identification was achieved via complementary analytical techniques. Finally, this work found that fungal cell wall compounds, likely chitin, were not degraded, and were still detectable even after high UV irradiation doses. The implications for the preservation and detection of biosignatures in extraterrestrial environments are discussed.

Key words: biosignature, dark pigments, polysaccharides, polychromatic radiation, simulated conditions, Mars, life detection

2.3 Introduction

The detection of biosignatures on Mars is of outstanding interest in the current field of astrobiology, and drives various fields of research, ranging from new sample collection strategies to the development of more sensitive detection techniques. The effects of radiation on the stability of biosignatures are essential. On Earth, the preservation of organic biosignatures is principally influenced by the rates of biological records production and alterations from biological recycling and abiotic factors (e.g., radiation), the latter of which must not exceed the former. Some types of biosignatures have been found to be more resistant to certain degradation processes, while some environments may be more favourable in preserving some types than others (Simoneit et al., 1998; Engel and Macko, 2013; Aerts et al., 2014). Research on these issues is a driving factor in designing explorative strategies for life detection missions throughout the Solar System. Ultraviolet (UV) radiation, especially shorter-wavelength UV-C, is known to be a damaging factor for organisms and potential organic biosignatures. On Mars, for example, exposure to the surface UV radiation can degrade common biologically relevant organic molecules to simple organics that may confound identification via biosignatures, even on relatively recently exposed surfaces (Cockell et al., 2005; Dartnell et al., 2012; Poch et al., 2013; Dartnell and Patel, 2014). On Earth, the interiors of rocks provide a protected environment for extant life in some of the most inhospitable terrestrial environments, including the Antarctic Dry Valleys. The endolithic habitat provides thermal buffering, physical stability, and protection from incident UV, solar radiation, and dryness (Friedmann and Ocampo-Friedmann, 1984). Microorganisms can be found at depths of a few to tens of millimetres in rock interiors; these are so-called cryptoendolithic organisms.

The UV environment on Mars differs significantly from that on present-day Earth, and it can significantly influence how biosignatures persist. The Martian atmosphere (primarily composed of CO_2) effectively absorbs all UV radiation below 190 nm and has a modest absorbing effect from 190 to 200 nm, but atmospheric absorbance at longer wavelengths is negligible, and therefore UV with wavelengths >200 nm interacts with the surface (Patel et al., 2002). On Earth, most of the UV-B (280–315 nm) and UV-C (200–280 nm) radiation is absorbed by the ozone (O_3); conversely, this molecule is present in low concentrations in the current Martian atmosphere (Rothschild and Cockell, 1999). The actual UV flux reaching the surface of Mars is influenced by various factors, such as latitude, season, and the orbital position of the planet, and can also fluctuate due to small seasonal build-ups of O_3, as well as dust load in the atmosphere (Patel et al., 2002; Gómez-Elvira et al., 2014). The average UV irradiance (200–400 nm) at the Martian surface has been modelled to be ~50 J/m^{2}s (Kuhn and Atreya, 1979; Schuerger et al., 2003). UV-

B and UV-C represent Mars' UV incident radiation wavelengths that are extremely harmful to DNA and other common biological molecules (Cockell et al., 2005; Stalport et al., 2009; Dartnell et al., 2012; Poch et al., 2013). Several direct measurements of UV irradiance have been made by the Curiosity rover, showing that the maximum total UV flux at the Gale Crater may be closer to 20 J/m^{2}s, which is less severe than the typically modelled irradiance level but is still not favourable for surface habitability (Gómez-Elvira et al., 2014). Additional factors, such as ionising radiation, the presence of oxidants or other reactive species in the atmosphere, and regolith on Mars, would appear to make the long-term survival of organisms or organic biosignatures on the surface highly unlikely (Encrenaz et al., 2012; Glavin et al., 2013; Quinn et al., 2013; Hassler et al., 2014; Ming et al., 2014; Carrier and Kounaves, 2015). Considering that few works have dealt with the interactions of incident UV flux with minerals and rocks (Patel et al., 2002; Patel et al., 2003; Moores et al., 2007; Schuerger et al., 2012), even in preparation for in situ missions to Mars (such as ExoMars and Mars 2020 (Kinch et al., 2020; Lopez-Reyes et al., 2020), the issue is not yet well understood, and therefore a further necessary step is to identify the extent to which rocks and minerals can provide effective shielding against UV radiation.

The present study was performed in the context of the Biology and Mars Experiment (BIOMEX), part of the EXPOSE-R2 mission of the European Space Agency (ESA) along with three other astrobiological experiments, which facilitated 16-month exposure on the outer side of the International Space Station (ISS) from August 2014 to February 2016 (Rabbow et al., 2017; de Vera et al., 2019). The aim of the study was to investigate the resistance and stability of biomolecules to UV irradiation, assessed via the Experiments Verification Test (EVT) ground-based experiments in preparation for the space-exposure BIOMEX project, as support for the ongoing life detection missions on Mars (e.g., ExoMars' Rosalind Franklin mission). These included the exposure of *C. antarcticus* MNA-CCFEE 515, a cryptoendolithic black fungus isolated from Antarctic rocks, to increasing doses of polychromatic UV (200–400 nm) irradiation (up to 5.5×10^5 kJ/m^2). Samples were grown on Martian mineral analogues (Phyllosilicatic and Sulphatic Mars Regolith Simulants) and dried before the irradiation treatment. The stability of fungal biomolecules within Martian analogue minerals was investigated through quantitative PCR (qPCR), UV–Visible (UV-Vis) spectrophotometry, Raman and FT-IR spectroscopy.

2.4 Materials and methods

2.4.1 Sample preparation and cultivation conditions

The cryptoendolithic black fungus *C. antarcticus* MNA-CCFEE 515 of the Mycological Section of the University of Tuscia (Viterbo, Italy) was isolated by R. Ocampo-Friedmann from sandstone collected by H. Vishniac at Linnaeus Terrace in McMurdo Dry Valleys (Southern Victoria Land, AQ) during the 1980-1981 Antarctic expedition (Selbmann et al., 2005).

The homogenised cell suspension from fungal colonies (2.0×10^4 cells/ml) was spread on Malt Extract Agar (MEA) medium (malt extract, powdered: 30 g/l; peptone: 5 g/l; agar: 15 g/l; Applichem GmbH) in Petri dishes and mixed with three separate substrates: Antarctic sandstone (15 g/l) and two Martian regolith analogues (10 g/l). Antarctic sandstone was the original substrate (OS) where the fungus occurs naturally, while the Phyllosilicatic Mars Regolith Simulant (P-MRS) and the Sulphatic Mars Regolith Simulant (S-MRS) mimicked the regolith of the phyllosilicate deposits formed mainly on early Mars and the regolith of sulphate deposits currently observed on Mars, respectively (**Figure 5**). The mineralogical composition of both Martian analogues was provided by Böttger et al. (2012). These Martian regolith analogues have been chosen to evaluate whether they may interfere with fungal biomolecule detection. All samples were incubated for 3 months at 15 °C; once fungal colonies were grown, circular portions were cut to fit within the wells (12 mm) of the exposure carrier and then dehydrated in a sterile hood at room temperature overnight.

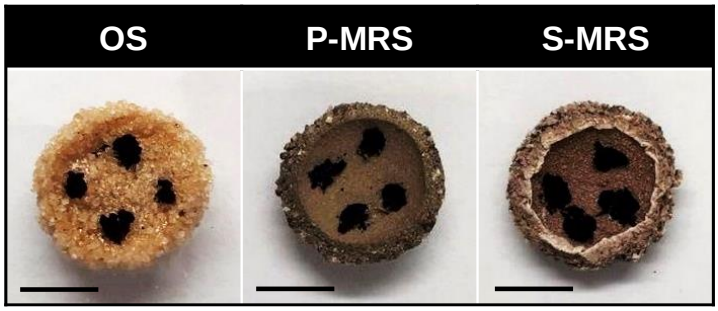

Figure 5. View of EVT2 samples with fungal colonies of *C. antarcticus*. Scale bar: 1 cm.

2.4.2 Test facilities and exposure conditions

In the context of the BIOMEX project, ground-based environmental and space simulations were performed using the Planetary and Space Simulation facilities (PSI) at the Institute of Aerospace Medicine (German Aerospace Centre, DLR, Köln, Germany). The exposure conditions

of the two parts of the EVTs (Experiment Verification Test part 1: performed to simulate several space and Mars-like parameters; Experiment Verification Test part 2: performed to simulate the UV irradiance as expected during a 12-month mission in Low Earth Orbit) were reported by de Vera et al. (2019). All tests were performed in triplicate, and untreated samples, kept in the dark at room temperature, were used as laboratory controls (CTRs). Samples of each substrate were either not irradiated or irradiated with one of the fluences from 5.5×10^2 kJ/m^2 up to 5.5×10^5 kJ/m^2 in the respective irradiation times using a Solar Simulator at 1271 J/m^{2}s as listed in **Table 1**. For each substrate (OS, P-MRS, S-MRS), we investigated pivotal samples from the EVT2 treatment i.e., CTRs, 5.5×10^2 kJ/m^2, and 5.5×10^5 kJ/m^2 samples; moreover, the *C. antarcticus* colonies grown under physiological conditions on MEA without substrate mixing were used as positive controls (POS CTRs).

Table 1. Sample exposure conditions during the UV irradiation treatment of the EXPOSE-R2 Experiment Verification Tests part 2 (EVT2) from the BIOMEX project.

Polychromatic UV irradiance with SOL2000 (200–400 nm)	Exposure time	Final UV dose	Martian days [1]	Substrate
0 J/m^{2}s → CTR (laboratory control)	0 s	0 kJ/m^2	-	MEA + OS/ MEA + P-MRS/ MEA + S-MRS
0 J/m^{2}s → Dark (transport control)	0 s	0 kJ/m^2	-	
1271 J/m^{2}s	7 min, 12 s	5.5×10^2 kJ/m^2 (0.1 % ND [2])	0.37	
1271 J/m^{2}s	1 h, 12 min	5.5×10^3 kJ/m^2 (1.0 % ND [2])	3.70	
1271 J/m^{2}s	30 h	1.4×10^5 kJ/m^2	94.15	
1271 J/m^{2}s	60 h	2.7×10^5 kJ/m^2	181.57	
1271 J/m^{2}s	120 h	5.5×10^5 kJ/m^2	369.87	
Physiological conditions (0 J/m^{2}s) → POS CTR (positive control)	0 s	0 kJ/m^2	-	MEA

[1] Calculated from Cockell et al. (2000). [2] ND: neutral density filter. Modified from de Vera et al. (2019). In yellow, the EVT2 samples used in this work.

2.4.3 DNA integrity assay

2.4.3.1 DNA extraction and quantification

Genomic DNA was extracted from the EVT2 and POS CTR samples using NucleoSpin Plant II Kit/2011 (MACHEREY-NAGEL GmbH & Co. KG, Düren, Germany) and following the protocol optimised for fungi (Selbmann et al., 2005). Samples were quantified using the Qubit Fluorometer (Invitrogen) and the Qubit dsDNA High Sensitivity (HS) Assay Kit (Invitrogen). The assay was performed at room temperature, and three readings for each sample were performed.

Dilution factors were calculated after achieving sample concentrations, and DNA samples were diluted up to the same concentration (0.018 ng/µL) before running the qPCR analysis.

2.4.3.2 DNA amplification

A real-time qPCR was conducted to quantify the number of fungal Large Subunit (LSU) ribosomal DNA restricted fragments (~330 bp) using LR3R (GTC TTG AAA CAC GGA CC) (Vilgalys and Hester, 1990) and LR5 (TCC TGA GGG AAA CTT CG) (Hopple and Vilgalys, 1999) primers. The qPCR reactions were performed in the Bio Rad CFX96 Real-Time PCR Detection System, and the Bio Rad CFX Manager software processed the results in graphs. The reactions were carried out in triplicate in the 96-well plate with a solution containing 7.5 µL iQ SYBR Green Supermix (Bio Rad, Milan, Italy), 1.0 µL each primer solution (5 pmol/µL), and 5.5 ng DNA template in a final volume of 15 µL; for the No Template Control (NTC) sample, 5.5 µL sterile deionised water was added instead of DNA template. The amplification conditions of the LSU region were derived from Selbmann et al. (2011). Fluorescence measurements were performed at the end of each annealing cycle. A melt curve analysis was performed by raising the temperature from 65 to 95 °C in 0.5 °C steps for 5 s each. To enable the quantification of PCR products, standard curves based on threshold cycles were produced by reamplifying tenfold dilution series of PCR products from genomic DNA. Aliquots of each dilution (equivalent to 1×10^2–1×10^8 LSU copies) in triplicate were used as templates in qPCR. Means and standard deviations were calculated for qPCR products.

2.4.3.3 Statistical analysis

The one-way analysis of variance (ANOVA) and the pairwise multiple comparison procedures (Tukey's HSD post-hoc test) were performed on log-transformed data using RStudio software (RStudio Team, 2016; R Core Team, 2018).

2.4.4 Fungal melanin assay

2.4.4.1 Pigment extraction and quantification

Melanin was extracted from the previous EVT2 and POS CTR samples following the optimised protocol for black fungi (Pacelli et al., 2020b). After the extraction, serial dilutions of purified pigments (1:5, 1:10, 1:20, 1:50 to 1:100) were made, allowing dissolution in an aqueous substrate

(NaOH 1 M). To define the correlation between absorbance and wavelength, spectral measurements of all sample solutions were recorded via UV-Vis spectrophotometry as described in Pacelli et al. (2020b). To determine the concentration of extracted melanin samples, synthetic DHN (1,8-dihydroxynaphthalene) melanin (Sigma-Aldrich) was prepared in NaOH 1 M at a concentration of 500 mg/ml, and a standard curve at 650 nm (A_{650}) was obtained (**Figure 6**). Dilutions at 1:5 for the OS and S-MRS samples and at 1:50 for the P-MRS samples were selected for measuring the A_{650}.

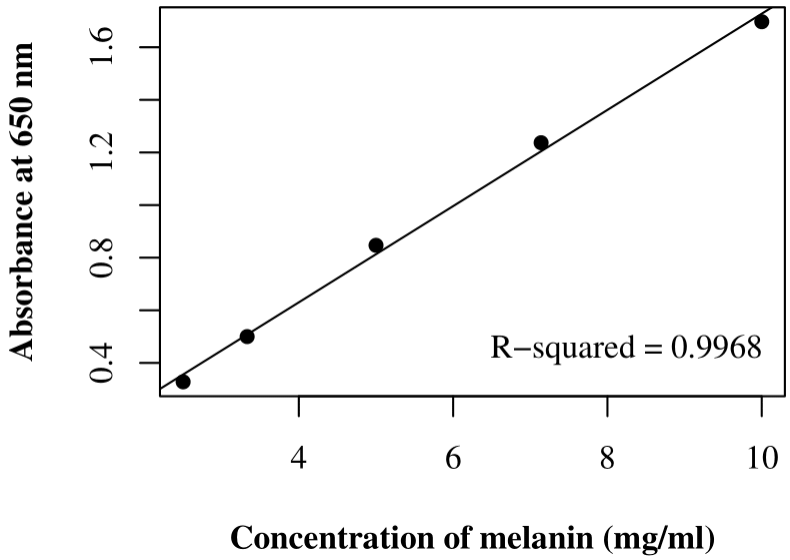

Figure 6. A_{650} standard curve of synthetic DHN melanin, which was calculated according to Raman and Ramasamy (2017). On the x-axis, the melanin concentration (in mg/ml); on the y-axis, the absorbance value at 650 nm (in absorbance units).

2.4.4.2 Pigment detection

Raman spectroscopic analysis was performed directly on the previous EVT2 samples at the Raman Laboratory of the German Aerospace Centre (DLR) in Berlin, with an alpha300 R Confocal Raman microscope (WITec) at room temperature and under ambient atmospheric conditions, according to the optimised protocol by Böttger et al. (2012). The Raman laser excitation wavelength was 532 nm, and the spectral resolution was 4-5 cm^{-1}. A Nikon 10× objective with a 0.25 numerical aperture was used to focus the laser on a 1.5 µm spot. Before the analysis, spectral calibration was performed with pure silicon and paracetamol test samples. For spectral data acquisitions, image scans were collected following the protocol reported by Pacelli et al. (2021) and the spectral data evaluation and processing – including background evaluation – were performed with WITec Project FOUR software.

2.4.4.3 Fungal organic compound detection

FT-IR spectroscopic analysis was performed directly on the previous EVT2 samples at the Planetary Emissivity Laboratory of DLR in Berlin. Spectra were recorded in triplicate on the Vertex 80v FT-IR Spectrometer (Bruker) in reflectance mode and read at a resolution of 4 cm^{-1} in the wavenumber region of 400–10,000 cm^{-1} with Spectragryph software (Menges, 2019). Measurements have been performed under evacuated atmosphere to remove atmospheric features from the spectra. For analysing the presence of specific organic molecules, the region of interest, 600–4000 cm^{-1}, was cropped.

2.5 Results

2.5.1 DNA damage assessment

The integrity of genomic DNA samples was tested by assessing its ability to serve as a PCR template after the polychromatic UV irradiation treatment. The results show reduced gene target amplifications when increasing the irradiation dose for all tested samples (**Figure 7**). Overall, an average of ~$3 \cdot 10^5$ copies were amplified in the POS CTR, whereas an average of ~2×10^5 copies were amplified in the non-irradiated (i.e., CTR) samples, ~$1.7 \cdot 10^4$ in the low-irradiated (i.e., 5.5×10^2 kJ/m^2) samples, and ~1×10^4 in the high-irradiated (i.e., 5.5×10^5 kJ/m^2) samples. Particularly, both OS 5.5×10^2 and OS 5.5×10^5 showed significantly fewer amplified copies than OS CTR (14 % and 11 %, respectively), as well as P-MRS 5.5×10^2 kJ/m^2 and P-MRS 5.5×10^5 kJ/m^2 with P-MRS CTR (2 % and 0.02 %, respectively), and S-MRS 5.5×10^2 kJ/m^2 and S-MRS 5.5×10^5 kJ/m^2 with S-MRS CTR (6 % and 1 %, respectively). To summarise, the amplification was successful in all OS, P-MRS, and S-MRS samples, even in the high-irradiated P-MRS (5.5×10^5 kJ/m^2) sample, which reported fewer than 100 copies.

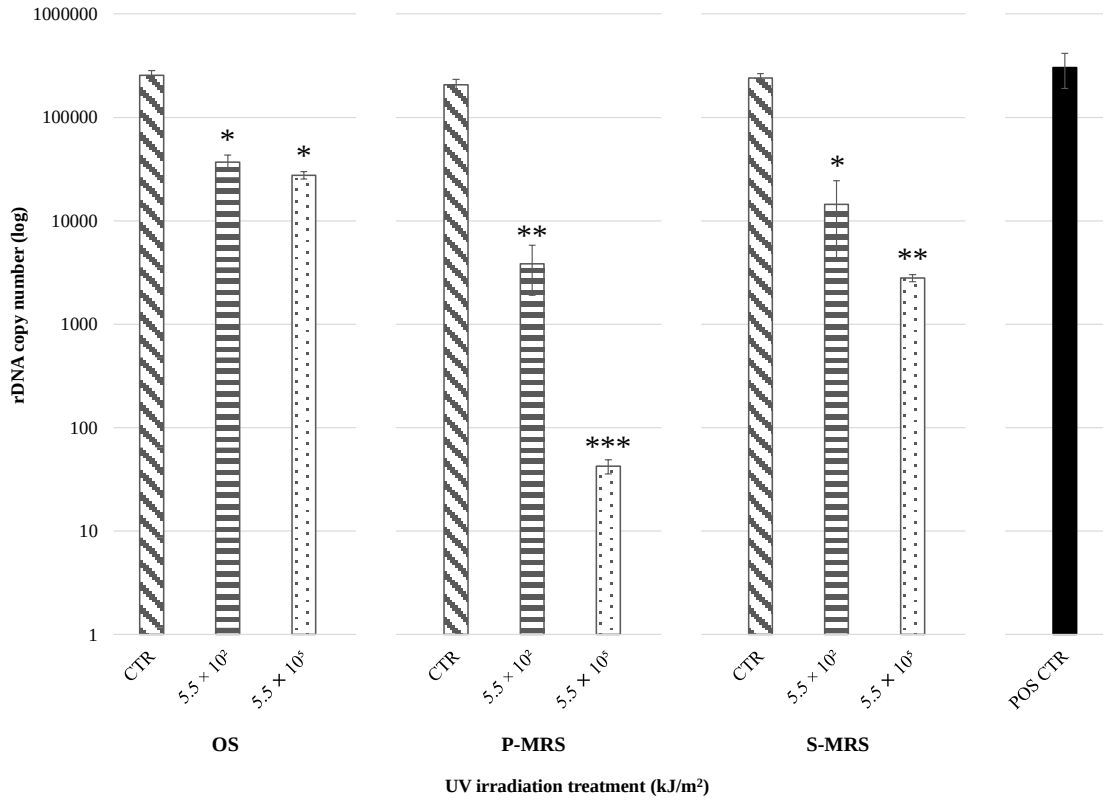

Figure 7. Real-time qPCR of an LSU gene fragment (~330 bp) from *C. antarcticus* after irradiation treatment within EVT2 simulations. On the x-axis, increasing polychromatic UV irradiation doses (CTR: non-irradiated sample; 5.5 × 10^2 kJ/m^2; 5.5 × 10^5 kJ/m^2: irradiated samples) for each substrate (OS: Antarctic sandstone; P-MRS: Phyllosilicatic Mars Regolith Simulant; S-MRS: Sulphatic Mars Regolith Simulant); on the y-axis, the number of amplified target gene copies (in logarithmic scale). Irradiation treatments were compared within analogues, whereas the positive control (POS CTR: *C. antarcticus* grown on MEA under physiological conditions) is shown for reference purposes. Statistically significant difference within substrate samples was calculated with Tukey's test (* < 0.05; ** < 0.001; *** < 0.0001); no significant differences were reported between each CTR and the POS CTR (*p*-value > 0.05).

2.5.2 Pigment characterisation by UV-Vis spectrophotometry

Among all the biological pigments, melanin absorbs all visible wavelengths, resulting in its characteristic dark colour (Bell and Wheeler, 1986). The nature of the purified pigments was thus confirmed by their spectral properties (**Figure 8**). Sample solutions were scanned from the UV to visible wavelength range (200 to 800 nm). Overall, every spectrum showed a strong absorbance in the UV region, reaching maximum values at ~230 nm and progressively decreasing as the wavelength increased. This property is due to the presence of a complex polymeric structure in the melanin molecule (Cockell and Knowland, 1999). Particularly, all P-MRS and S-MRS spectra showed similar profiles with POS CTR, but with wider and narrower absorption peaks in the UV region, respectively. To quantify the purified pigments, their concentration was estimated by comparing the absorbance values at 650 nm of each sample with the A_{650} standard curve (**Figure 6**). The mean and standard deviation values for melanin concentrations (in mg/ml) and the maximum absorbance wavelengths (in nm) are reported in **Table 2**.

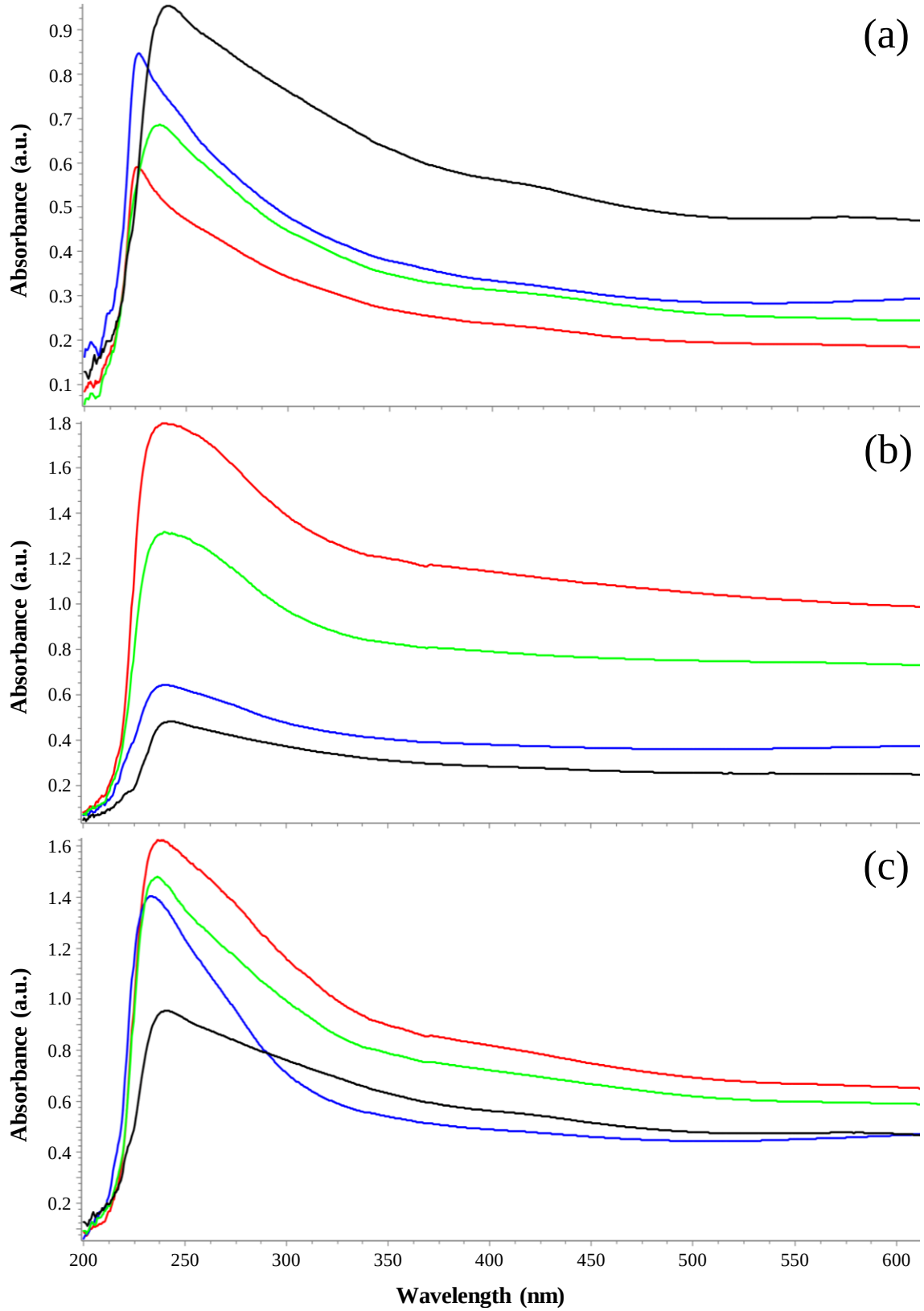

Figure 8. Ultraviolet–visible (UV-Vis) spectra of extracted melanin pigments from *C. antarcticus* dried colonies mixed with (a) OS: Antarctic sandstone; (b) P-MRS: Phyllosilicatic Mars Regolith Simulant; (c) S-MRS: Sulphatic Mars Regolith Simulant, after exposure to increasing polychromatic UV irradiation doses (CTR: red line; 5.5×10^2 kJ/m^2: blue line; 5.5×10^5 kJ/m^2: green line). On the x-axis, increasing wavelengths (in nm); on the y-axis, absorbance values (in absorbance units). Spectral profiles were compared within analogues, while the positive control (POS CTR: *C. antarcticus* grown on MEA under physiological conditions) is shown as the melanin spectrum reference (black line).

Table 2. Mean (± S.D.) values of the melanin concentration (in mg/ml) and the maximum UV absorbance wavelength (in nm) of purified pigments from the selected EVT2 and POS CTR samples.

Sample	Concentration (mg/ml)	Absorption peak (nm)
OS CTR	5.271 (± 2.705)	228 (± 4)
OS 5.5 × 10^2 kJ/m^2	12.116 (± 3.708)	230 (± 6)
OS 5.5 × 10^5 kJ/m^2	6.758 (± 7.760)	233 (± 7)
P-MRS CTR	322.409 (± 103.428)	234 (± 9)
P-MRS 5.5 × 10^2 kJ/m^2	100.973 (± 22.709)	236 (± 6)
P-MRS 5.5 × 10^5 kJ/m^2	237.980 (± 134.799)	234 (± 9)
S-MRS CTR	24.005 (± 15.427)	234 (± 6)
S-MRS 5.5 × 10^2 kJ/m^2	19.811 (± 3.545)	232 (± 7)
S-MRS 5.5 × 10^5 kJ/m^2	22.096 (± 14.595)	233 (± 6)
POS CTR	20.136 (± 5.752)	233 (± 6)

OS: Antarctic sandstone; P-MRS: Phyllosilicatic Mars Regolith Simulant; S-MRS: Sulphatic Mars Regolith Simulant; CTR: non-irradiated sample; 5.5 × 10^2 kJ/m^2 and 5.5 × 10^5 kJ/m^2: irradiated samples; POS CTR: *C. antarcticus* grown on MEA under physiological conditions.

2.5.3 Pigment characterisation by Raman spectroscopy

The Raman signal was obtained by focusing the exciting laser onto *C. antarcticus* dried colonies of the EVT2 samples without any previous preparation. All the acquired Raman spectra showed two clearly distinguishable broad peaks, located at 1323–1345 cm^{-1} and at 1565–1598 cm^{-1} (**Figure 9**). The Raman spectra obtained share key features with those reported in the literature for melanin pigments (Centeno and Shamir, 2008; Culka et al., 2017; Pacelli et al., 2021). However, the definite assignment of the two melanin bands is not entirely agreed upon. Some authors ascribe both bands to the C–C stretching bonds within the aromatic rings, whereas others mark a contribution of aromatic C–N and C–H deformation bonds in the 1400 cm^{-1} region (Huang et al., 2004; Samokhvalov et al., 2004; De Gussem et al., 2005; Maquelin et al., 2006; Rösch et al., 2006; Movasaghi et al., 2007; Saif et al., 2021). According to Culka et al. (2017), this uncertainty is probably due to the vibrations of the constituent monomers, resulting in many overlapping Raman bands. The specific positions of the main peaks serve as a proof that the samples did not undergo thermal degradation, and the signal acquired is of melanin and not burnt organic matter (or amorphous carbon), according to Pacelli et al. (2021). Furthermore, the presence of the peak around 1425 cm^{-1} is a clear sign of the *C. antarcticus*' melanin (Pacelli et al., 2021).

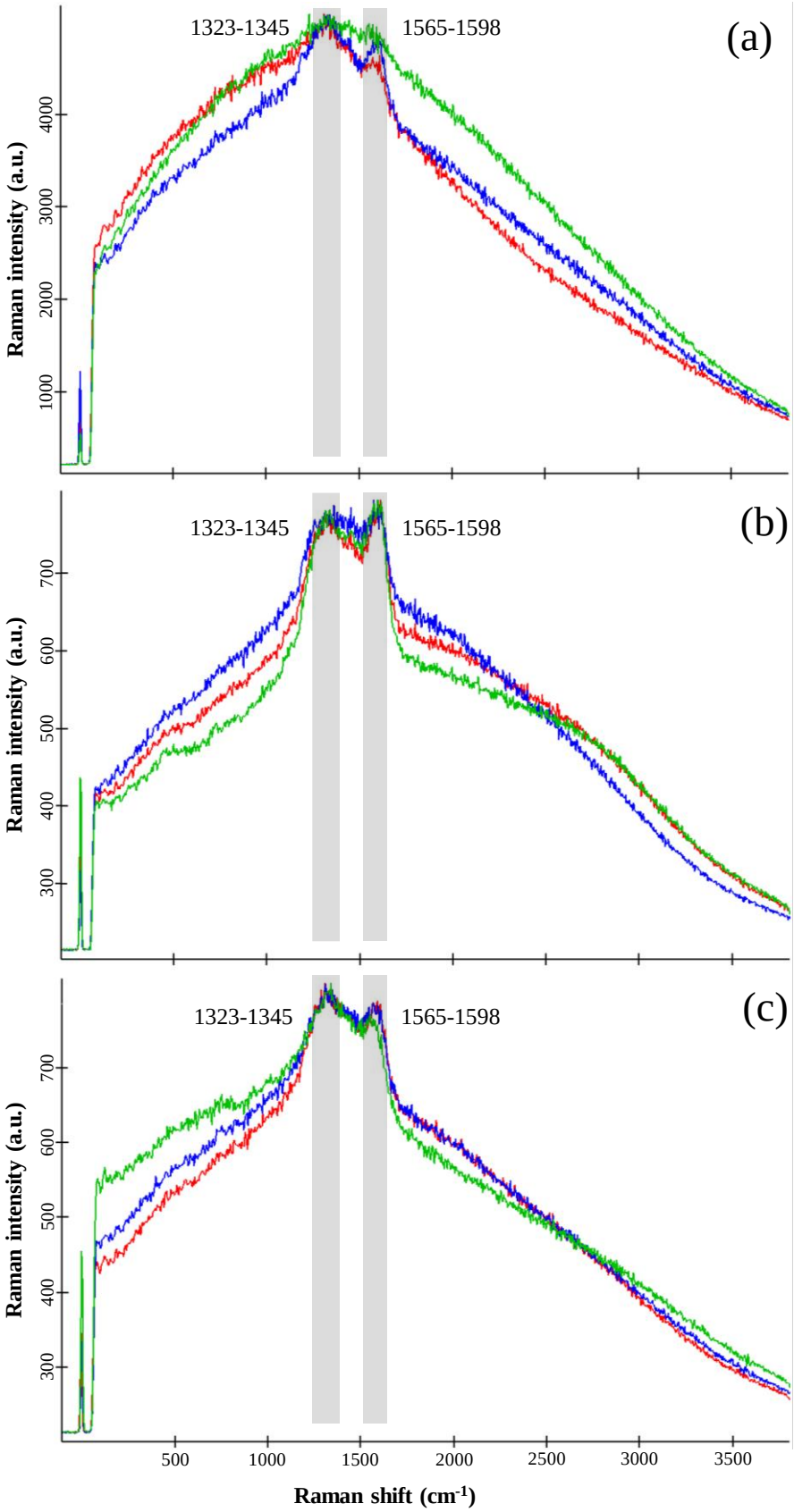

Figure 9. Raman spectra of *C. antarcticus* dried colonies mixed with (a) OS: Antarctic sandstone; (b) P-MRS: Phyllosilicatic Mars Regolith Simulant; (c) S-MRS: Sulphatic Mars Regolith Simulant, after exposure to polychromatic UV irradiation (CTR: red line; 5.5×10^2 kJ/m^2: blue line; 5.5×10^5 kJ/m^2: green line). On the x-axis, Raman shift (in cm^{-1}); on the y-axis, Raman intensity of the scattered light (in arbitrary units). Shared peaks are highlighted within grey squares.

2.5.4 Organic compounds characterisation by FT-IR spectroscopy

FT-IR spectroscopy was used to confirm the melanic nature of the *C. antarcticus* pigment, and to verify the possible presence of further organic compounds after exposure to UV irradiation treatment. Spectra were obtained directly from dried fungal colonies of the EVT2 samples without any previous preparation. All the acquired FT-IR spectra (**Figure 10**) revealed a strong, broad band at 3461–3372 cm^{-1}, which was attributed to the O–H groups linked by the NH_2 groups of phenolic and aromatic amino functions present in pyrrolic and indolic molecules (Jones, 1970; Magarelli et al., 2010; Hou et al., 2019).

Instead, the band duplet at 2931–2926 cm^{-1} and 2858–2851 cm^{-1} was ascribed to the CH stretching of saturated aliphatic hydrocarbons (Safar et al., 1994; Maquelin et al., 2006; Movasaghi et al., 2008). The small bands occurring between 1669 and 1632 cm^{-1} can be assigned to the alkenyl C=C and C=O stretching of the carboxylic or amide functions present in proteins (Stuart, 2004; Coates, 2006; Schulz and Baranska, 2007; Magarelli et al., 2010). The broad spectral region between 1250 and 1000 cm^{-1} can be related to phosphate groups, as well as the C–O, C–N, and C–O–C absorption peaks of carbohydrates or lipids (Maquelin et al., 2006; Schulz and Baranska, 2007; Salman et al., 2014; Kosa et al., 2017). Below 1000 cm^{-1}, the absorption bands were usually weak, and mostly could be assigned to aromatic C–H and O–H out-of-plane deformations (Stuart, 2004; Schulz and Baranska, 2007; Magarelli et al., 2010). Other specific absorption bands have been identified in **Table 3**.

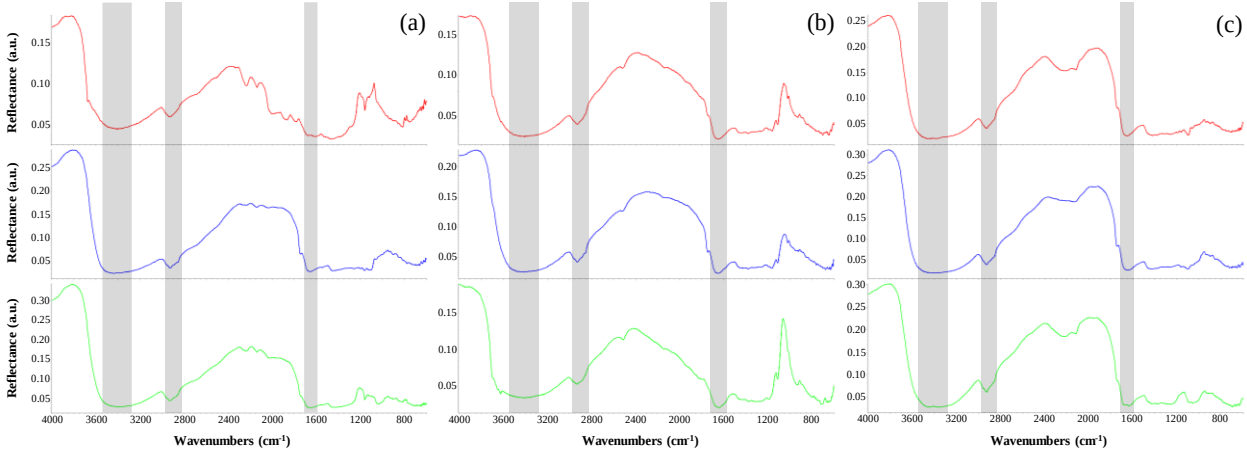

Figure 10. Fourier Transform Infrared (FT-IR) spectra of *C. antarcticus* dried colonies mixed with (a) OS: Antarctic sandstone (5.5×10^2 kJ/m^2: blue line; 5.5×10^5 kJ/m^2: green line), (b) P-MRS: Phyllosilicatic Mars Regolith Simulant (5.5×10^2 kJ/m^2: blue line; 5.5×10^5 kJ/m^2: green line) and (c): S-MRS: Sulphatic Mars Regolith Simulant (5.5×10^2 kJ/m^2: blue line; 5.5×10^5 kJ/m^2: green line). On the x-axis, decreasing wavenumbers (in cm^{-1}); on the y-axis, reflectance values (in arbitrary units). Shared peaks are highlighted within grey squares.

Table 3. Absorption bands (in cm^{-1}) observed in the EVT2 FT-IR spectra and their possible molecular bonding interpretation.

Wavenumber	Possible interpretation	Reference
3461-3372	NH_2/OH stretching of phenols and aromatic amines in indolic and pyrrolic systems	(Magarelli et al., 2010)
2931-2926	CH_2 asymmetric stretching of saturated aliphatic groups in fatty acids	(Safar et al., 1994; Coates, 2006)
2858-2851	CH_2 symmetric stretching of saturated aliphatic groups in fatty acids	(Safar et al., 1994; Coates, 2006)
2515-2511	OH stretching in carboxylic acids	(Stuart, 2004; Shurvell, 2006)
2249	Acetylenic C≡C/aliphatic nitrile C≡N stretching	(Stuart, 2004; Coates, 2006)
2233-2211	Acetylenic C≡C/aromatic nitrile C≡N stretching	(Stuart, 2004; Coates, 2006)
2136-2114	Acetylenic C≡C/aliphatic isonitrile N≡C stretching	(Stuart, 2004; Coates, 2006)
2037-1788	Several vibrations from overtones and combinations of substituted benzene rings	(Shurvell, 2006)
1743-1738	C=O stretching of aliphatic esters in triglycerides	(Guillén and Cabo, 1999; Stuart, 2004)
669-1632	Alkenyl C=C/C=O/C=N stretching of amide I in proteins	(Stuart, 2004; Coates, 2006)
1462-1445	CH_2 scissoring/CH_3 asymmetric bending of aliphatic compounds in proteins or fatty acids	(Irudayaraj et al., 2001; Stuart, 2004)
1422-1415	OH in-plane bending in carboxylic acids	(Shurvell, 2006)
1380-1374	CH_3 symmetric bending of aliphatic compounds in proteins or fatty acids	(Irudayaraj et al., 2001; Stuart, 2004)
1254-1252	P=O asymmetric/CO stretching of aliphatic phosphorus compounds, aromatic ethers and esters in carbohydrates or lipids	(Stuart, 2004; Kosa et al., 2017)
1193-1190	PO/CN/CO stretching of aromatic amines, phosphates, and phenols in carbohydrates or lipids	(Stuart, 2004; Shurvell, 2006)
1164-1158	CO stretching of aliphatic ethers, esters, and alcohols in carbohydrates	(Stuart, 2004; Shurvell, 2006)
1122-1085	CN/COC asymmetric/CO stretching of aliphatic amines, ethers, esters, and alcohols in carbohydrates	(Shurvell, 2006; Schulz and Baranska, 2007)
1061-1018	POC asymmetric/CO stretching of aliphatic phosphorus compounds, ethers, and alcohols in carbohydrates	(Stuart, 2004; Schulz and Baranska, 2007)
928-921	COH out-of-plane bending in carboxylic acids	(Stuart, 2004)
901-814	CH out-of-plane bending of benzenes	(Shurvell, 2006; Schulz and Baranska, 2007)
721-712	$–(CH_2)_n–$ rocking of methylene chains in hydrocarbons	(Irudayaraj et al., 2001; Stuart, 2004)
700-687	Olefinic *cis*-CH/phenolic OH out-of-plane bending	(Shurvell, 2006)
675-642	Acetylenic C=CH bending	(Coates, 2006)

2.6 Discussion

In this work, we investigated the stability of biomolecules in the black fungus *C. antarcticus* after exposure to the ground-based simulations performed in preparation for the space exposure BIOMEX project and in support of the biosignature detection method planned for the explorative mission on Mars. The search for life on Mars is necessarily informed by terrestrial biomolecules, the only form of life that we know; furthermore, it is reasonable that life on Mars could be related to life on Earth due to the massive meteoritic exchange between Earth and Mars (Melosh, 1988; Gladman et al., 1996; Mileikowsky et al., 2000). In addition, several papers have demonstrated that terrestrial life, if it landed on Mars, would be able to resist and live on Mars when protected by regolith from the harsh radiation environment of the Martian surface.

A prime consideration for the detection of organic biosignatures on Mars is their long-term preservation on the surface, where the presence of UV and ionising radiation is one of the main damaging factors. Although the preservation of complex organic molecules in the shallow subsurface (~10 cm) of Martian rocks drops 1000-fold due to ionising radiation (Pavlov et al., 2012), there are recent indications that the rapid burial of organic molecules, short surface exposures thanks to slower weathering rates, and the characteristics of certain mineral depositions are key factors enhancing biosignature preservation in the subsurface of Mars (Hays et al., 2017; Williams et al., 2020). Therefore, we exposed dried fungal colonies, once grown on Martian rock analogues, to increasing doses of Mars-relevant polychromatic UV irradiation (200–400 nm) up to 5.5×10^5 kJ/m^2, which simulates 369.87 days on the Martian surface (Cockell et al., 2000). Here, we investigate the stability of the fungus itself and its related biomolecules in relation to the potential detectability of Martian biosignatures.

C. antarcticus DNA was showed to be resistant to the increasing UV doses, since its detection and amplification was achieved in all samples, even in those highly irradiated (5.5×10^5 kJ/m^2) and using very low DNA concentrations (0.018 ng/µL) (**Figure 7**). Although further data are required to confirm any potential role of the different substrates in providing protection against UV radiation, greater damages were reported for samples grown on Martian analogues. Although nucleic acids are organic compounds that are highly sensitive to degradation over geological timescales (Aerts et al., 2014) and their preservation may be precluded (National Academies of Sciences, 2018), labile/polar compounds of these types are utile to assessing whether life processes are currently active, or were active in recent geological times (Simoneit et al., 1998; Summons et al., 2011). Hence, we corroborate the possibility of using DNA as a potential biosignature in the search for extant or recently extinct life forms on Mars, considering its

unambiguous biological origin. Since the Viking missions in the 1970s, nucleic acid detection instruments have not been included onboard life detection rovers; however, the miniaturisation of PCR devices could allow their integration in future missions. Indeed, the development of, e.g., the MinION device (Oxford Nanopore Technologies), a portable nanopore real-time sequencer that requires just small DNA or RNA amounts, would enable the clear detection of signs of life (Maggiori et al., 2020).

Among the other potential biosignatures investigated, we have focused on melanin pigments (present in all domains of terrestrial life) as they belong to those biomolecule classes (i.e., lipids and biopolymers) that exhibit the highest molecular stability and potential preservation among all organic compounds on Earth, i.e., over timescales of billions of years (Simoneit et al., 1998; Engel and Macko, 2013), while also being abundant in *C. antarcticus* cell walls (Selbmann et al., 2005) and well-known to be involved in photoprotection (Culka et al., 2017; Pacelli et al., 2017; Pacelli et al., 2020a). We used three different approaches to detect the pigments: (i) UV-Vis spectrophotometry; (ii) Raman spectroscopy; (iii) FT-IR spectroscopy.

(i) Since dark melanin pigments act as a blackbody, they absorb radiation at all visible wavelengths; the percentage of absorption is generally greater in the UV region and decreases progressively as the wavelength is increased to the far-red region (Bell and Wheeler, 1986). The UV-Vis results of the purified pigments reported the typical spectral profile of fungal melanins (Suryanarayanan et al., 2004; Meeßen et al., 2013; Pal et al., 2014; Raman and Ramasamy, 2017) in the OS, P-MRS, and S-MRS spectra of all three irradiation treatments (**Figure 8**), showing the maximum absorbance peak at around 230 nm (**Table 2**). The greater absorption in the UV region is a property of aromatic organic compounds (Yuan et al., 2007), and this absorbance peak suggests the detectability of melanin only: if proteins and nucleic acids were present, the peak would be shifted to the wavelength region between 250 and 320 nm (Mach et al., 1995).

Melanin has been proven to be well detectable and quantifiable. Nevertheless, it has been noted that the P-MRS analogue, because it contains phyllosilicatic minerals or clays, presents high adsorption/absorption properties, with respect to the other substrates. It is likely that some minerals were still present in the purified melanin pigments interfering with the UV-Vis analysis, as reported in Pacelli et al. (2020a); the presence of minerals may have altered melanin absorbance values at 650 nm, thus explaining the unusual spectral profile with a second large peak around 245 nm. In the context of searching for traces of extinct or extant life on Mars, the melanin concentration results from both P-MRS and S-MRS samples (**Table 2**) led us to assume that, although the estimation of melanin concentration from fungal colonies in Martian analogue regolith can be altered by the presence of the soil itself, it is still possible to clearly detect the

absorbance of purified melanin pigments, even with the presence of mineral compounds and in irradiated samples (up to 5.5×10^5 kJ/m^2).

(ii) The UV-Vis results of melanin pigment identification are supported by data from Raman and FT-IR analyses (**Figure 9**, **Figure 10**). The sample spectra clearly show the presence of unaltered melanin pigments, even in samples exposed at a dose of 5.5×10^5 kJ/m^2. The specific peaks' positions, and the presence of the intermediate peak at 1425 cm^{-1}, allow us to discriminate melanin pigments from organic or inorganic carbon, which have similar features in the Raman spectrum, according to our previous study (Pacelli et al., 2021). Neither the UV irradiation treatment nor dried conditions altered the melanin spectral properties, and thus melanin was successfully detected in all samples. Previous works have reported the degradative effect of UV and ionising radiation on photosynthetic pigments (e.g., carotenoids), with the significant diminishment of spectral peak intensity and fluorescence (Dartnell et al., 2011; Dartnell et al., 2012; Baqué et al., 2018). Our results show the absence of the phenomenon on melanin pigments, demonstrating a successful detection even in samples irradiated with high UV doses (i.e., 5.5×10^5 kJ/m^2). This corroborates the initial proposal of using melanin as a potential biosignature due to its remarkable detectability in highly UV-irradiated environments.

(iii) Considering that two IR instruments are included in the ExoMars payloads (Bibring et al., 2017; De Sanctis et al., 2017; Rull et al., 2017; Vago et al., 2017), along with a Raman Laser Spectrometer, it is important to study biomolecules with a spectroscopic approach. FT-IR spectroscopy is an absorption-based optical analytical technique. The major benefits of using FT-IR imaging over traditional methods are that it is non-disruptive, label-free, and requires a very limited number of samples. Through the acquisition of a biochemical fingerprint, FT-IR can provide information about the content, structure, and chemical modification of major biomolecules present in the investigated sample (Kendall et al., 2009). Raman and FT-IR spectroscopies are related techniques with respective complementary spectra (McCreery, 2000). The synergy of both techniques is a powerful tool when performing organic and inorganic compound characterisation.

The results obtained by FT-IR spectroscopy reveal the presence of some main functional groups in all EVT2 spectra (**Figure 10**), and their presence was related to common organic compounds (**Table 3**). For instance, the ubiquitous presence of peaks at 3461–3372 cm^{-1}, 2931–2926 cm^{-1}, 2858–2851 cm^{-1}, and 1669–1632 cm^{-1}, along with the narrow one at 1061–1018 cm^{-1}, is related to *C. antarcticus*' melanin pigments (Pacelli et al., 2020b). In particular, peaks at 3461–3372 cm^{-1} and 1669–1632 cm^{-1} are generally attributed to melanin pigments (Bonner and Duncan, 1962; Kannan and Ganjewala, 2009; Magarelli et al., 2010; Sajjan et al., 2010), while additional

peaks at 2931–2926 cm^{-1}, 2858–2851 cm^{-1} and 1061–1018 cm^{-1} are typically attributed to fungal melanins (Paim et al., 1990; Pal et al., 2014; Sun et al., 2016; Raman and Ramasamy, 2017). Besides this, the peaks observed in the fingerprint region of all spectra could eventually be identified as phenolic compounds, whose presence could be correlated to that of fungal melanins or other secondary metabolites (Schulz and Baranska, 2007; Centeno and Shamir, 2008).

As for the detection of fungal biomolecules other than melanin pigments, many narrow peaks between 1254 and 1018 cm^{-1} related to carbohydrates as well as to amino and phosphate compounds could be associated with polysaccharides of the fungal cell wall (e.g., chitosan, β-glucan, mannan, etc.) (Maquelin et al., 2006; Salman et al., 2014; Forfang et al., 2017; Kosa et al., 2017). Furthermore, the peaks observed in relation to the amide I band (1669-1632 cm^{-1}), the CH2 bending signal (1462–1445 cm^{-1}), and CO stretching (1164–1158 cm^{-1}) suggest the detection of chitin-characteristic vibrations (Rinaudo, 2006; Ivshin et al., 2007; Salman et al., 2014; Forfang et al., 2017). To conclude, the FT-IR results confirm the presence of melanin pigments in all EVT2 samples; this evidence corroborates the suggestion of using the biomolecule as a biosignature, since it is highly detectable via different analytical techniques. Furthermore, all these results show the importance of using multiple and interconnected analytical techniques in the search for life, since they can provide complementary and useful information for detecting and characterising biosignatures.

Moreover, our outcomes have identified chitin, the main component of the fungal cell wall, as a resistant biomolecule to UV irradiation. So far, it has also been reported in the context of the BIOMEX experiments via Raman analysis of *Circinaria gyrosa*'s fungal symbiont (Böttger et al., 2014). Chitin is known as one of the few biosignatures specific to fungi, and it has been reported in organically preserved fossils (Briggs and Summons, 2014). Nevertheless, the detection of chitin in geological materials is a difficult task: its occurrence in 25-million-year-old fossils has shown that the primary criterion for chitin preservation is not geological time, but rather the conditions of the depositional environment and the absence of diagenetic processes, such as alteration and decomposition (Ivarsson et al., 2011). Following the previous interpretation of FTIR results, we consider the possibility of using chitin as a potential, stable biosignature, since it is detectable in fungal samples even after exposure to high UV irradiation (i.e., 5.5×10^5 kJ/m^2 dose) and is intrinsically related to terrestrial life.

2.7 Conclusions

In the light of previous investigations (Culka et al., 2017; Pacelli et al., 2017; Pacelli et al., 2020a; Pacelli et al., 2020b), we confirm the potential of using melanin pigments as a possible biosignature, and propose the further study of the chitin molecule as a possible new one, because both are highly stable biosynthesised molecules that could still be detected if exposed to extreme UV radiation – an extreme environmental condition that normally occurs on the Martian surface. Even if the Martian subsurface offers protection against solar UV radiation and those oxidising conditions found at the surface (only a few millimetres of dust coverage is required to shield against harmful UV radiation for survivable durations, in contrast to shorter-wavelength ionising radiation that could penetrate up to 1.5 m beneath the surface) (Cockell and Raven, 2004), this work addresses the case of recently surface-exposed rocks, where the photolytic destruction of organic compounds can rapidly occur. Therefore, this work can help broaden our knowledge on those terrestrial biomolecules that could be searched for in upcoming life detection missions.

2.8 Acknowledgments

This work was supported by the Italian Space Agency (BIOMEX MicroColonial Fungi-Experiment on ISS for tracking biomarkers on Martian and lunar rock analogues – ASI grant no. 2013-063-R.0, BioSigN MicroFossils – ASI grant no. 2018-6- U.0.). The Italian National Antarctic Research Program (PNRA) and the Italian National Antarctic Museum ‘Felice Ippolito’ (MNA) are also acknowledged for funding the collection of MNA-CCFEE Antarctic samples. M.B. acknowledges the support of the Deutsche Forschungsgemeinschaft (DFG – German Research Foundation) for the project ‘Raman Biosignatures for Astrobiology Research’ (RaBioFAM; project number: 426601242).

2.9 References

Aerts, J.W., Roling, W.F., Elsaesser, A., and Ehrenfreund, P. (2014) Biota and biomolecules in extreme environments on Earth: Implications for life detection on Mars. *Life* **4**: 535-565.

Baqué, M., Hanke, F., Böttger, U., Leya, T., Moeller, R., and de Vera, J.-P. (2018) Protection of cyanobacterial carotenoids' Raman signatures by Martian mineral analogues after high-dose gamma irradiation. *J Raman Spectrosc* **49**: 1617-1627.

Bell, A.A., and Wheeler, M.H. (1986) Biosynthesis and functions of fungal melanins. *Ann Rev Phytopathol* **24**: 411-451.

Bibring, J.-P., Hamm, V., Pilorget, C., Vago, J.L., and the MicrOmega, T. (2017) The MicrOmega investigation onboard ExoMars. *Astrobiology* **17**: 621-626.

Bonner, T.G., and Duncan, A. (1962) Infra-red spectra of some melanins. *Nature* **194**: 1078-1079.

Böttger, U., de Vera, J.P., Fritz, J., Weber, I., Hübers, H., and Schulze-Makuch, D. (2012) Optimizing the detection of carotene in cyanobacteria in a Martian regolith analogue with a Raman spectrometer for the ExoMars mission. *Planet Space Sci* **60**: 356-362.

Böttger, U., Hübers, H.W., Martinez-Frias, J., Meessen, J., Rull, F., Sánchez, F.J. et al. (2014) Raman spectroscopic analysis of the calcium oxalate producing extremotolerant lichen *Circinaria gyrosa*. *Int J Astrobiology* **13**: 19-27.

Briggs, D.E.G., and Summons, R.E. (2014) Ancient biomolecules: their origins, fossilization, and role in revealing the history of life. *BioEssays* **36**: 482-490.

Carrier, B.L., and Kounaves, S.P. (2015) The origins of perchlorate in the Martian soil. *Geophys Res Lett* **42**: 3739-3745.

Centeno, S.A., and Shamir, J. (2008) Surface enhanced Raman scattering (SERS) and FTIR characterization of the sepia melanin pigment used in works of art. *J Mol Struct* **873**: 149-159.

Coates, J. (2006) Interpretation of infrared spectra, a practical approach. In *Encyclopedia of Analytical Chemistry*. Meyers, R.A. (ed). Chichester: John Wiley & Sons Ltd, pp. 10815-10837.

Cockell, C.S., and Knowland, J. (1999) Ultraviolet radiation screening compounds. *Biol Rev* **74**: 311-345.

Cockell, C.S., and Raven, J.A. (2004) Zones of photosynthetic potential on Mars and the early Earth. *Icarus* **169**: 300-310.

Cockell, C.S., Schuerger, A.C., Billi, D., Friedmann, E.I., and Panitz, C. (2005) Effects of a simulated Martian UV flux on the cyanobacterium, *Chroococcidiopsis* sp. 029. *Astrobiology* **5**: 127-140.

Cockell, C.S., Catling, D.C., Davis, W.L., Snook, K., Kepner, R.L., Lee, P., and McKay, C.P. (2000) The ultraviolet environment of Mars: biological implications past, present, and future. *Icarus* **146**: 343-359.

Culka, A., Jehlička, J., Ascaso, C., Artieda, O., Casero, C.M., and Wierzchos, J. (2017) Raman microspectrometric study of pigments in melanized fungi from the hyperarid Atacama desert gypsum crust. *J Raman Spectrosc* **48**: 1487-1493.

Dartnell, L.R., and Patel, M.R. (2014) Degradation of microbial fluorescence biosignatures by solar ultraviolet radiation on Mars. *Int J Astrobiology* **13**: 112-123.

Dartnell, L.R., Patel, M.R., Storrie-Lombardi, M.C., Ward, J.M., and Muller, J.-P. (2012) Experimental determination of photostability and fluorescence-based detection of PAHs on the Martian surface. *Meteorit Planet Sci* **47**: 806-819.

Dartnell, L.R., Storrie-Lombardi, M.C., Mullineaux, C.W., Ruban, A.V., Wright, G., Griffiths, A.D. et al. (2011) Degradation of cyanobacterial biosignatures by ionizing radiation. *Astrobiology* **11**: 997-1016.

De Gussem, K., Vandenabeele, P., Verbeken, A., and Moens, L. (2005) Raman spectroscopic study of *Lactarius* spores (Russulales, Fungi). *Spectrochim Acta A Mol Biomol Spectrosc* **61**: 2896-2908.

De Sanctis, M.C., Altieri, F., Ammannito, E., Biondi, D., De Angelis, S., Meini, M. et al. (2017) Ma_MISS on ExoMars: mineralogical characterization of the Martian subsurface. *Astrobiology* **17**: 612-620.

de Vera, J.P., Alawi, M., Backhaus, T., Baqué, M., Billi, D., Böttger, U. et al. (2019) Limits of life and the habitability of Mars: the ESA space experiment BIOMEX on the ISS. *Astrobiology* **19**: 145-157.

Encrenaz, T., Greathouse, T.K., Lefèvre, F., and Atreya, S.K. (2012) Hydrogen peroxide on Mars: Observations, interpretation and future plans. *Planet Space Sci* **68**: 3-17.

Engel, M.H., and Macko, S.A. (eds) (2013) *Organic Geochemistry: Principles and Applications*. New York, NY: Springer.

Forfang, K., Zimmermann, B., Kosa, G., Kohler, A., and Shapaval, V. (2017) FTIR spectroscopy for evaluation and monitoring of lipid extraction efficiency for oleaginous fungi. *PLoS One* **12**.

Friedmann, E.I., and Ocampo-Friedmann, R. (1984) The Antarctic cryptoendolithic ecosystem: Relevance to exobiology. *Origins Life Evol Biosphere* **14**: 771-776.

Gladman, B.J., Burns, J.A., Duncan, M., Lee, P., and Levison, H.F. (1996) The exchange of impact ejecta between terrestrial planets. *Science* **271**: 1387-1392.

Glavin, D.P., Freissinet, C., Miller, K.E., Eigenbrode, J.L., Brunner, A.E., Buch, A. et al. (2013) Evidence for perchlorates and the origin of chlorinated hydrocarbons detected by SAM at the Rocknest aeolian deposit in Gale Crater. *J Geophys Res Planets* **118**: 1955-1973.

Gómez-Elvira, J., Armiens, C., Carrasco, I., Genzer, M., Gómez, F., Haberle, R. et al. (2014) Curiosity's rover environmental monitoring station: Overview of the first 100 sols. *J Geophys Res Planets* **119**: 1680-1688.

Guillén, M.D., and Cabo, N. (1999) Usefulness of the frequency data of the Fourier Transform Infrared spectra to evaluate the degree of oxidation of edible oils. *J Agric Food Chem* **47**: 709-719.

Hassler, D.M., Zeitlin, C., Wimmer-Schweingruber, R.F., Ehresmann, B., Rafkin, S., Eigenbrode, J.L. et al. (2014) Mars' surface radiation environment measured with the Mars Science Laboratory's Curiosity Rover. *Science* **343**: 1244797.

Hays, L.E., Graham, H.V., Des Marais, D.J., Hausrath, E.M., Horgan, B., McCollom, T.M. et al. (2017) Biosignature preservation and detection in Mars analog environments. *Astrobiology* **17**: 363-400.

Hopple, J.S., and Vilgalys, R. (1999) Phylogenetic relationships in the mushroom genus *Coprinus* and dark-spored allies based on sequence data from the nuclear gene coding for the Large Ribosomal Subunit RNA: divergent domains, outgroups, and monophyly. *Mol Phylogenet Evol* **13**: 1-19.

Hou, R., Liu, X., Xiang, K., Chen, L., Wu, X., Lin, W. et al. (2019) Characterization of the physicochemical properties and extraction optimization of natural melanin from *Inonotus hispidus* mushroom. *Food Chem* **277**: 533-542.

Huang, Z., Lui, H., Chen, M., Alajlan, A., McLean, D., and Zeng, H. (2004) Raman spectroscopy of *in vivo* cutaneous melanin. *J Biomed Opt* **9**.

Irudayaraj, J., Sivakesava, S., Kamath, S., and Yang, H. (2001) Monitoring chemical changes in some foods using Fourier Transform Photoacoustic Spectroscopy. *J Food Sci* **66**: 1416-1421.

Ivarsson, M., Broman, C., Holmström, S.J.M., Ahlbom, M., Lindblom, S., and Holm, N.G. (2011) Putative fossilized fungi from the lithified volcaniclastic apron of Gran Canaria, Spain. *Astrobiology* **11**: 633-650.

Ivshin, V.P., Artamonova, S.D., Ivshina, T.N., and Sharnina, F.F. (2007) Methods for isolation of chitin-glucan complexes from higher fungi native biomass. *Polym Sci Ser B* **49**: 305-310.

Jones, R.A. (1970) Physicochemical Properties of Pyrroles. In *Advances in Heterocyclic Chemistry*. Katritzky, A.R., and Boulton, A.J. (eds): Academic Press, pp. 383-472.

Kannan, P., and Ganjewala, D. (2009) Preliminary characterization of melanin isolated from fruits and seeds of *Nyctanthes arbor-tristis*. *J Sci Res* **1**: 655-661.

Kendall, C., Isabelle, M., Bazant-Hegemark, F., Hutchings, J., Orr, L., Babrah, J. et al. (2009) Vibrational spectroscopy: a clinical tool for cancer diagnostics. *Analyst* **134**: 1029-1045.

Kinch, K.M., Madsen, M.B., Bell, J.F., Maki, J.N., Bailey, Z.J., Hayes, A.G. et al. (2020) Radiometric calibration targets for the Mastcam-Z camera on the Mars 2020 rover mission. *Space Sci Rev* **216**: 141.

Kosa, G., Kohler, A., Tafintseva, V., Zimmermann, B., Forfang, K., Afseth, N.K. et al. (2017) Microtiter plate cultivation of oleaginous fungi and monitoring of lipogenesis by high-throughput FTIR spectroscopy. *Microb Cell Fact* **16**: 101.

Kuhn, W.R., and Atreya, S.K. (1979) Solar radiation incident on the Martian surface. *J Mol Evol* **14**: 57-64.

Lopez-Reyes, G., Pilorget, C., Moral, A.G., Manrique, J.A., Sanz, A., Berrocal, A. et al. (2020) Raman Laser Spectrometer (RLS) calibration target design to allow onboard combined science between the RLS and MicrOmega instruments on the ExoMars rover. *J Raman Spectrosc* **51**: 1718-1730.

Mach, H., Volkin, D.B., Burke, C.J., and Russell Middaugh, C. (1995) Ultraviolet absorption spectroscopy. In *Protein stability and folding: theory and practice*. Shirley, B.A. (ed). Totowa, NJ: Humana Press, pp. 91-114.

Magarelli, M., Passamonti, P., and Renieri, C. (2010) Purification, characterization and analysis of sepia melanin from commercial sepia ink (*Sepia officinalis*). *CES Med Vet Zootec* **5**: 18-28.

Maggiori, C., Stromberg, J., Blanco, Y., Goordial, J., Cloutis, E., García-Villadangos, M. et al. (2020) The limits, capabilities, and potential for life detection with MinION sequencing in a paleochannel Mars analog. *Astrobiology* **20**: 375-393.

Maquelin, K., Choo-Smith, L., Kirschner, C., Ngo-Thi, N.A., Naumann, D., and Puppels, G.J. (2006) Vibrational spectroscopic studies of microorganisms. In *Handbook of vibrational spectroscopy*. Chalmers, J.M., and Griffiths, P.R. (eds): John Wiley & Sons, Ltd.

McCreery, R.L. (2000) Raman spectroscopy for chemical analysis. In *Chemical analysis*. Winefordner, J.D. (ed): John Wiley & Sons, Inc.

Meeßen, J., Sánchez, F.J., Sadowsky, A., de la Torre, R., Ott, S., and de Vera, J.P. (2013) Extremotolerance and resistance of lichens: Comparative studies on five species used in astrobiological research II. Secondary lichen compounds. *Orig Life Evol Biosph* **43**: 501-526.

Melosh, H.J. (1988) The rocky road to panspermia. *Nature* **332**: 687-688.

Menges, F. (2019). Spectragryph—Optical Spectroscopy Software. Version 1.2.14. Available at https://www.effemm2.de/spectragryph/ (accessed on 7 February 2020).

Mileikowsky, C., Cucinotta, F.A., Wilson, J.W., Gladman, B., Horneck, G., Lindegren, L. et al. (2000) Natural transfer of viable microbes in space: 1. From Mars to Earth and Earth to Mars. *Icarus* **145**: 391-427.

Ming, D.W., Archer, P.D., Glavin, D.P., Eigenbrode, J.L., Franz, H.B., Sutter, B. et al. (2014) Volatile and organic compositions of sedimentary rocks in Yellowknife Bay, Gale Crater, Mars. *Science* **343**: 1245267.

Moores, J.E., Smith, P.H., Tanner, R., Schuerger, A.C., and Venkateswaran, K.J. (2007) The shielding effect of small-scale martian surface geometry on ultraviolet flux. *Icarus* **192**: 417-433.

Movasaghi, Z., Rehman, S., and Rehman, I.U. (2007) Raman spectroscopy of biological tissues. *Appl Spectrosc Rev* **42**: 493-541.

Movasaghi, Z., Rehman, S., and Rehman, I.U. (2008) Fourier Transform Infrared (FTIR) spectroscopy of biological tissues. *Appl Spectrosc Rev* **43**: 134-179.

National Academies of Sciences, Engineering, Medicine (2018) *An astrobiology strategy for the search for life in the universe*. Washington, DC: National Academies Press.

Pacelli, C., Bryan, R.A., Onofri, S., Selbmann, L., Shuryak, I., and Dadachova, E. (2017) Melanin is effective in protecting fast and slow growing fungi from various types of ionizing radiation. *Environ Microbiol* **19**: 1612-1624.

Pacelli, C., Cassaro, A., Aureli, L., Moeller, R., Fujimori, A., and Onofri, S. (2020a) The responses of the black fungus *Cryomyces antarcticus* to high doses of accelerated helium ions radiation within Martian regolith simulants and their relevance for Mars. *Life* **10**: 130.

Pacelli, C., Cassaro, A., Maturilli, A., Timperio, A.M., Gevi, F., Cavalazzi, B. et al. (2020b) Multidisciplinary characterization of melanin pigments from the black fungus *Cryomyces antarcticus*. *Appl Microbiol Biotechnol* **104**: 6385-6395.

Pacelli, C., Cassaro, A., Baqué, M., Selbmann, L., Zucconi, L., Maturilli, A. et al. (2021) Fungal biomarkers are detectable in Martian rock-analogues after space exposure: implications for the search of life on Mars. *Int J Astrobiology* **20**: 345-358.

Paim, S., Linhares, L.F., Mangrich, A.S., and Martin, J.P. (1990) Characterization of fungal melanins and soil humic acids by chemical analysis and infrared spectroscopy. *Biol Fertil Soils* **10**: 72-76.

Pal, A.K., Gajjar, D.U., and Vasavada, A.R. (2014) DOPA and DHN pathway orchestrate melanin synthesis in *Aspergillus* species. *Med Mycol* **52**: 10-18.

Patel, M.R., Zarnecki, J.C., and Catling, D.C. (2002) Ultraviolet radiation on the surface of Mars and the Beagle 2 UV sensor. *Planet Space Sci* **50**: 915-927.

Patel, M.R., Bérces, A., Kolb, C., Lammer, H., Rettberg, P., Zarnecki, J.C., and Selsis, F. (2003) Seasonal and diurnal variations in Martian surface ultraviolet irradiation: biological and chemical implications for the Martian regolith. *Int J Astrobiology* **2**: 21-34.

Pavlov, A.A., Vasilyev, G., Ostryakov, V.M., Pavlov, A.K., and Mahaffy, P. (2012) Degradation of the organic molecules in the shallow subsurface of Mars due to irradiation by cosmic rays. *Geophys Res Lett* **39**.

Poch, O., Noblet, A., Stalport, F., Correia, J.J., Grand, N., Szopa, C., and Coll, P. (2013) Chemical evolution of organic molecules under Mars-like UV radiation conditions simulated in the laboratory with the "Mars organic molecule irradiation and evolution" (MOMIE) setup. *Planet Space Sci* **85**: 188-197.

Quinn, R.C., Martucci, H.F.H., Miller, S.R., Bryson, C.E., Grunthaner, F.J., and Grunthaner, P.J. (2013) Perchlorate radiolysis on Mars and the origin of Martian soil reactivity. *Astrobiology* **13**: 515-520.

R Core Team (2018). R: A Language and Environment for Statistical Computing. Version 3.5.2. Vienna, Austria: R Foundation for Statistical Computing. Available at https://www.r-project.org/ (accessed on 8 August 2019).

Rabbow, E., Rettberg, P., Parpart, A., Panitz, C., Schulte, W., Molter, F. et al. (2017) EXPOSE-R2: The astrobiological ESA mission on board of the International Space Station. *Front Microbiol* **8**: 1533.

Raman, N.M., and Ramasamy, S. (2017) Genetic validation and spectroscopic detailing of DHN-melanin extracted from an environmental fungus. *Biochem Biophys Rep* **12**: 98-107.

Rinaudo, M. (2006) Chitin and chitosan: Properties and applications. *Prog Polym Sci* **31**: 603-632.

Rösch, P., Harz, M., Peschke, K.-D., Ronneberger, O., Burkhardt, H., and Popp, J. (2006) Identification of single eukaryotic cells with micro-Raman spectroscopy. *Biopolymers* **82**: 312-316.

Rothschild, L.J., and Cockell, C.S. (1999) Radiation: microbial evolution, ecology, and relevance to Mars missions. *Mutat Res-Fund Mol M* **430**: 281-291.

RStudio Team (2016). RStudio: Integrated Development for R; Computer Software. Version 1.1.423. Boston, MA, USA: RStudio, PBC. Available at https://posit.co/ (accessed on 8 August 2019).

Rull, F., Maurice, S., Hutchinson, I., Moral, A., Perez, C., Diaz, C. et al. (2017) The Raman Laser Spectrometer for the ExoMars rover mission to Mars. *Astrobiology* **17**: 627-654.

Safar, M., Bertrand, D., Robert, P., Devaux, M.F., and Genot, C. (1994) Characterization of edible oils, butters and margarines by Fourier transform infrared spectroscopy with attenuated total reflectance. *J Am Oil Chem Soc* **71**: 371-377.

Saif, F.A., Yaseen, S.A., Alameen, A.S., Mane, S.B., and Undre, P.B. (2021) Identification and characterization of *Aspergillus* species of fruit rot fungi using microscopy, FT-IR, Raman and UV–Vis spectroscopy. *Spectrochim Acta A Mol Biomol Spectrosc* **246**: 119010.

Sajjan, S., Kulkarni, G., Yaligara, V., Lee, K., and Karegoudar, T. (2010) Purification and physiochemical characterization of melanin pigment from *Klebsiella* sp. GSK. *J Microbiol Biotechnol* **20**: 1513-1520.

Salman, A., Shufan, E., Tsror, L., Moreh, R., Mordechai, S., and Huleihel, M. (2014) Classification of *Colletotrichum coccodes* isolates into vegetative compatibility groups using infrared attenuated total reflectance spectroscopy and multivariate analysis. *Methods* **68**: 325-330.

Samokhvalov, A., Liu, Y., and Simon, J.D. (2004) Characterization of the Fe(III)-binding site in *Sepia* eumelanin by resonance Raman confocal microspectroscopy. *Photochem Photobiol* **80**: 84-88.

Schuerger, A.C., Mancinelli, R.L., Kern, R.G., Rothschild, L.J., and McKay, C.P. (2003) Survival of endospores of *Bacillus subtilis* on spacecraft surfaces under simulated martian environments: implications for the forward contamination of Mars. *Icarus* **165**: 253-276.

Schuerger, A.C., Moores, J.E., Clausen, C.A., Barlow, N.G., and Britt, D.T. (2012) Methane from UV-irradiated carbonaceous chondrites under simulated Martian conditions. *J Geophys Res* **117**.

Schulz, H., and Baranska, M. (2007) Identification and quantification of valuable plant substances by IR and Raman spectroscopy. *Vib Spectrosc* **43**: 13-25.

Selbmann, L., Isola, D., Zucconi, L., and Onofri, S. (2011) Resistance to UV-B induced DNA damage in extreme-tolerant cryptoendolithic Antarctic fungi: detection by PCR assays. *Fungal Biol* **115**: 937-944.

Selbmann, L., de Hoog, G.S., Mazzaglia, A., Friedmann, E.I., and Onofri, S. (2005) Fungi at the edge of life: cryptoendolithic black fungi from Antarctic desert. *Stud Mycol* **51**: 1-32.

Shurvell, H.F. (2006) Spectra–structure correlations in the mid- and far-infrared. In *Handbook of vibrational spectroscopy*: John Wiley & Sons, Ltd.

Simoneit, B.R.T., Summons, R.E., and Jahnke, L.L. (1998) Biomarkers as tracers for life on early Earth and Mars. *Orig Life Evol Biosph* **28**: 475-483.

Stalport, F., Coll, P., Szopa, C., Cottin, H., and Raulin, F. (2009) Investigating the photostability of carboxylic acids exposed to Mars surface ultraviolet radiation conditions. *Astrobiology* **9**: 543-549.

Stuart, B.H. (2004) *Infrared spectroscopy: fundamentals and applications*: John Wiley & Sons, Ltd.

Summons, R.E., Amend, J.P., Bish, D., Buick, R., Cody, G.D., Des Marais, D.J. et al. (2011) Preservation of Martian organic and environmental records: final report of the Mars biosignature working group. *Astrobiology* **11**: 157-181.

Sun, S., Zhang, X., Sun, S., Zhang, L., Shan, S., and Zhu, H. (2016) Production of natural melanin by *Auricularia auricula* and study on its molecular structure. *Food Chem* **190**: 801-807.

Suryanarayanan, T.S., Ravishankar, J.P., Venkatesan, G., and Murali, T.S. (2004) Characterization of the melanin pigment of a cosmopolitan fungal endophyte. *Mycol Res* **108**: 974-978.

Vago, J.L., Westall, F., Pasteur Instrument Teams, L.S.S.W.G., Other, C., Coates, A.J., Jaumann, R. et al. (2017) Habitability on early Mars and the search for biosignatures with the ExoMars rover. *Astrobiology* **17**: 471-510.

Vilgalys, R., and Hester, M. (1990) Rapid genetic identification and mapping of enzymatically amplified ribosomal DNA from several *Cryptococcus* species. *J Bacteriol* **172**: 4238-4246.

Williams, A.J., Craft, K.L., Millan, M., Johnson, S.S., Knudson, C.A., Juarez Rivera, M. et al. (2020) Fatty acid preservation in modern and relict hot-spring deposits in Iceland, with implications for organics detection on Mars. *Astrobiology* **21**: 60-82.

Yuan, W., Burleigh, S.H., and Dawson, J.O. (2007) Melanin biosynthesis by *Frankia* strain CeI5. *Physiol Plant* **131**: 180-190.

Chapter 3

Deletion of the polyketide synthase-encoding gene *pks1* prevents melanisation in the extremophilic fungus *Cryomyces antarcticus*

Ilaria Catanzaro [1,2], Ruben Gerrits [1], Ines Feldmann [1], Anna A. Gorbushina [1,3], Silvano Onofri [2], and Julia Schumacher [1,3] *

[1] Bundesanstalt für Materialforschung und -prüfung (BAM), Berlin, Germany

[2] Università degli Studi della Tuscia, Viterbo, Italy

[3] Freie Universität Berlin, Germany

Under publication in *IUBMB Life*. DOI: 10.1002/iub.2895

3.1 Author contributions

Conceptualization: S.O.; Methodology: A.A.G., J.S.; Validation: **I.C.**, J.S.; Formal analysis: **I.C.**, R.G., I.F., J.S.; Investigation: **I.C.**, J.S.; Resources: A.A.G., S.O.; Writing – original draft preparation: **I.C.**, J.S.; Writing – review and editing: **I.C.**, R.G., I.F., A.A.G., S.O., J.S.; Visualization: **I.C.**, R.G., J.S.; Supervision: S.O., J.S.; Project administration: **I.C.**, S.O.; Funding acquisition: A.A.G., S.O.

3.2 Abstract

Cryomyces antarcticus, a melanised cryptoendolithic fungus endemic to Antarctica, can tolerate environmental conditions as severe as those in space. Particularly, its ability to withstand ionising radiation has been attributed to the presence of thick and highly melanised cell walls, which – according to a previous investigation – may contain both 1,8-dihydroxynaphthalene (DHN) and L-3,4 dihydroxyphenylalanine (L-DOPA) melanin. The genes putatively involved in the synthesis of DHN melanin were identified in the genome of *C. antarcticus.* Most important is *capks1* encoding a non-reducing polyketide synthase (PKS) and being the ortholog of the functionally characterised *kppks1* from the rock-inhabiting fungus *Knufia petricola*. The co-expression of CaPKS1 or KpPKS1 with a 4'-phosphopantetheinyl transferase in *Saccharomyces cerevisiae* resulted in the formation of a yellowish pigment, suggesting that CaPKS1 is the enzyme providing the precursor for DHN melanin. To dissect the composition and function of the melanin layer in the outer cell wall of *C. antarcticus*, non-melanised mutants were generated by CRISPR/Cas9-mediated genome editing. Notwithstanding its slow growth (up to months), three independent non-melanised Δ*capks1* mutants were obtained. The mutants exhibited growth similar to the wild type and a light pinkish pigmentation, which is presumably due to carotenoids. Interestingly, visible light had an adverse effect on growth of both melanised wild type and non-melanised Δ*capks1* strains. Further evidence that light can pass the melanised cell walls derives from a mutant expressing a H2B-GFP fusion protein which can be detected by fluorescence microscopy. In conclusion, the study reports the first genetic manipulation of *C. antarcticus*, resulting in non-melanised mutants and demonstrating that the melanin is rather of the DHN type. These mutants will allow to elucidate the relevance of melanisation for surviving extreme conditions found in the natural habitat as well as in space.

Key words: black fungi, cryptoendolithism, DHN melanin, carotenoids, CRISPR/Cas9, astrobiology, stress tolerance

3.3 Introduction

Cryomyces antarcticus (class Dothideomycetes) is a cryptoendolithic black fungus endemic to Antarctica (Selbmann et al., 2005; Selbmann et al., 2013). In addition to displaying morpho-physiological traits shared among microcolonial fungi, *C. antarcticus* exhibits an extremely slow meristematic growth – an isodiametric cellular expansion optimising the surface/volume ratio and a stable character of psychrophilic fungi even under optimal culture conditions (Gostinčar et al., 2022). Isolated from sandstone sampled at Linnaeus Terrace (McMurdo Dry Valleys, Southern Victoria Land), the fungus has been preserved in the National Antarctic Museum - Culture Collection of Fungi from Extreme Environments (MNA-CCFEE) at the University of Tuscia in Viterbo, Italy (Onofri et al., 2020).

Since the discovery of black fungi within cryptoendolithic microbial communities in Antarctic rocks (Friedmann et al., 1988), large attention has been directed towards the fungi due to their distinctive adaptations to extreme environmental conditions (Onofri et al., 2007). *C. antarcticus* strain MNA-CCFEE 515 has been particularly studied under a variety of conditions, from those typical of its habitat (e.g., severe thermal fluctuations, intense UV-B irradiation), to the more exotic found in space or extraplanetary environments (e.g., vacuum, ionising radiation) (Onofri et al., 2020). Its remarkable ability to thrive in such diverse extreme conditions has been ascribed to its unique morpho-physiological adaptations (Selbmann et al., 2015), specifically melanin cross-linked to the thick cell walls (Gessler et al., 2014), rather than to a robust DNA repair system (Toreno et al., 2018).

Indeed, fungal melanins contribute to the structural integrity of the cell wall and protection against cellular stress (Gow et al., 2017). These heterogenic macromolecules result from the oxidative polymerisation of phenolic/indolic precursors and are known for their negatively charge and hydrophobic nature (Butler and Day, 1998). Fungi may employ two distinct biosynthetic approaches: the 1,8-dihydroxynaphthalene (DHN) pathway, which entails a polyketide synthase (PKS) catalysing the *de novo* synthesis of phenolic substrates for DHN melanin polymerisation, and the L-3,4 dihydroxyphenylalanine (L-DOPA) pathway, which converts tyrosine or L-DOPA through tyrosinase and laccase activity into dopaquinone for spontaneous DOPA melanin polymerisation (Eisenman and Casadevall, 2012). The former is the prevalent strategy found in Ascomycetes, while the latter appears to be more common in Basidiomycetes and human pathogens (Toledo et al., 2017; Eisenman et al., 2020). An additional dark pigment found in fungi, the water-soluble pyomelanin, lacks its own biosynthesis pathway and derives from polymerisation of an L-tyrosine degradation product (Schmaler-Ripcke et al., 2009; Perez-Cuesta

et al., 2020). Though the tyrosine from primary metabolism can be used for both DOPA melanin and pyomelanin synthesis, fungi usually produce these pigments only when the precursors are exogenously supplied (Smith and Casadevall, 2019).

Investigations into the melanin of *C. antarcticus* have primarily relied on chemical analytical methods (Pacelli et al., 2017a; Pacelli et al., 2020b), without a clear assessment of the genetic basis behind the biosynthesis process. Our objective is to fill this research gap by adopting a genetic engineering approach in *C. antarcticus*. This methodology offers more consistent and reproducible results compared to chemical inhibitors and other destructive techniques (Cao et al., 2021), and allows to study the functions *in vivo*. However, the development of effective molecular tools for meristematic black fungi has traditionally faced challenges compared to filamentous fungi. Their slow-growth and heavy melanisation make them difficult to manipulate genetically. The development of the CRISPR (Clustered Regularly Interspaced Short Palindromic Repeats)/Cas9 (CRISPR-associated protein 9) technology represents the opportunity to establish techniques for targeted genome editing, even in hard-to-reach fungi, as it was recently demonstrated for the rock-inhabiting fungus *Knufia petricola* (Eurotiomycetes/Chaetothyriales) (Voigt et al., 2020). With a relatively faster growth compared to *C. antarcticus*, this fungus displays morpho-physiological traits typical of black fungi (Wollenzien et al., 1997; Nai et al., 2013; Mitchison-Field et al., 2019). The production of DHN melanin, carotenoids, mycosporines, and extracellular polysaccharides (EPS) has been well-characterised (Volkmann and Gorbushina, 2006; Breitenbach et al., 2018; Flieger et al., 2018; Dittrich et al., 2023). Originally isolated from a marble surface in Athens, Greece (Gorbushina et al., 2008), the strain A95 (CBS 123872) serves as model for exploring the lifestyle and physiology of material-colonising black fungi (Knabe and Gorbushina, 2018). The annotated genome sequence and toolkits for genetic engineering and comparative phenotyping (Voigt et al., 2020; Erdmann et al., 2022) supply essential resources for targeted gene knock-out and knock-in approaches and the functional characterisation of the generated strains. For instance, *K. petricola* mutants deficient in the synthesis of DHN melanin, carotenoids or both pigments are used to elucidate their roles in traits such as the dissolution of minerals and penetration of carbonate substrates (Gerrits et al., 2020; Tonon et al., 2020; Breitenbach et al., 2022).

In this work, we made *C. antarcticus* the first Antarctic fungus to undergo genetic engineering, for facilitating the study of the role of its pigments in withstanding extreme natural and extraterrestrial conditions in future investigations. The availability of CRISPR/Cas9 editing techniques, along with previous experiences in transforming *K. petricola*, facilitated the establishment of transformation protocols for *C. antarcticus*. Our approach involved the targeting

of the key enzyme-encoding gene for DHN melanogenesis (*capks1*) and the putative carotenogenic genes (*caphs1*, *caphd1*). It resulted in the successful generation of DHN melanin- and carotenoid-deficient *C. antarcticus* mutants, demonstrating the feasibility of genetically manipulating less amenable fungi.

3.4 Materials and methods

3.4.1 Cultivation of C. antarcticus

C. antarcticus and *K. petricola* strains listed in **Table 4** were cultivated on the standard media used for maintenance of *K. petricola* strains i.e., on malt extract broth/agar [MEB/MEA: 2.0 % malt extract (Carl Roth GmbH + Co. KG), 0.1 % peptone from casein (Carl Roth GmbH + Co. KG), 2.0 % D-glucose, 2.0 % kobe agar (AppliChem GmbH)], a synthetic-defined–nitrate–glucose medium [SDNG: 0.17 % Difco Yeast Nitrogen Base without Amino Acids and Ammonium Sulfate (BD Biosciences), 0.3 % $NaNO_3$, 2.0 % D-glucose, 2.0 % kobe agar], or an additional malt extract agar [MEAV: 3.0 % malt extract (Carl Roth GmbH + Co. KG), 1.5 % bacteriological agar (AppliChem GmbH)]. MEA and SDNG media were supplemented with the selective agents hygromycin B (HYG; AppliChem), nourseothricin (NTC; Werner BioAgents GmbH), geneticin (G418; Sigma-Aldrich), or glufosinate ammonium (GFS; ChemPur) as specified.

C. antarcticus biomass from eight-week-old MEA cultures were homogenised using a Retsch mixer mill (5 min at 30 Hz). Titres of colony forming units (CFU) were determined using a Thoma cell counting chamber and adjusted with 1x phosphate-buffered saline (PBS) to 5×10^6 cells/ml for growth assays and 1×10^6 cells/ml for drop assays. For growth assays, serial dilutions down to 5×10^3 cells/ml were prepared, and 200 µl (1×10^6 to 1×10^3 cells) were evenly distributed with ten glass beads (3-5 mm) on agar, while 100 µl of the highest diluted cell suspension (5×10^2 cells) were used as inoculum per quarter with four-compartment Petri dishes. For drop assays, serial dilutions down to 1×10^3 cells/ml were prepared, and 10 µl (1×10^4 to 1×10^1 cells) were dropped in a grid pattern onto agar. For liquid cultures, 20 ml of MEB were inoculated with 200 µl of homogenised cell suspensions. *K. petricola* strains on solidified media were incubated at 25 °C in the dark, and *C. antarcticus* strains at 15 °C in constant darkness (DD) or in a 12 h light/12 h dark (LD) cycle (Philips F32T8/TL741 cool white, 118 µmol photons/m^2/s).

Table 4. Fungal strains used in this study.

Strain name	GMO ID	Genotype	Reference
***C. antarcticus* MNA-CCFEE 515**		WT	(Selbmann et al., 2005)
Δ*capks1*	CA-0002	515, Δ*pks1* [(T*niaD*::*hph*::P*trpC*)]	This study
Δ*caphs1-phd1*	CA-0017	515, Δ*phs1-phd1* [(T*niaD*::*hph*::P*trpC*)]	This study
h2b-gfp	CA-0021	515, Δ*phs1-phd1* [(T*niaD*::*hph*::P*trpC*)–(P*oliC*::*h2b-gfp*::T*gluc*)]	This study
***K. petricola* A95**		WT	(Nai et al., 2013)
Δ*kpsdh1*	KP-0053	A95, Δ*sdh1* [(T*niaD*::*nat1*::P*trpC*)]	(Voigt et al., 2020)
Δ*kppks1*	KP-0033	A95, Δ*pks1* [(T*niaD*::*nat1*::P*trpC*)]	(Voigt et al., 2020)
kppks1 ^{COMiL}	KP-0505	A95, P*pks1*::[(*pks1*::T*gluc*)-(T*niaD*::*nat1*::P*trpC*)]	This study
***S. cerevisiae* FY834**		*MAT*α *his3-*Δ*200 ura3-52 leu2-*Δ*1 lys2-*Δ*202 trp1-*Δ*63*	(Winston et al., 1995)
control	SC-0271	FY834, p425 GAL1, p426 GAL1	This study
kpppt1	SC-0272	FY834, pLEU-*kpppt1*, p426 GAL1	This study
kppks1	SC-0273	FY834, p425 GAL1, pURA-*kppks1*	This study
kpppt1* + *kppks1	SC-0274	FY834, pLEU-*kpppt1*, pURA-*kppks1*	This study
capks1	SC-0277	FY834, p425 GAL1, pURA-*capks1*	This study
kpppt1* + *capks1	SC-0278	FY834, pLEU-*kpppt1*, pURA-*capks1*	This study

3.4.2 Bioinformatics analyses

C. antarcticus nucleotide and protein sequences of putative melanogenic (**Figure S1**) and carotenogenic genes listed in **Table S1** were extracted from the *C. antarcticus* CBS 116301 v3.0 database (https://mycocosm.jgi.doe.gov/Cryan3) at the Joint Genome Institute. Accession numbers of protein sequences used for sequence comparisons are listed in **Table S2**. For muscle alignments, phylogenetic trees, and the identification of CRISPR sites, the corresponding tools of Geneious Prime 2023.2.1 (Biomatters Ltd.) were used. Conserved protein domains were identified by InterPro (https://www.ebi.ac.uk/interpro) (Paysan-Lafosse et al., 2023). Plasmid maps were generated with SnapGene 4.0.8 (GSL Biotech LLC).

3.4.3 Standard molecular methods

Genomic DNA from *C. antarcticus* was extracted as described previously for *K. petricola* (Voigt et al., 2020). DNA and the 1 kb Plus DNA Ladder (New England Biolabs, NEB), mixed with Midori Green Direct (Biozym Scientific GmbH), were separated in 1 % agarose gels in a Mupid exU gel electrophoresis chamber filled with 0.5 % tris-acetate-EDTA (TAE) buffer and visualised by using a ChemiDoc XRS+ Imager equipped with the Image Lab 6.0.1 software (Bio-

Rad Laboratories Inc.). DNA was amplified with the Q5 High-Fidelity DNA Polymerase (New England Biolabs, NEB) for cloning and transformation, and with the *Taq* DNA Polymerase (NEB) for diagnostic applications. Primers listed in **Table S3** were obtained from Eurofins Genomics. Plasmids listed in **Table S4** were assembled *in vivo* i.e., in *Saccharomyces cerevisiae* FY843 (Schumacher, 2012), or *in-vitro* by using the NEBuilder HiFi DNA Assembly Master Mix (NEB). Plasmid DNA from *Escherichia coli* and *S. cerevisiae* was extracted with the Monarch Plasmid Miniprep Kit (NEB). Larger amounts of plasmid DNA from *E. coli* were extracted with the NucleoBond Xtra Midi Kit (Macherey-Nagel). Sanger sequencing of plasmid DNA was accomplished at Eurofins Genomics.

3.4.4 Gene expression in S. cerevisiae

Vectors for galactose-inducible expression of *kpppt1* (GenBank: MT859418.1), *kppks1* (GenBank: PP374627.1) and *capks1* (Cryan3 scaffold_6:122131-129243) in *S. cerevisiae* (pLEU-*kpppt1*, pURA-*kppks1*, pURA-*capks1*) were assembled *in vivo* using p425 GAL or p426 GAL1 (Mumberg et al., 1994) as entry plasmid, as described in **Figure S2A** and **Table S4**. *S. cerevisiae* FY834 was transformed using the LiAc/single-stranded carrier DNA/PEG method from Gietz and Schiestl (2007). Plasmid-propagating strains (**Table 4**) were maintained on glucose-containing SD medium lacking the respective nutrients. SD/GLU-HLWU medium [2.0 % D-glucose, 0.17 % Difco Yeast Nitrogen Base without Amino Acids and Ammonium Sulfate (BD Biosciences), 0.5 % $(NH_4)_2SO_4$, 0.06 % drop-out supplement –HIS/–LEU/–TRP/–URA (Takara Bio Inc.), 2.0 % kobe agar; pH 5.8] was supplemented with 10 mg/l of histidine, 50 mg/l of tryptophane, 100 mg/l of leucine and/or 50 mg/l of uracil. For induction of gene expression, the strains were cultivated on SD/GAL-LU agar containing 4.0 % D-galactose instead of D-glucose as carbon source at 30 °C in darkness.

3.4.5 Genetic manipulation of C. antarcticus

Procedures for editing the genome of *C. antarcticus* were adopted from those established in *K. petricola* (Noack-Schönmann et al., 2014; Voigt et al., 2020; Erdmann et al., 2022) (**Figure S3**). For introducing double strand breaks (DSBs) in the *gene of interest* (*goi*), target-specific sgRNA and Cas9 were transiently expressed from a circular plasmid. Plasmids coding for Cas9 and one or two sgRNA (pAMA/tRNA-*capks1*^{PS1}-*capks1*^{PS4}, pAMA/tRNA-*caphs1*^{PS1}-*caphd1*^{PS1}, pAMA/tRNA-*hph*^{PS1}, and pAMA/tRNA-*nat1*^{PS1}) were cloned by assembly of

sgRNA/tRNA fragments amplified from pFC902 (Nødvig et al., 2018) in *Pac*I-digested pFC332 (Nødvig et al., 2015) as described in detail in **Table S4**. Linear donor DNA for replacing genes of interest was generated by amplification or by digestion of plasmid DNA. Replacement fragments with 75-bp-long homologous sequences were amplified from pNDH-OGG, pNDN-OGG (Schumacher, 2012) or pNDH-ONGG (Erdmann et al., under review) with primers *goi*-SH5F, *goi*-SH3R/T*gluc-goi*-SH3R as exemplarily shown in **Figure S4**. For reintroduction of genes in replacement mutants into their native genomic loci, the expression constructs with long homologous sequences were isolated with *Swa*I from cloned pN-*capks1* ^{COMIL} and pH-*kppks1* ^{COMIL} (**Table S4**, **Table S5**, **Figure S5**).

Protoplasts of *C. antarcticus* strains were generated by enzymatic digestion of the cell walls (**Figure S3**). For that, 200 to 300 mg of biomass from a four-week-old MEB culture of the *C. antarcticus* strain of interest was washed twice with protoplast buffer (KPB), and then resuspended in 20 ml of protoplast buffer (KPB) containing 40 mg/ml of VinoTaste Pro (Novozymes) and 1 mg/ml of Yatalase (Takara Bio Inc.). Cell wall lysis was performed at 27 °C and 80 rpm overnight. Protoplasts were collected using a 15-µm cell strainer (pluriSelect), followed by centrifugation at 1,000 × g and 4 °C for 5 min. Protoplasts were washed twice with transformation buffer (KTB), and re-suspended in the same buffer at a final concentration of $\geq 3.5 \times 10^6$ protoplasts/ml. 1-4 × 10^6 protoplasts in volumes of 100 to 200 µl were mixed with 40 µg of plasmid DNA and 15-30 µl of donor DNA (resistance cassettes) and transformed in a 1:2:15 volume ratio with 24 % PEG 6000 and liquid transformation medium (KTM).

Transformation reactions were gently distributed over 20 ml of osmotically stabilised MEA (MEAS) for obtaining ~10^6 protoplasts per Petri dish. After incubation for 24 h at 15 °C, the plates were overlaid with 5 ml of KTM top agar supplemented with either 125 µg/ml of HYG (final conc. 25 µg/ml) or 25 µg/ml of NTC (final conc. 5 µg/ml). Putative resistant transformants were transferred to MEA containing equal HYG or NTC concentrations after two to four months. Growing strains were repeatedly transferred to fresh selective MEA, before DNA from chosen transformants was extracted. Homologous recombination (HR) events resulting in the replacement of the gene of interest by a resistance cassette were detected by diagnostic PCR using primers binding in the used resistance cassette (T*niaD*-hiF, *hph*-hiF, *hph*-hiR, *ogfp*-sF1) and the up- and downstream of the targeted gene (*goi*-hi5F, *goi*-hi3R) as specified in **Figure S4**, **Figure S5**, and **Figure S6**.

3.4.6 Microscopic analyses

For scanning electron microscopy (SEM), samples were cut out of solid agar medium covered with either the *C. antarcticus* wild type or the Δ*capks1* mutant (two for each) and prepared according to Spurr (1969). This protocol included a fixation with 2.5 % glutaraldehyde, a wash with PBS and a dehydration using an ethanol dilution series with gradually increasing concentration (i.e., 30 % to 100 %). Afterwards, samples were dried via critical point drying (Leica EM CPD300) and fixed onto SEM sample holders using adhesive carbon tape. After sputter coating with a 30 nm conducting gold layer (EM ACE600), they were analysed by SEM (FEI XL30 ESEM) at the electron microscopy centre at BAM. SEM images were acquired with a secondary electron detector at an accelerating voltage of 20 kV.

For transmission electron microscopy (TEM), *C. antarcticus* wild type and Δ*capks1* colonies were collected in quadruplicates from eight-week-old MEA cultures and prepared according to an optimised protocol (Pacelli et al., 2017c). Sections obtained using the Reichert Ultracut ultramicrotome were stained with uranyl acetate and lead citrate, and image acquisition was performed at the Great Equipment Centre, section of Electron Microscopy of the University of Tuscia, as previously reported (Pacelli et al., 2017b).

For fluorescence microscopy, cells were homogenised using a Retsch mixer mill (5 min at 30 Hz), washed twice with PBS and transferred to microscope slides. For staining the nuclei, cells were resuspended in PBS containing 20 µg/ml of DAPI (4′,6-diamidino-2-phenylindole) (Sigma-Aldrich), incubated for three minutes in the dark at room temperature and washed twice with PBS. DAPI and GFP fluorescence was detected with a Leica SP8 confocal laser scanning microscope using a 100x objective with immersion oil. GFP was exited at 485 nm and the emission was recorded at 530/40 nm using a PMT detector. DAPI was exited at 405 nm and the emission was detected at 460/40 nm using a HyD detector.

3.5 Results and discussion

3.5.1 Identification of the putative DHN melanogenic genes in C. antarcticus

DHN melanin is produced by many Ascomycetes. Filamentous fungi often incorporate DHN melanin in the cell walls of their reproductive structures such as conidiophores and conidia, fruiting bodies and sexual spores or sclerotia, while the vegetive mycelia are often not melanised.

For example, DHN melanogenesis, its regulation and functions have been studied in detail in *Aspergillus fumigatus* (Tsai et al., 1999), *Alternaria alternata* (Gao et al., 2022), *Neurospora crassa* (Ao et al., 2019), and *Botrytis cinerea* (Schumacher, 2016). In contrast, black fungi that reproduce asexually by budding or meristematic growth only, produce the dark pigment constitutively (Gorbushina et al., 2003). The biosynthetic routes for the phenolic precursor DHN are rather conserved (**Figure S1**), though the organisation and regulation of the involved genes differ among species. Not yet well understood is how the DHN is polymerised outside the cell and which chemical structure or modifications the final DHN polymers have. As DHN can be cross-linked with other metabolites and components of the cell wall including chitin, glucan and glycoproteins, the final polymer may have heterogenous compositions.

To identify the putative DHN melanogenic genes in the genome of *C. antarcticus* (**Table S1**), BlastP searches were conducted using the amino acid sequences of the *A. fumigatus* melanogenic enzymes as queries (**Table S2**). Genes for all necessary enzymatic steps were found (**Figure 11A**). This includes a polyketide synthase (PKS1) with a characteristic domains structure (**Figure 12A**) and a phosphopantetheinyl transferase (PPT1), both needed for the formation of the phenolic backbone, and enzymes for converting the intermediates to DHN (YGH1, YGH2, THR1, THR2, SDH1) (**Figure S1**). The sequences of the *C. antarcticus* enzymes were compared with orthologs from DHN melanin-producing fungi of other classes. As expected, the *C. antarcticus* sequences display the highest amino acid identities (51-82 %) with those of *A. alternata* (Dothideomycetes), the closest relative among the four fungi compared. All fungi examined exhibit two THR reductases, except for *A. fumigatus*, which possess only one carrying out both reduction steps in the DHN pathway (Tsai et al., 1999). According to the findings in other fungi where both THN reductases have a redundant function but prefer T4HN or T3HN as substrate (Thompson et al., 2000), *C. antarcticus* THR1 and THR2 may also be redundant exhibiting preference for T4HN and T3HN, respectively.

Best known for their relevance for DHN polymerisation are the two enzymes ABR1 and ABR2, which are encoded by genes in the DHN melanin cluster of *A. fumigatus*. Both are multicopper oxidases (MCO), whose deletions cause altered pigmentation (Tsai et al., 1999). BlastP searches in the database of annotated *C. antarcticus* proteins revealed ten proteins (**Figure 11B**) containing the three characteristic Cu-oxidase domains and the conserved patterns for coordinating the four copper atoms which are characteristic for fungal LCCs (Giardina et al., 2010), namely HxH (L1), HxH (L2), HxxHxH (L3) and HCHxxxHxxxG[M/F/L] (L4). Interestingly, CaMCO8 and CaMCO9 have extended N-terminal regions bearing one and three predicted chitin-binding domains, respectively. N-terminal signal peptides for secretion were predicted for all

C. antarcticus proteins except for CaMCO7. Because of similarity to *A. fumigatus* FetC (62 % aa identity), the characteristic C-terminal transmembrane domain and physical linkage of *cafet1* with an iron permease-encoding gene, CaFET1 was identified as a ferroxidase putatively involved in reductive iron assimilation. In sum, the *C. antarcticus* genome bears all genes for the synthesis of DHN and its extracellular polymerisation by secreted MCOs.

A

Name	Description	*A. fumigatus*	*A. alternata*	*N. crassa*	*B. cinerea*
CaPPT1	4'-phosphopantetheinyl transferase	**NpgA** [33 %]	**PPT1** [51 %]	**PPT-1** [32 %]	**PPT1** [37 %]
CaPKS1	Polyketide synthase	**Alb1** [44 %]	**PKSA** [69 %]	**PER-1** [47 %]	**PKS12** [48 %]
CaYGH1	Yellowish-green hydrolase	*no ortholog*	**AYGA** [71 %]	**PKH-2** [54 %]	*no ortholog*
CaYGH2	Yellowish-green hydrolase	**Ayg1** [51 %]	**AYGB** [65 %]	**PKH-1** [41 %]	**YGH1** [55 %]
CaTHR1	Tetrahydroxynaphthalene reductase	**Arp2** [47 %]	**BRM3** [82 %]	**PKR-2** [74 %]	**BRN2** [57 %]
CaTHR2	Trihydroxynaphthalene reductase	*no ortholog*	**BRM2** [76 %]	**PKR-1** [77 %]	**BRN1** [75 %]
CaSDH1	Scytalone dehydratase	**Arp1** [53 %]	**BRM1** [70 %]	**SCY-1** [66 %]	**SCD1** [50 %]
CaCMR1	C2H2-Zn2Cys6 transcription factor	**RegA** [19 %]	**CMR1** [64 %]	**SAH-12** [17%]	**SMR1** [40 %]

B

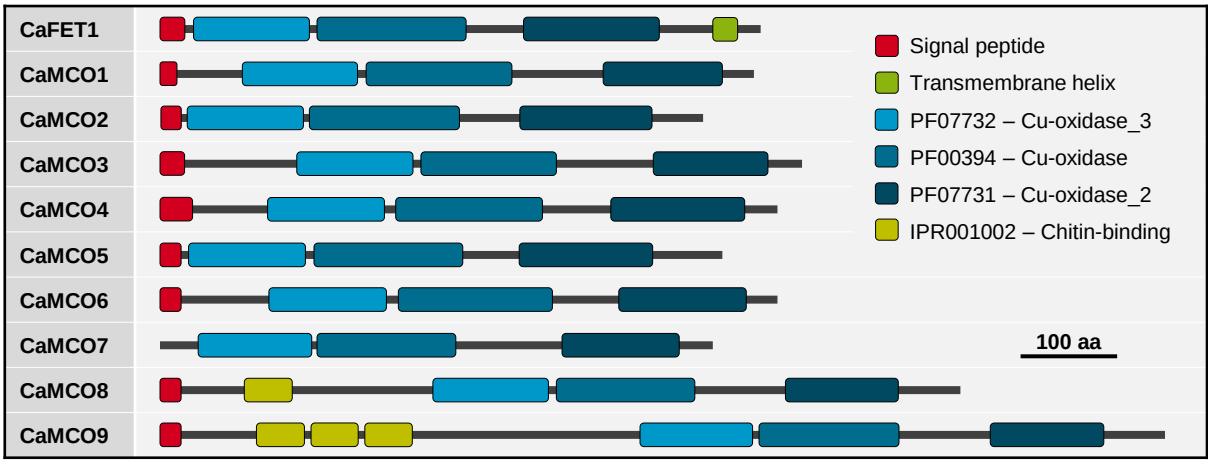

Figure 11. Putative DHN melanogenic enzymes of *C. antarcticus*.

A. Enzymes putatively involved in the formation of DHN. Orthologs from *Aspergillus fumigatus* (Eurotiomycetes), *Alternaria alternata* (Dothideomycetes), *Neurospora crassa* (Sordariomycetes), and *Botrytis cinerea* (Leotiomycetes) [color code intensity is related to the % amino acid identity with *C. antarcticus* proteins in brackets] are shown. See **Table S1** and **Table S2** for accession numbers. **B. Multicopper oxidases (MCOs) that might be involved in polymerisation of DHN.** Proteins shown were identified by the presence of the three conserved Cu-oxidase domains. FET1 contains a C-terminal transmembrane helix typical for ferroxidases. MCOs with an N-terminal signal peptide might be secreted.

3.5.2 C. antarcticus *PKS1 produces a yellowish pigment when expressed in* S. cerevisiae

Fungal non-reducing PKSs produce precursors for differently coloured pigments by using acetyl-coA and malonyl-coA as substrates (Kroken et al., 2003). The precursors themselves may be already coloured. Clade I enzymes such as *A. fumigatus* ALB1, *A. nidulans* wA and *Fusarium graminearum* PKS12 release the yellowish heptaketide YWA1, which is then modified in different pathways (**Figure S1**). In *A. fumigatus*, YWA1 is deacetylated by the hydrolase

AYG1 to yield the pentaketide T4HN, with is further converted to DHN and DHN melanin (Tsai et al., 2001). In *A. nidulans*, YWA1 is oxidised in the conidia by the laccase yA to a greenish pigment (Mayorga and Timberlake, 1990). In *F. graminearum*, YWA1 is converted in several steps to the red pigment aurofusarin (Frandsen et al., 2011). Clade II PKSs produce different polyketides for DHN melanin synthesis: PKS1 from *Colletotrichum orbiculare* releases T4HN, which is immediately converted by the T4HN reductase (Fujii et al., 2000) while PKS1 of the black yeast *Exophiala dermatitidis* releases the hexaketide AT4HN, which is modified to T4HN by YG1, an ortholog of AYG1 (Wheeler et al., 2008). In a phylogenetic tree based on amino acid identity (**Figure 12B**), *C. antarcticus* PKS1 groups with PKS from other Dothideomycetes (68-73 %), and *E. dermatitidis* PKS1 (48 %), *K. petricola* PKS1 (47 %), and *B. cinerea* PKS13 (49 %). For all these fungi, the requirement of the PKS for DHN melanin formation was experimentally shown (Kawamura et al., 1997; Feng et al., 2001; Schumacher, 2016; Jiang et al., 2017; Derbyshire et al., 2018; Voigt et al., 2020). The close relationship of CaPKS1 with these PKSs suggests that CaPKS1 is involved in DHN melanogenesis as well.

To see whether CaPKS1 is a functional protein, putatively producing the same product as the PKS1 from the black fungus *K. petricola*, both PKSs were heterologously expressed from plasmid DNA in the budding yeast *Saccharomyces cerevisiae*. For this, intron-free sequences of the *C. antarcticus* and *K. petricola* genes were fused to a galactose-inducible promoter in yeast expression vectors. Thus, gene expression in plasmid-carrying *S. cerevisiae* strains occurred during cultivation in presence of galactose but not in presence of glucose (**Figure 12C**, **Figure S2**). As expected, the expression of either *capks1* or *kppks1* alone did not induce the production of any metabolite, as the *S. cerevisiae* PPT (LYS5) cannot activate PKSs (Tippelt and Nett, 2021). Consistent with this, the co-expression of the PKSs with the Sfp-type phosphopantetheinyl transferase PPT1 from *K. petricola* resulted in the production and accumulation of similar looking yellowish metabolites. As T4HN is colourless and its oxidation product flaviolin reddish-brown, KpPKS1 and CaPKS1 may release another polyketide that must be converted in an additional step to T4HN as demonstrated in *A. fumigatus* (Tsai et al., 2001), *E. dermatitidis* (Wheeler et al., 2008), and *B. cinerea* (Schumacher, 2016) (**Figure S1**). With the 'yellowish-green hydrolases' CaYGH1 and CaYGH2, *C. antarcticus* possesses two proteins orthologous to AYG1, EdYG1 and BcYGH1, which may produce T4HN from a longer polyketide. However, the PKSs may also release all YWA1, AT4HN and T4HN in different quantities as recently found for *A. alternata* PksA (Gao et al., 2022). Although the two PKSs may release different products in *K. petricola* and *C. antarcticus*, CaPKS1 has been demonstrated to

be a functional protein with the potential to provide the phenolic precursor for the formation of DHN melanin.

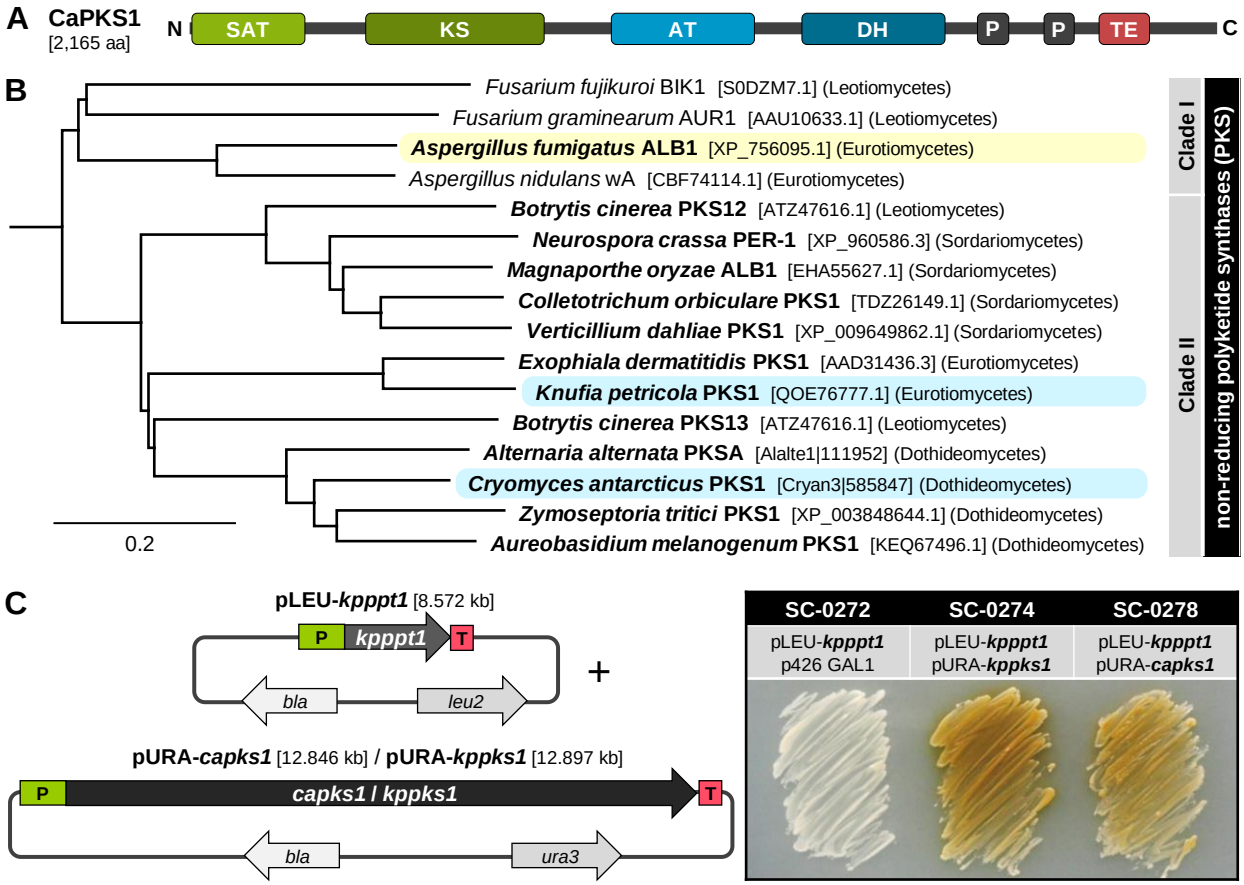

Figure 12. The polyketide synthase PKS1 of *C. antarcticus*.

A. Domain organisation of CaPKS1. SAT – starter unit: ACP transacylase [PF16073], KS – β-ketoacyl synthase [PF00109, PF02801], AT – acyl transferase [PF00698], DH – dehydratase [PF14765], P – phosphopantetheine attachment site [PF00550], TE – thioesterase [PF00975]. **B. CaPKS1 belongs to clade II of non-reducing PKS.** Species indicated in bold produce DHN melanin. ALB1, the only melanin-producing PKS in clade I is highlighted yellow, the PKSs of rock-inhabiting species in clade II are highlighted blue. **C. Expression of CaPKS1 in *Saccharomyces cerevisiae* results in a yellowish pigment.** *S. cerevisiae* strain FY834 was transformed with two plasmids for the expression of one or two genes from *K. petricola* [*kpppt1* encodes a phosphopantetheinyl transferase (PPT), *kppks1* the PKS for DHN melanogenesis] or *C. antarcticus* [*capks1*]. P – promoter, T – terminator. Plasmid-propagating *S. cerevisiae* strains were cultivated for three days at 30 °C on SD/GAL-LU agar for induction of gene expression. For further details and controls see **Table S1** and **Figure S2**.

3.5.3 *Development of protocols for protoplast-mediated transformation of* C. antarcticus

Gene functions in the native organism can be studied by targeted mutation or overexpression approaches as far as the organism is genetically amendable. Different strategies for the transformation of fungi exist (Lichius et al., 2020). In all fungi, but especially in black fungi, the cell wall constitutes the main barrier for the uptake of recombinant DNA. Given that protoplasts can be obtained from the fungus of interest, their transformation allows for different options, as

different types of DNA (linear, circular plasmid DNA) as well as ribonucleoproteins (RNPs) for CRISPR/Cas9-mediated genome editing can be introduced (Schuster and Kahmann, 2019).

Protocols for the generation and transformation of protoplasts of *K. petricola* have been optimised over the years (Noack-Schönmann et al., 2014; Voigt et al., 2020; Erdmann et al., 2022) and can serve as a blueprint for the transformation of other black fungi. First, it was verified that *C. antarcticus* did grow well on media, i.e., SDNG (synthetic defined nitrate glucose) and MEA (malt extract agar), that are used for the transformation and transformant maintenance of *K. petricola* (**Figure 13A**,**B**). Further, protoplasts from the highly melanised *C. antarcticus* cells were obtained following the same protocol i.e., incubation of cells for 16 h at 27 °C in an osmotically stabilised buffer containing a mixture of cell wall-degrading enzymes. As for *K. petricola*, cells and protoplasts cannot completely be separated by size from each other, but protoplasts are easily identified by their clear cell wall and turgid shape in contrast to the heavily melanised cells (**Figure 13C**). The number of protoplasts obtained from melanised *C. antarcticus* biomass was 7.7 x 10^6 on average. The protoplast/cell ratio ranged between 0.4 and 0.6.

Independent of the transformation method, it is necessary to select transformants i.e., cells that have been taken up and integrated the recombinant DNA into their genomes. Selection can be achieved using toxic compounds (selective agents) and using donor DNA carrying a cassette for conferring resistance to the corresponding toxic compound. Frequently used selection marker systems in fungi, including *K. petricola*, are hygromycin B (HYG)/hygromycin phosphotransferase (HPH), nourseothricin (NTC)/nourseothricin acetyltransferase (NAT1), geneticin (G418)/neomycin phosphotransferase (NPTII), or glufosinate ammonium (GFS)/phosphinothricin N-acetyltransferase (BAR) (Lichius et al., 2020; Erdmann et al., 2022). However, fungi may exhibit different or even no sensitivity to these compounds, and thus appropriate selective agents and their optimal concentrations for inhibiting growth of the respective fungus must be figured out. Therefore, growth of *C. antarcticus* on MEA and SDNG supplemented with various concentrations of HYG, NTC, or G418 was evaluated by plating 10^4, 10^5 or 10^6 cells per Petri dish. Overall, the *C. antarcticus* cell viability after incubation for three months decreased with increasing concentrations of HYG, NTC and G418 (**Figure 13A**). Remarkably, the fungus showed higher sensitivity to the compounds on MEA compared to SDNG. As expected from observations made for *K. petricola*, the sensitivity correlated with the numbers of cells plated. Thus, concentrations of 25 µg/ml of the three selective agents prevented growth of 10^5 cells/Petri dish on both media. However, it must be considered that protoplasts might be more sensitive to the selective agents than cells. Growth of *C. antarcticus* on SDNG after six weeks of incubation was unaffected by 40 µg/ml of GFS, a dose preventing growth of

K. petricola in the amino acid-free SDNG medium (**Figure 13B**). The observed ineffectiveness of GFS may be ascribed to either the tolerance of *C. antarcticus* to the tested concentration or the instability of the chemical compound over the long incubation time.

With the possibility to obtain protoplasts of *C. antarcticus* and the identification of appropriate compounds (HYG, NTC, G418) and selective concentrations, the prerequisites for the transformation of *C. antarcticus* with recombinant DNA were fulfilled.

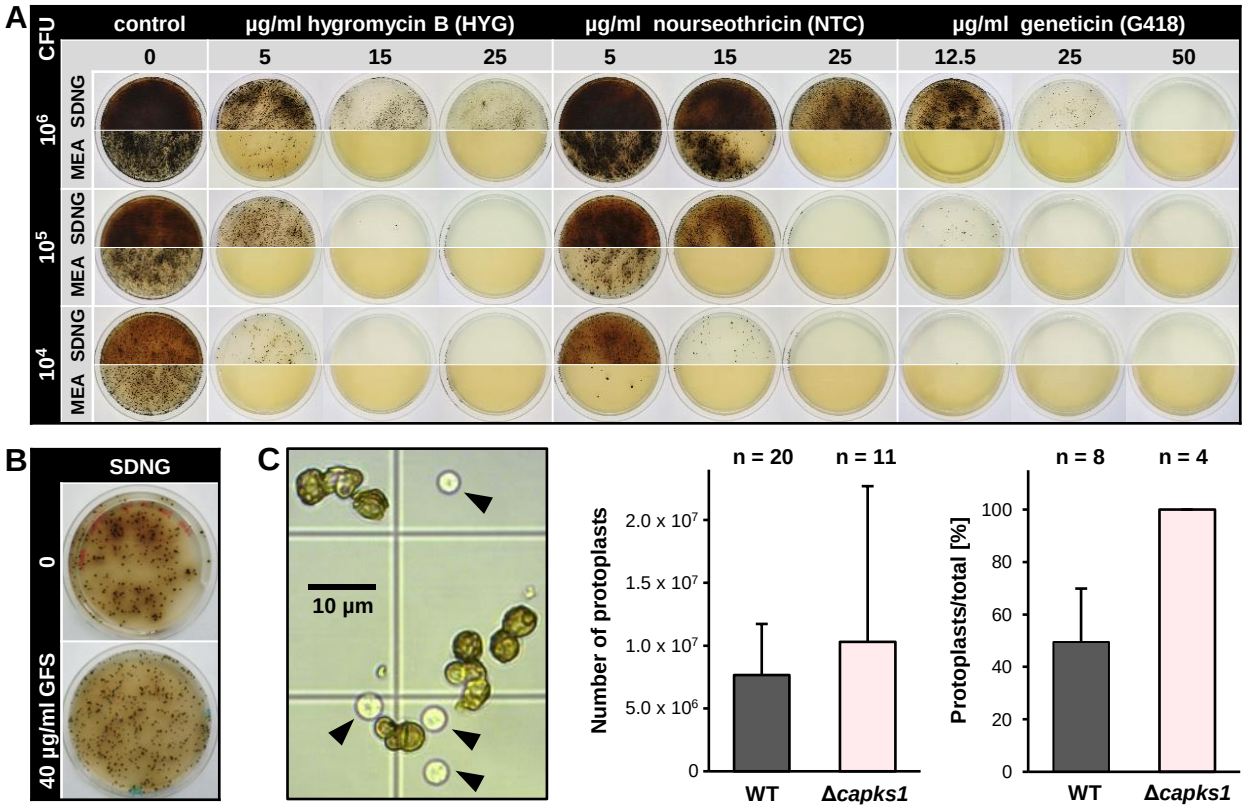

Figure 13. Prerequisites for genetic transformation of *C. antarcticus*.

A. *C. antarcticus* wild type is sensitive to the aminoglycosides hygromycin B, nourseothricin and geneticin. MEA and SDNG agar plates were inoculated with different numbers of colony forming units (CFU) and incubated for three months at 15 °C in darkness. **B. Glufosinate ammonium (GFS) does not prevent growth of *C. antarcticus*.** SDNG agar without or supplemented with GFS was inoculated with 2 x 10^3 CFU and incubated for three months at 15 °C in the dark. **C. Protoplasts from highly melanised *C. antarcticus* cells can be obtained.** Incubation of biomass in osmotically stabilised buffer with cell wall-degrading enzymes yielded protoplasts (black arrows) for the melanised WT after 14-16 h and for the non-melanised Δ*capks1* mutant already after 3-4 h. Protoplast numbers and the protoplast cell ratio were calculated from *n* approaches. Mean values and standard deviations are shown.

3.5.4 Deletion of capks1 *by a CRISPR/Cas9-assisted replacement approach*

With supporting evidence that CaPKS1 provides precursors for the DHN melanin, a targeted replacement strategy for *capks1* was considered to generate a non-melanised *C. antarcticus* strain. When exploring the genomic location of *capks1*, it was found that *capks1* is physically linked

with further genes putatively associated with DHN melanogenesis (**Figure 14A**). Clustering of DHN melanogenic genes is frequently observed. Thereby, all genes (e.g., *A. fumigatus*), few genes (e.g., *B. cinerea*) or even none (e.g., *N. crassa*) are physically linked in the genome (Jia et al., 2021). *Cathr2*, *cacmr1* and *capks1* are organised in the same manner as in *A. alternata* and other Dothideomycetes, which is in accordance with their close relationships. *Cathr2* and *camco1* might be involved in the synthesis of DHN and its polymerisation, respectively. *Cacmr1* encodes a putative transcription factor, whose orthologs such as *C. orbiculare* CMR1 (Tsuji et al., 2000), *A. alternata* CMR1 (Fetzner et al., 2014) and *B. cinerea* SMR1 (Schumacher, 2016) regulate the expression of the DHN melanogenic genes. In accordance with the studied orthologs, CaCMR1 contains the two conserved DNA-binding domains in its N-terminal region, which is a C2H2-zinc finger and a Zn(2)-Cys(6) binuclear cluster. Based on the sequence similarities, the activity of CaCMR1 may regulate the expression of all the other melanin-encoding genes in *C. antarcticus*. A gene deletion approach was designed to replace *capks1* with a resistance cassette by

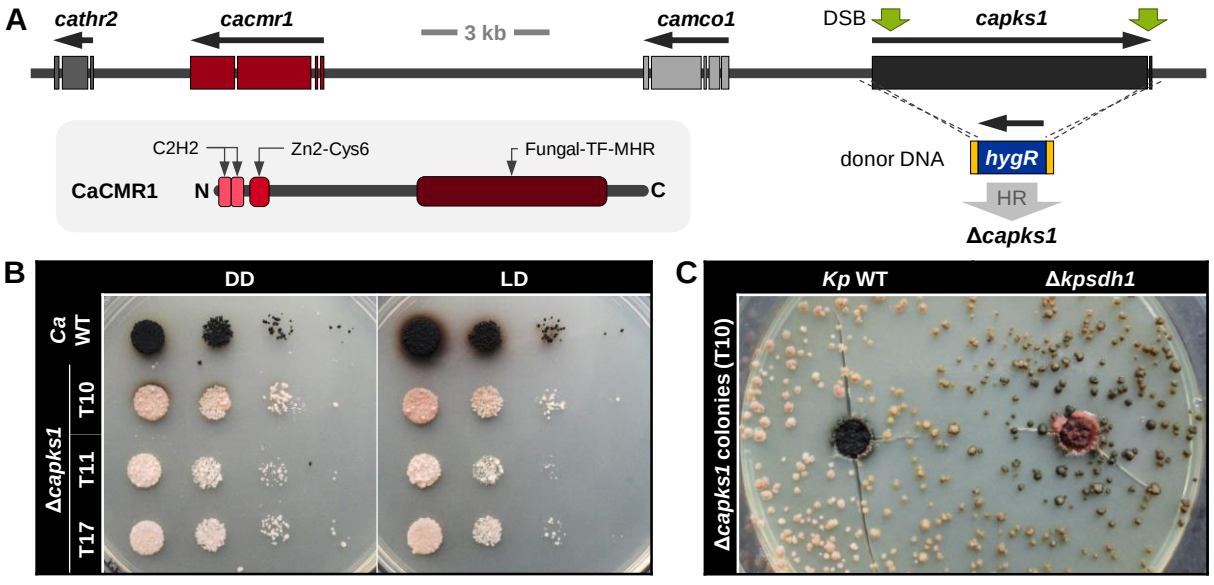

Figure 14. Deletion of *pks1* in *C. antarcticus* abolishes melanisation.

A. The PKS1-encoding gene is physically linked with other putative melanogenic genes. The protein domains (C2H2 zinc finger [PF00096], fungal Zn(2)-Cys(6) binuclear cluster domain [PF00172], fungal transcription factor regulatory middle homology region [cd12148]) of the putative transcription factor CaCMR1 are shown. The *capks1* coding region was deleted from the genome by a CRISPR/Cas9-assisted replacement approach. Two double strand breaks (DSBs; green arrows) were introduced for triggering homologous recombination (HR) using the provided donor DNA (a hygromycin resistance cassette flanked by 75-bp-long sequences homologous to the *capks1* flanking sequences) as template. Three hygromycin Δ*capks1* mutants were obtained (see **Figure S4** for details). **B. The three independent Δ*capks1* mutants exhibit an identical phenotype.** Cell suspensions (10^4, 10^3, 10^2, 10^1 CFU per droplet) of the wild-type strain (*Ca* WT) and the deletion mutants were dropped onto MEA and incubated for five weeks at 15 °C in constant darkness (DD) or in 12 h light/12 h darkness (LD). **C. Pathway intermediates secreted by Δ*kpsdh1* restore melanisation of the Δ*capks1* mutant.** MEA was inoculated with ~500 CFU of Δ*capks1* and incubated for three months at 15 °C in darkness. Then, two agar plugs were replaced by agar plugs covered with biomass of *K. petricola* A95 (*Kp* WT) and of a mutant that secretes DHN pathway intermediates (Δ*kpsdh1*), respectively. The picture was taken after additional incubation for two weeks at 15 °C in darkness.

homologous recombination (HR) (**Figure 14A**, **Figure S4A**). For triggering DNA repair in that specified genomic location, two double strand breaks (DSBs) at both ends of *capks1* should be introduced by the CRISPR/Cas9 technology. Consequently, the DSBs would be repaired by HR when a resistance cassette flanked by sequences homologous to the 5'- and 3'-noncoding regions of *capks1* is provided as repair template (donor DNA). The plasmid pAMA/tRNA-*capks1*^{PS1}-*capks1*^{PS4} for the transient expression of Cas9 and two *capks1*-specific sgRNAs was cloned. It contained *cas9* fused to a nuclear localisation signal with the codon usage of *A. niger* and under control of the regulatory sequences of *A. nidulans tef1*, and a tRNA-sgRNA cassette under control of the regulatory sequences of *A. fumigatus* U3 for transcription by the RNA polymerase III. This plasmid was developed for genome editing in *Aspergillus* spp. (Nødvig et al., 2018) but is also used in *K. petricola* (Erdmann et al., 2022). Donor DNAs, containing a hygR or a natR cassette flanked by 75-bp-long sequences homologous to the *C. antarcticus* genome, were generated using primers binding via the 3' region to the resistance cassette in pNDR-OGG plasmids, and having 75-bp-long 5' overhangs for attaching the *C. antarcticus* sequences (**Figure S4A**).

Protoplasts were transformed with the circular plasmid and linear donor DNA, either mediating hygR or natR, plated on osmotically stabilised medium (MEAS) and overlaid after 24 h with medium supplemented with the respective selective agents to obtain final concentrations of 25 µg/ml for HYG and 5 µg/ml for NTC, respectively. For control, protoplasts were transformed with H_2O and overlaid with selective medium (control for background growth) or non-selective medium (control for recovery of protoplasts). Initially, protoplasts could regenerate a cell wall when incubated in the osmotically stabilised media used for the transformation of *K. petricola*, and growth of recovered wild-type cells was suppressed by the concentrations of the selective agents that were used for *K. petricola*. For the transformation samples, numerous dark and light-coloured colonies appeared after four months of incubation at 15 °C on the top of the selective medium. For confirmation of the transformation events resulting in hygR or natR, mainly light-coloured but also some black colonies were transferred to MEA supplemented with HYG (25 µg/ml) and NTC (5 µg/ml), respectively. While most of the light-coloured cells grew with HYG, proofing them as hygR transformants, the ones from the transformation with the natR approach failed to grow on NTC-containing medium. In a few cases, the streaking of light-coloured cells from the transformation plates onto HYG-containing agar yielded a mixture of wild-type-like and non-melanised colonies. For these transformants, cells from non-melanised colonies were repeatedly spread and isolated to clear out melanised cells. The transformation of wild type protoplasts with the *capks1*-hygR replacement fragment yielded non-melanised colonies in four different experiments (**Table S5**), demonstrating the reproducibility of the approach.

In total, twenty-seven hygR Δ*capks1* transformants from two transformation experiments were submitted to diagnostic PCR for detecting the replacement of *capks1* by the hygR cassette, as consequence of HR events at 5' and 3' of the DSBs/*capks1*. For this, primers binding in the hygR cassette were combined with those binding up and downstream of *capks1* in the genome. Further, *capks1* was detected with primers binding in the native coding regions in between the two Cas9 cutting sites. The expected amplicon pattern was observed in the three transformants T10, T11, and T17 (**Figure S4C**), resulting in a deletion rate of 11 % (3 out of 27 tested). Remarkably, all strains tested were not melanised indicating the absence of a functional allele of *capks1*. However, in 24 strains either the HR events could not be detected and/or *capks1* was detected (data not shown) suggesting that the Cas9-mediated DSBs were repaired by non-homologous end-joining rather than by HR resulting in random mutations. A drop assay was performed to compare the growth phenotype of the three verified Δ*capks1* mutants with that of the wild type on MEA when incubated in complete darkness (DD) or in a diurnal light-dark (LD) cycle (**Figure 14B**). All three mutants exhibited a light pinkish pigmentation and growth rates comparable with that of the wild type. Therefore, three independent hygR Δ*capsk1* mutants were generated that are not melanised. This demonstrates that genetic engineering of *C. antarcticus* is feasible (**Figure S3**), though it is very lengthy (eight to nine months) due to the very slow growth rates of both the WT and mutant strains.

*3.5.5 Restoration of melanisation in Δ*capks1 *by DHN precursors secreted by* K. petricola

The genetic complementation of the Δ*capks1* mutants by adding back the *capks1* was envisaged as control. To prevent the disruption of other genes by an ectopic integration of a *capks1* expression construct, a targeted knock-in strategy was considered. As no suitable non-coding/intergenic regions for the targeted integration were available, a strategy was designed to reinsert *capks1* in its native genomic region under control of its native 5'-noncoding region for comparable transcription levels in the complemented strains and the wild type. A construct was cloned containing the coding region of *capks1* with 0.364 kb of the 5'-noncoding region upstream of the *B. cinerea gluc* terminator and a natR cassette (**Figure S5A**). Upon introduction of a DSB in the resistance gene (*hph*) of the Δ*capks1* locus, the sequences homologous to the 5'-noncoding sequence of *capks1* (0.364 kb) and the *trpC* promoter present in both hygR and natR cassettes (0.357 kb) would allow for HR events, replacing the former hygR cassette by the *capks1*-natR expression construct. Protoplasts of the Δ*capks1* mutant were obtained and transformed with the circular pAMA/tRNA-*hph*^{PS1} for expression of Cas9 and a *hph*-specific sgRNA, and the linear

capks1-natR construct isolated by digestion from pN-*capks1*^{COMIL}. However, no natR transformants were obtained. To rule out mistakes in the complementation strategy, the same strategy was used to complement a natR *K. petricola* Δ*pks1* mutant (**Figure S5B**). Numerous colonies with a wild-type-like pigmentation grew on the transformation medium. Four of them were isolated and analysed by diagnostic PCR, which confirmed the envisaged HR events in three strains. These strains produced DHN melanin like the wild type and grew with HYG but not with NTC as expected (**Figure S5B**). Thus, the pursued complementation strategy was correct, indicating that the failure in obtaining complemented Δ*capks1* strains was rather due to the hypersensitivity of the non-melanised *C. antarcticus* cells and protoplasts to NTC (similar observations were made for the natR Δ*capks1* transformants) or to the transformation procedure itself.

Nonetheless, the ability to restore melanogenesis in Δ*capks1* was assessed through delivery of DHN precursors. As can be seen in the drop assay, the edges of the pinkish Δ*capks1* colonies next to the *C. antarcticus* wild-type colonies turned dark (**Figure 14B**). In another assay, the Δ*capks1* mutant was co-cultivated with the *K. petricola* wild type and the Δ*kpsdh1* mutant, which secretes pathway intermediates due to the mutation of the scytalone dehydratase-encoding gene (**Figure 14C**). The colonies around the Δ*kpsdh1* mutant but not those surrounding the wild type became pigmented, suggesting that those Δ*capks1* colonies took up the brownish metabolites secreted by Δ*kpsdh1* and converted them into DHN melanin. By both approaches, it was shown that the other DHN melanogenic genes in Δ*capks1* mutants remained intact, and the *C. antarcticus* wild type unlike *K. petricola* secretes DHN pathway intermediates into the medium. These metabolites either remain colourless or are taken up again during incubation in constant darkness. Under diurnal cycles (LD), they are oxidised to their unusable shunt products, resulting in brownish halos around melanised colonies. The fact that the secretion of the same dark pigments in both DD and LD was prevented in Δ*capks1* demonstrates that they all derive from CaPKS1 as the key enzyme in DHN melanogenesis.

3.5.6 Replacement of the carotenogenic genes by a H2B-GFP expression construct

The deletion of *capks1* causing the inability to produce precursors for DHN melanin resulted in mutants with a light pinkish pigmentation. Similar observations, i.e., that other pigments become visible after blocking melanisation, have been made in other fungi. Most striking is the intense pink to reddish pigmentation of non-melanised *K. petricola* mutants (Δ*kppks1*) (**Figure S5B**). Other black fungi lacking the ability to produce DHN melanin, including

E. dermatitidis, exhibit a light pinkish pigmentation comparable to that of Δ*capks1* mutants. While the pigmentation of *E. dermatitidis* Δ*pks1* mutants was found to be more pronounced during cultivation in the light than in the dark (Chen et al., 2014), the light conditions did not significantly affect the pigmentation of the Δ*capks1* mutant (**Figure 14B**) or the Δ*kppks1* mutant (data not shown). The pink to reddish pigmentation in the latter mutant is due to the accumulation of carotenoids, as the deletion of the carotenogenic genes abolishes their synthesis resulting in albino mutants (Voigt et al., 2020). Carotenogenic genes are contained in the genome of many DHN melanin-producing fungi (Schumacher and Gorbushina, 2020), and are often clustered with genes encoding a carotenoid oxygenase for the formation of retinal and a green light-driven proton pump, such as in *Fusarium fujikuroi* and *B. cinerea* (Avalos and Estrada, 2010; Schumacher et al., 2014). To see whether *C. antarcticus* has the capability to produce carotenoids, BlastP searches using the sequences of the *K. petricola* carotenogenic enzymes were performed. This led to the identification of a bifunctional phytoene synthase/lycopene cyclase (CaPHS1, 49 % aa identity with KpPHS1) and a phytoene desaturase (CaPHD1, 59 % aa identity with KpPHD1) (**Figure 15A**, **Table S1**). While *phs1* and *phd1* have the same orientation in most fungi including *K. petricola*, *caphs1* and *caphd1* share a terminator region.

To validate carotenoid production in *C. antarcticus*, an approach was considered to delete both adjacent carotenogenic genes in a single step. pAMA/tRNA-*caphs1*^{PS1}-*caphd1*^{PS1} was cloned for the expression of ribonucleoproteins introducing DSBs in the 5'-coding regions of the two genes. Two types of donor DNA were used to replace the genes either by a resistance cassette only (hygR or natR) or by a resistance cassette fused to a cassette for the expression of a histone 2B-green fluorescent protein (H2B-GFP) fusion protein. Each donor DNA contained 75-bp-long sequences homologous to the 5'-noncoding regions of *caphs1* and *caphd1* (**Figure 15A**, **Figure S6**). The transformation of *C. antarcticus* wild type protoplasts with the hygR-containing donor DNA yielded seventeen transformants for the hygR cassette only (Δ*caphs1-caphd1*; CA-0017) and five hygR transformants for the *h2b-gfp* expression construct (*h2b-gfp*; CA-0021). To detect the desired replacement events in the resistant transformants, diagnostic PCR analyses were carried out as specified in **Figure S6**. This revealed the correct HR events and the absence of *caphs1-caphd1* in thirteen out of seventeen (CA-0017) and five out of five transformants (CA-0021). These deletion rates of 76 % and 100 % were significantly higher than that for the deletion of *capks1* (deletion rate of 11 %), for which only non-melanised transformants were analysed by diagnostic PCR. Thus, these deletion approaches proved the effectiveness of editing the *C. antarcticus* genome using HYG/*hph* as selection system. Unfortunately, no transformation of wild type protoplasts with the Δ*caphs1-caphd1*-natR fragment was carried out in parallel. This

might have shown if the failure to obtain non-melanised natR transformants was due to an increased sensitivity to NTC.

The obtained Δ*caphs1-caphd1* mutants displayed a wild-type-like phenotype but putatively lack carotenoids (**Figure 15B**). The H2B-GFP fusion protein, expected to be localised in the nuclei of *C. antarcticus*, could be detected by confocal fluorescence microscopy (**Figure 15C**). The signal intensity was rather low – likely as consequences of the thick melanised cell wall and slow metabolism – but the approach showed that the *B. cinerea*-optimised *gfp* under control of the *A. nidulans* P*oliC* is expressed in *C. antarcticus* and thus is suitable for studying its cell biology. Furthermore, this experiment revealed that *C. antarcticus* cells contain a single nucleus. The attempt to stain the nuclei with the DAPI dye failed due to unspecific binding of the dye to the cell wall, suggesting that the dye cannot enter the cell to bind the DNA.

However, the transformation of Δ*capks1* protoplasts with pAMA/tRNA-*caphs1*^{PS1}-*caphd1*^{PS1} and a *capks1*-natR replacement fragment did not yield any transformants. Therefore, the question of whether the light pinkish pigmentation of the Δ*capks1* mutants is due to accumulation of carotenoids remains unanswered.

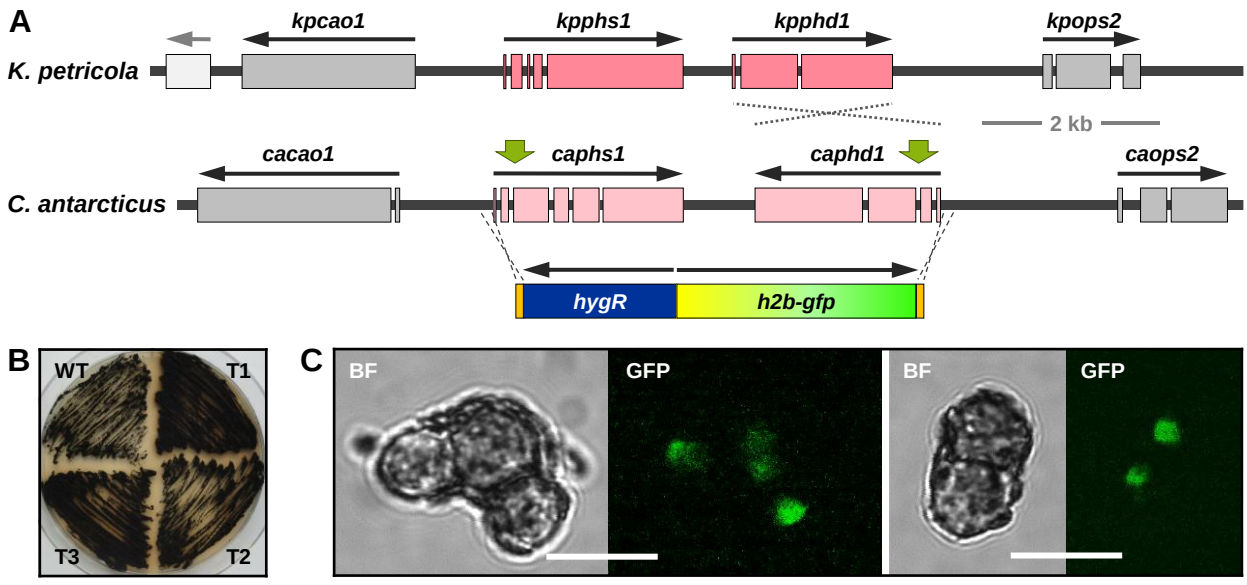

Figure 15. Insertion of an expression construct in the carotenogenic gene cluster of *C. antarcticus*.

A. The putative carotenogenic genes *caphs1* and *caphd1*. The four physically linked genes in the genomes of *K. petricola* (GenBank: MT859420.1) and *C. antarcticus* (Cryan3 scaffold 55: 150,000-163,000) are shown: *phs1* – phytoene synthase/lycopene cyclase, *phd1* – phytoene desaturase, *cao1* – carotenoid oxygenase, *ops2* – microbial opsin. For the expression of a histone 2B-GFP fusion protein in *C. antarcticus*, adjacent *caphs1* and *caphd1* were replaced by a hygR cassette-containing expression construct. Cas9 cutting sites (green arrows) and the donor DNA with 75-bp-long sequences homologous to the 5'-noncoding regions of both genes (orange bars) are shown. See **Figure S6** for further details. **B. Deletion of *caphs1* and *caphd1* does not alter the pigmentation.** Wild type and three Δ*caphs1-caphd1* mutants with the *h2b-gfp* construct (CA-0021) were cultivated for three weeks on MEA at 25 °C in DD. **C. Δ*caphs1-caphd1* mutants with the *h2b-gfp* expression construct exhibit green fluorescence in the nuclei.** GFP fluorescence in cells of transformant T1 (CA-0021) is shown. BF – brightfield, scale bars – 10 µm.

3.5.7 Growth of C. antarcticus *strains is attenuated by visible light*

Initial results on the *C. antarcticus* wild type and non-melanised Δ*capks1* mutants indicated that their phenotypes differ when incubated in DD (complete darkness) in comparison to LD (diurnal light-dark) conditions (**Figure 14B**). To confirm this observation and to see whether it is related with the culture medium used, serial dilutions of wild type and the Δ*capks1* cells were dropped onto three different solid media. MEA, used previously, is a rich medium containing glucose and peptone as additional carbon and nitrogen sources, allowing fast growth. SDNG is a synthetic medium, containing vitamins and trace elements, and glucose and nitrate as carbon and nitrogen source, respectively. MEAV is an alternative malt extract medium which is used for the cultivation of Antarctic fungi (Pacelli et al., 2020a); it lacks additional carbon and nitrogen sources (**Figure 16**, **Figure S7**). After six weeks of incubation in DD, the wild type and the Δ*capks1* mutant exhibited similar growth rates across all media. But during exposure to LD cycles, both strains showed decreased cell viability on MEA and SDNG, and neither strain did grow on the glucose- and peptone-free MEAV. The secretion of brownish pigments by the wild type colonies was affected by light on MEA as observed before, but also by the medium. Thus, the colonies secreted on SDNG agar more metabolites in DD compared to LD. Brownish metabolites, likely intermediate products of DHN melanin, were observed being taken up by the mutant strains in DD. Conversely, a rapid oxidation of the secreted metabolites by light prevented their uptake by mutants under LD conditions. Assuming that in this experiment cells in droplets may have shielded underlying cells from light, single-cell growth assays were conducted with the wild type and the three Δ*capks1* strains. For this, cells were spread onto agar in compartmentalised Petri dishes to prevent metabolites from wild type colonies from impacting on the non-melanised mutants (**Figure 16**). Consistent observations of reduced (MEA/SDNG) or absent growth (MEAV) of both wild type and mutant strains under LD conditions confirmed light sensitivity across all strains. These observations suggest that light may act as a stress-inducing factor for *C. antarcticus*, yet growth can be sustained when more nutrients are readily available.

Sensitivity to visible light has not been reported for *C. antarcticus* so far. The fungus lives in association with cryptoendolithic microbial communities in Antarctic sandstone rocks (Selbmann et al., 2005). These communities typically display a vertical zonation pattern, assumed to be formed in response to the surrounding sunlight regime. As sandstones are sedimentary rocks with quartz grains, incident sunlight can penetrate inside the rock and be transmitted to deeper layers due to mineral transparency, interacting with both the photosynthetic and non-photosynthetic components of microbial communities (Sajjad et al., 2022). Black fungi are typically found in the

first colonised zone, located just a few millimetres below the rock crust. This area has been estimated to receive up to 10 % of the surface light flux (Nienow et al., 1988), and therefore dark melanins in these fungi are believed to act as light filters, alleviating photo-oxidative damage caused by the excessive solar irradiation on the rest of the community (Coleine et al., 2021). Observations made from our experiments imply that the sensitivity of *C. antarcticus* to visible light is an inherent trait and not contingent upon DHN melanin production. However, the meaning of this effect in the natural habitat of the fungus remains elusive and requires further investigation.

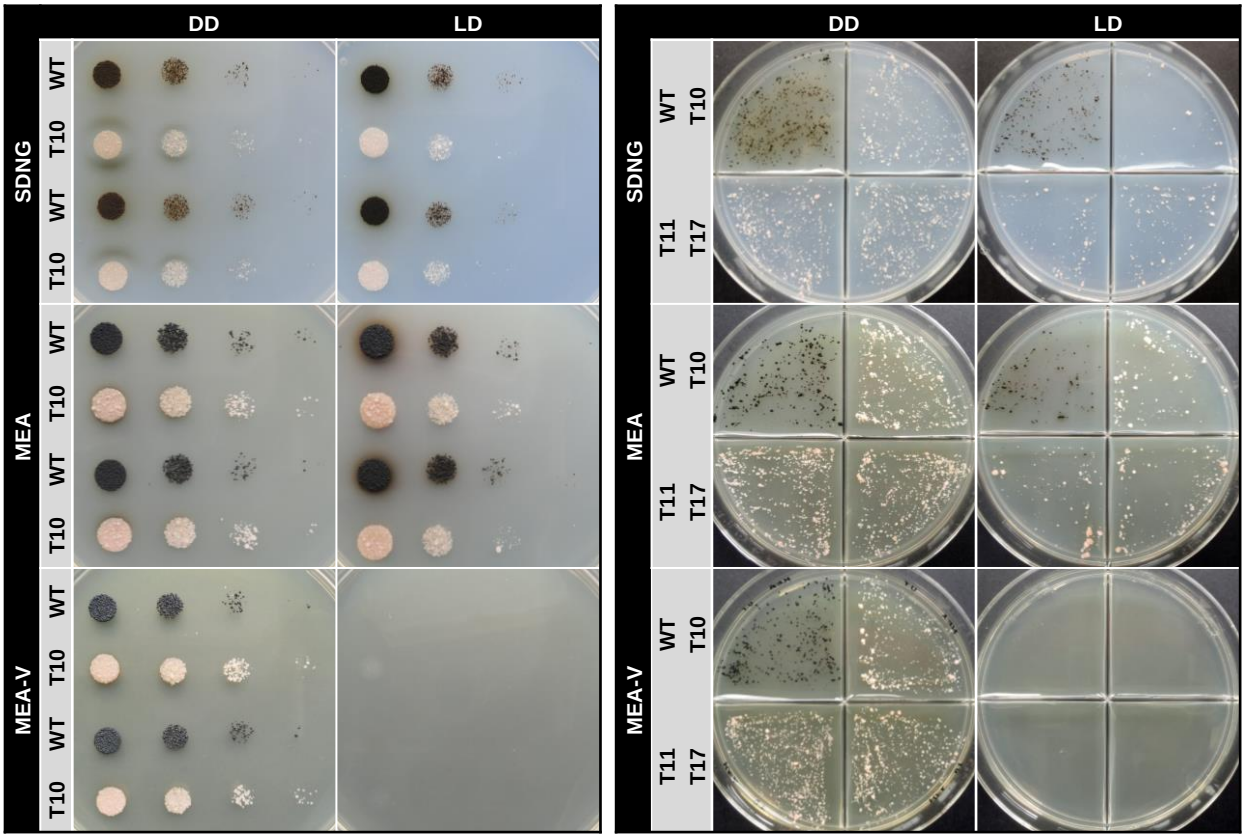

Figure 16. Melanised and non-melanised *C. antarcticus* strains are equally sensitive to visible light.

The wild-type strain and Δ*capks1* mutants were cultured for six weeks at 15 °C in DD or LD conditions. Solidified media on the left were inoculated with droplets of cells suspensions (10^4, 10^3, 10^2, 10^1 CFU per droplet of each technical replicate) (see the same plates on white background in **Figure S7** for brownish metabolites secreted by the wild type). The media on the right were inoculated with ~500 CFU per Petri dish compartment. MEAV in contrast to MEA does not contain glucose and peptone.

3.5.8 The deletion of capks1 *affects the cell wall organisation*

Melanins are best-known for their function to protect cells from harmful UV radiation, but they may have further specific functions in fungi depending on their habitats and life cycles. Thus, DHN melanin-containing cell walls may function as mechanical barrier and give strength and shape to infection or reproduction structures, thereby protecting the fungal cells from abiotic and

biotic stress factors and contributing to dispersal and survival of the reproductive units (Cordero and Casadevall, 2017).

To see whether DHN melanin or its absence alters the morphology of *C. antarcticus* cells and colonies, optical and electron microscopy were applied (**Figure 17**). Stereomicroscopic analyses revealed a consistent colony-forming ability in the Δ*capks1* mutant, with colony sizes comparable with those of the wild type. The distinctive trait of Δ*capks1* colonies was the light pinkish pigmentation and a fluffier appearance. Assuming that these pinkish pigments are carotenoids, they may be incorporated in the membranes of *C. antarcticus* as found in *K. petricola*. Carotenoid production is supposed to occur in both mutant and wild type yet being hidden in the latter due to the dark cell wall. Scanning electron microscopy demonstrated that the cell aggregation in Δ*capks1* colonies resembles that of the wild type colonies. Both melanised and non-melanised cells are covered with extracellular polysaccharides (EPS), though the Δ*capks1* mutant produce more EPS as was found for the non-melanised *K. petricola* Δ*pks1* mutant (Breitenbach et al., 2022). The EPS has been characterised before in several melanised strains of *C. antarcticus* (Selbmann et al., 2005), but not in the one used in this study. Therefore, composition and amounts of EPS might be compared between wild type and the non-melanised Δ*capks1* mutant to clarify whether the absence of DHN melanin affects the EPS production in *C. antarcticus* as well. Transmission electron microscopy revealed wild-type and Δ*capks1* cells with intact plasma membranes and cell walls. Consistent with previous studies on the wild-type strain (Pacelli et al., 2019; Cassaro et al., 2022), the deposition of DHN melanin manifested as tiny, highly electron-dense granules (approx. 20-100 nm in diameter) in the outer layers of the cell wall and on top. Conversely, no electron-dense depositions were observed in the cell walls of the non-melanised mutant. These structural changes in the cell wall are thus associated with DHN melanin. Interestingly, the arrangement of DHN melanin in the cell walls of *C. antarcticus* and *K. petricola* differs. Dark melanin granules are found throughout the multi-layered cell wall of *C. antarcticus*, while a smoother DHN layer is observed in the outer wall of budding *K. petricola* cells (Knabe and Gorbushina, 2018; Breitenbach et al., 2022).

In summary, melanin-deficient and carotenoid-deficient *C. antarcticus* mutants were successfully generated by a genetic engineering approach in this study. Utilisation of these mutants in further phenotypic studies will gain new insights into the role of DHN melanin in the extraordinary survival capabilities of *C. antarcticus*.

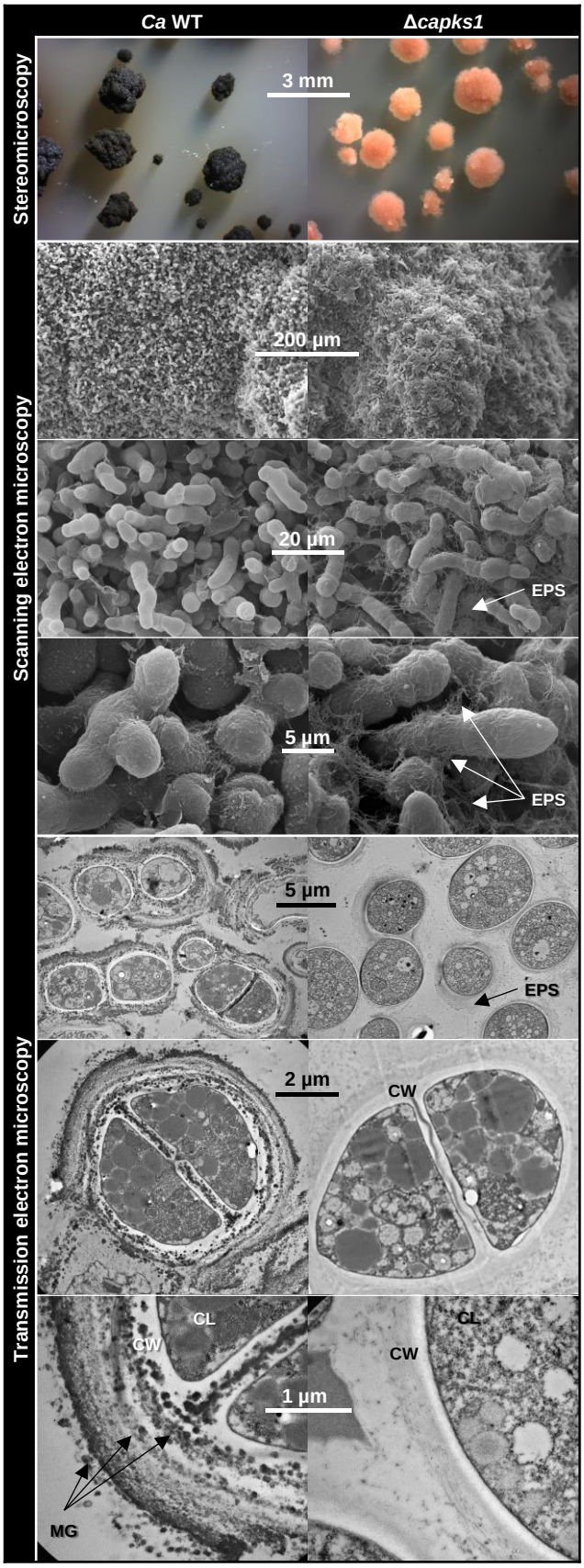

Figure 17. Deletion of *pks1* in *C. antarcticus* alters the organisation of the cell wall.

Microscopic analyses of melanised wild type and non-melanised Δ*capks1* colonies from biofilm cultures (MEA). Extracellular polysaccharides (EPS), cell wall (CW), cell lumen (CL), melanin granules (MG).

3.6 Conclusions

The Antarctic black fungus *C. antarcticus* is a slow growing fungus originating from a cold desert - the closest terrestrial analogue to conditions on early Mars. Its ability to resist 'absolute' (i.e. *par excellence*) extreme environments was repeatedly demonstrated. The role of the dark pigment melanin for survivability of this fungus has been postulated. Here, we further improved *C. antarcticus* as a test organism by implementing genetic engineering tools for the targeted mutation of genes in its genome. The tools developed and optimised in the model black fungus *K. petricola* were successfully transferred to the *C. antarcticus* system demonstrating their reliability and efficiency. Only minimal technical modifications in the procedure were necessary. But the largest difference in genetically manipulating the two black fungi is the time needed to complete this task: three to four weeks in *K. petricola* and eight to nine months in *C. antarcticus*. Using the annotated genome sequence of *C. antarcticus* available at the JGI, genes putatively involved in the synthesis of DHN melanin and carotenoids were identified allowing to propose the synthesis pathways. To generate mutants defective in DHN melanogenesis, *capks1* encoding the key enzyme of the pathway was deleted. Resulting deletion mutants were non-melanised and exhibited a light pinkish pigmentation, perhaps due to the accumulation of carotenoids. Thus, the carotenogenic genes were targeted by a deletion approach in the wild type and the non-melanised mutants. While the deletion of the two adjacent genes in the wild type (Δ*caphs1-phd1*) was successful, no Δ*capks1*/Δ*caphs1-phd1* mutants were obtained. Therefore, the link between the pinkish pigments and the carotenogenic genes could not be established in this study, but both DHN melanin- and carotenoid-deficient mutants have become available for functional and chemical characterisation.

Due to its polyextremotolerant nature *C. antarcticus* has become a prominent test organism in the field of astrobiology. With the now introduced availability of CRISPR/Cas9-mediated genome editing, *C. antarcticus* becomes an even better test organism for astrobiology and related research.

3.7 Acknowledgements

We thank Sarah Nitsche and Eileen Erdmann for discussion, Antonia Brandhorst and Jenny Straßner for supporting the cloning work, and Anna Rita Taddei for her contribution to the TEM analysis. The Italian National Program of Antarctic Research (PNRA) and the Italian National

Antarctic Museum ‘Felice Ippolito’ (MNA) are acknowledged for funding the collection of Antarctic samples MNA-CCFEE. This work was supported financially by internal funds of the BAM and the grant of the Italian Space Agency (ASI), Life in Space – ASI N. 2019-3-U.0.

3.8 References

Ao, J., Bandyopadhyay, S., and Free, S.J. (2019) Characterization of the *Neurospora crassa* DHN melanin biosynthetic pathway in developing ascospores and peridium cells. *Fungal Biol* **123**: 1-9.

Avalos, J., and Estrada, A.F. (2010) Regulation by light in *Fusarium*. *Fungal Genet Biol* **47**: 930-938.

Breitenbach, R., Silbernagl, D., Toepel, J., Sturm, H., Broughton, W.J., Sassaki, G.L., and Gorbushina, A.A. (2018) Corrosive extracellular polysaccharides of the rock-inhabiting model fungus *Knufia petricola*. *Extremophiles* **22**: 165-175.

Breitenbach, R., Gerrits, R., Dementyeva, P., Knabe, N., Schumacher, J., Feldmann, I. et al. (2022) The role of extracellular polymeric substances of fungal biofilms in mineral attachment and weathering. *npj Mater Degrad* **6**.

Butler, M.J., and Day, A.W. (1998) Fungal melanins: a review. *Can J Microbiol* **44**: 1115-1136.

Cao, W., Zhou, X., McCallum, N.C., Hu, Z., Ni, Q.Z., Kapoor, U. et al. (2021) Unraveling the structure and function of melanin through synthesis. *J Am Chem Soc* **143**: 2622-2637.

Cassaro, A., Pacelli, C., and Onofri, S. (2022) Survival, metabolic activity, and ultrastructural damages of Antarctic black fungus in perchlorates media. *Front Microbiol* **13**: 992077.

Chen, Z., Martinez, D.A., Gujja, S., Sykes, S.M., Zeng, Q., Szaniszlo, P.J. et al. (2014) Comparative genomic and transcriptomic analysis of *Wangiella dermatitidis*, a major cause of phaeohyphomycosis and a model black yeast human pathogen. *G3 (Bethesda)* **4**: 561-578.

Coleine, C., Stajich, J.E., de Los Rios, A., and Selbmann, L. (2021) Beyond the extremes: Rocks as ultimate refuge for fungi in drylands. *Mycologia* **113**: 108-133.

Cordero, R.J.B., and Casadevall, A. (2017) Functions of fungal melanin beyond virulence. *Fungal Biol Rev* **31**: 99-112.

Derbyshire, M.C., Gohari, A.M., Mehrabi, R., Kilaru, S., Steinberg, G., Ali, S. et al. (2018) Phosphopantetheinyl transferase (Ppt)-mediated biosynthesis of lysine, but not siderophores or DHN melanin, is required for virulence of *Zymoseptoria tritici* on wheat. *Sci Rep* **8**: 17069.

Dittrich, M., Paulo, C., Knabe, N., Sturm, H., Zaitsev, V., and Gorbushina, A.A. (2023) Microscopic Raman study of fungal pigment using the genetically amenable rock inhabitant *Knufia petricola* as a model organism. *Spectrochim Acta A Mol Biomol Spectrosc* **303**: 123250.

Eisenman, H.C., and Casadevall, A. (2012) Synthesis and assembly of fungal melanin. *Appl Microbiol Biotechnol* **93**: 931-940.

Eisenman, H.C., Greer, E.M., and McGrail, C.W. (2020) The role of melanins in melanotic fungi for pathogenesis and environmental survival. *Appl Microbiol Biotechnol* **104**: 4247-4257.

Erdmann, E.A., Nitsche, S., Gorbushina, A.A., and Schumacher, J. (2022) Genetic engineering of the rock inhabitant *Knufia petricola* provides insight into the biology of extremotolerant black fungi. *Front Fungal Biol* **3**: 862429.

Feng, B., Wang, X., Hauser, M., Kaufmann, S., Jentsch, S., Haase, G. et al. (2001) Molecular cloning and characterization of WdPKS1, a gene involved in dihydroxynaphthalene melanin biosynthesis and virulence in *Wangiella (Exophiala) dermatitidis*. *Infect Immun* **69**: 1781-1794.

Fetzner, R., Seither, K., Wenderoth, M., Herr, A., and Fischer, R. (2014) *Alternaria alternata* transcription factor CmrA controls melanization and spore development. *Microbiology* **160**: 1845-1854.

Flieger, K., Knabe, N., and Toepel, J. (2018) Development of an improved carotenoid extraction method to characterize the carotenoid composition under oxidative stress and cold temperature in the rock inhabiting fungus *Knufia petricola* A95. *J Fungi* **4**: 124.

Frandsen, R.J., Schutt, C., Lund, B.W., Staerk, D., Nielsen, J., Olsson, S., and Giese, H. (2011) Two novel classes of enzymes are required for the biosynthesis of aurofusarin in *Fusarium graminearum*. *J Biol Chem* **286**: 10419-10428.

Friedmann, E.I., Hua, M., and Ocampo-Friedmann, R. (1988) Cryptoendolithic lichen and cyanobacterial communities of the Ross Desert, Antarctica. *Polarforschung* **58**: 251-259.

Fujii, I., Mori, Y., Watanabe, A., Kubo, Y., Tsuji, G., and Ebizuka, Y. (2000) Enzymatic synthesis of 1,3,6,8-tetrahydroxynaphthalene solely from malonyl coenzyme A by a fungal iterative type I polyketide synthase PKS1. *Biochemistry* **39**: 8853-8858.

Gao, J., Wenderoth, M., Doppler, M., Schuhmacher, R., Marko, D., and Fischer, R. (2022) Fungal melanin biosynthesis pathway as source for fungal toxins. *Mbio*: e00219-00222.

Gerrits, R., Pokharel, R., Breitenbach, R., Radnik, J., Feldmann, I., Schuessler, J.A. et al. (2020) How the rock - inhabiting fungus *K. petricola* A95 enhances olivine dissolution through attachment. *Geochim Cosmochim Ac* **282**: 76-97.

Gessler, N.N., Egorova, A.S., and Belozerskaya, T.A. (2014) Melanin pigments of fungi under extreme environmental conditions. *Appl Biochem Microbiol* **50**: 105-113.

Giardina, P., Faraco, V., Pezzella, C., Piscitelli, A., Vanhulle, S., and Sannia, G. (2010) Laccases: a never-ending story. *Cell Mol Life Sci* **67**: 369-385.

Gietz, R.D., and Schiestl, R.H. (2007) High-efficiency yeast transformation using the LiAc/SS carrier DNA/PEG method. *Nat Protocols* **2**: 31-34.

Gorbushina, A., Kotlova, E., and Sherstneva, O. (2008) Cellular responses of microcolonial rock fungi to long-term desiccation and subsequent rehydration. *Stud Mycol* **61**: 91-97.

Gorbushina, A.A., Whitehead, K., Dornieden, T., Niesse, A., Schulte, A., and Hedges, J.I. (2003) Black fungal colonies as units of survival: hyphal mycosporines synthesized by rock-dwelling microcolonial fungi. *Can J Botany* **81**: 131-138.

Gostinčar, C., Zalar, P., and Gunde-Cimerman, N. (2022) No need for speed: slow development of fungi in extreme environments. *Fungal Biol Rev* **39**: 1-14.

Gow, N.A.R., Latge, J.-P., and Munro, C.A. (2017) The fungal cell wall: structure, biosynthesis, and function. *Microbiol Spectr* **5**: 1-25.

Jia, S.-L., Chi, Z., Chen, L., Liu, G.-L., Hu, Z., and Chi, Z.-M. (2021) Molecular evolution and regulation of DHN melanin-related gene clusters are closely related to adaptation of different melanin-producing fungi. *Genomics* **113**: 1962-1975.

Jiang, H., Liu, G.-L., Chi, Z., Wang, J.-M., Zhang, L.-L., and Chi, Z.-M. (2017) Both a *PKS* and a PPTase are involved in melanin biosynthesis and regulation of *Aureobasidium melanogenum* XJ5-1 isolated from the Taklimakan desert. *Gene* **602**: 8-15.

Kawamura, C., Moriwaki, J., Kimura, N., Fujita, Y., Fuji, S., Hirano, T. et al. (1997) The melanin biosynthesis genes of *Alternaria alternata* can restore pathogenicity of the melanin-deficient mutants of *Magnaporthe grisea*. *Mol Plant Microbe Interact* **10**: 446-453.

Knabe, N., and Gorbushina, A.A. (2018) Territories of rock-inhabiting fungi: survival on and alteration of solid air-exposed surfaces. In *Methods in Microbiology*. V. Gurtler, and Trevors, J.T. (eds): Elsevier Ltd, pp. 145-169.

Kroken, S., Glass, N.L., Taylor, J.W., Yoder, O.C., and Turgeon, B.G. (2003) Phylogenomic analysis of type I polyketide synthase genes in pathogenic and saprobic ascomycetes. *Proc Natl Acad Sci U S A* **100**: 15670-15675.

Lichius, A., Ruiz, D.M., and Zeilinger, S. (2020) Genetic Transformation of Filamentous Fungi: Achievements and Challenges. In *Grand Challenges in Fungal Biotechnology*. Nevalainen, H. (ed): Springer International Publishing, pp. 123-164.

Mayorga, M.E., and Timberlake, W. (1990) Isolation and molecular characterization of the *Aspergillus nidulans* wA gene. *Genetics* **126**: 73-79.

Mitchison-Field, L.M.Y., Vargas-Muniz, J.M., Stormo, B.M., Vogt, E.J.D., Van Dierdonck, S., Pelletier, J.F. et al. (2019) Unconventional cell division cycles from marine-derived yeasts. *Curr Biol* **29**: 3439-3456 e3435.

Mumberg, D., Müller, R., and Funk, M. (1994) Regulatable promoters of *Saccharomyces cerevisiae*: comparison of transcriptional activity and their use for heterologous expression. *Nucleic Acids Res* **22**: 5767.

Nai, C., Wong, H.Y., Pannenbecker, A., Broughton, W.J., Benoit, I., de Vries, R.P. et al. (2013) Nutritional physiology of a rock-inhabiting, model microcolonial fungus from an ancestral lineage of the Chaetothyriales (Ascomycetes). *Fungal Genet Biol* **56**: 54-66.

Nienow, J.A., McKay, C.P., and Friedmann, E.I. (1988) The cryptoendolithic microbial environment in the Ross Desert of Antarctica: light in the photosynthetically active region. *Microbial Ecol* **16**: 271-289.

Noack-Schönmann, S., Bus, T., Banasiak, R., Knabe, N., Broughton, W.J., Den Dulk-Ras, H. et al. (2014) Genetic transformation of *Knufia petricola* A95 - a model organism for biofilm-material interactions. *AMB Express* **4**: 80.

Nødvig, C.S., Nielsen, J.B., Kogle, M.E., and Mortensen, U.H. (2015) A CRISPR-Cas9 system for genetic engineering of filamentous fungi. *PLoS One* **10**: e0133085.

Nødvig, C.S., Hoof, J.B., Kogle, M.E., Jarczynska, Z.D., Lehmbeck, J., Klitgaard, D.K., and Mortensen, U.H. (2018) Efficient oligo nucleotide mediated CRISPR-Cas9 gene editing in Aspergilli. *Fungal Genet Biol* **115**: 78-89.

Onofri, S., Pacelli, C., Selbmann, L., and Zucconi, L. (2020) The amazing journey of *Cryomyces antarcticus* from Antarctica to space. In *Extremophiles as astrobiological models*. Seckbach, J., and Stan-Lotter, H. (eds): Scrivener Publishing LLC, pp. 237-254.

Onofri, S., Zucconi, L., Selbmann, L., Hoog, S.d., Ríos, D.A.d.l., Ruisi, S., and Grube, M. (2007) Fungal associations at the cold edge of life. In *Algae and cyanobacteria in extreme environments*. Seckbach, J. (ed): Springer, pp. 735-757.

Pacelli, C., Bryan, R.A., Onofri, S., Selbmann, L., Shuryak, I., and Dadachova, E. (2017a) Melanin is effective in protecting fast and slow growing fungi from various types of ionizing radiation. *Environ Microbiol* **19**: 1612-1624.

Pacelli, C., Cassaro, A., Aureli, L., Moeller, R., Fujimori, A., and Onofri, S. (2020a) The responses of the black fungus *Cryomyces antarcticus* to high doses of accelerated helium Ions radiation within Martian regolith simulants and their relevance for Mars. *Life (Basel)* **10**.

Pacelli, C., Selbmann, L., Zucconi, L., Raguse, M., Moeller, R., Shuryak, I., and Onofri, S. (2017b) Survival, DNA integrity, and ultrastructural damage in Antarctic cryptoendolithic eukaryotic microorganisms exposed to ionizing radiation. *Astrobiology* **17**: 126-135.

Pacelli, C., Selbmann, L., Zucconi, L., De Vera, J.P., Rabbow, E., Horneck, G. et al. (2017c) BIOMEX experiment: Ultrastructural alterations, molecular damage and survival of the fungus *Cryomyces antarcticus* after the Experiment Verification Tests. *Orig Life Evol Biosph* **47**: 187-202.

Pacelli, C., Selbmann, L., Zucconi, L., Coleine, C., de Vera, J.P., Rabbow, E. et al. (2019) Responses of the black fungus *Cryomyces antarcticus* to simulated Mars and space conditions on rock analogs. *Astrobiology* **19**: 209-220.

Pacelli, C., Cassaro, A., Maturilli, A., Timperio, A.M., Gevi, F., Cavalazzi, B. et al. (2020b) Multidisciplinary characterization of melanin pigments from the black fungus *Cryomyces antarcticus*. *Appl Microbiol Biotechnol* **104**: 6385-6395.

Paysan-Lafosse, T., Blum, M., Chuguransky, S., Grego, T., Pinto, B.L., Salazar, G.A. et al. (2023) InterPro in 2022. *Nucleic Acids Res* **51**: D418-D427.

Perez-Cuesta, U., Aparicio-Fernandez, L., Guruceaga, X., Martin-Souto, L., Abad-Diaz-de-Cerio, A., Antoran, A. et al. (2020) Melanin and pyomelanin in *Aspergillus fumigatus*: from its genetics to host interaction. *Int Microbiol* **23**: 55-63.

Sajjad, W., Ilahi, N., Kang, S., Bahadur, A., Zada, S., and Iqbal, A. (2022) Endolithic microbes of rocks, their community, function and survival strategies. *Int Biodeterior Biodegradation* **169**.

Schmaler-Ripcke, J., Sugareva, V., Gebhardt, P., Winkler, R., Kniemeyer, O., Heinekamp, T., and Brakhage, A.A. (2009) Production of pyomelanin, a second type of melanin, via the tyrosine degradation pathway in *Aspergillus fumigatus*. *Appl Environ Microbiol* **75**: 493-503.

Schumacher, J. (2012) Tools for *Botrytis cinerea*: new expression vectors make the gray mold fungus more accessible to cell biology approaches. *Fungal Genet Biol* **49**: 483-497.

Schumacher, J. (2016) DHN melanin biosynthesis in the plant pathogenic fungus *Botrytis cinerea* is based on two developmentally regulated key enzyme (PKS)-encoding genes. *Mol Microbiol* **99**: 729-748.

Schumacher, J., and Gorbushina, A.A. (2020) Light sensing in plant- and rock-associated black fungi. *Fungal Biol* **124**: 407-417.

Schumacher, J., Simon, A., Cohrs, K.C., Viaud, M., and Tudzynski, P. (2014) The transcription factor BcLTF1 regulates virulence and light responses in the necrotrophic plant pathogen *Botrytis cinerea*. *PLoS Genet* **10**: e1004040.

Schuster, M., and Kahmann, R. (2019) CRISPR-Cas9 genome editing approaches in filamentous fungi and oomycetes. *Fungal Genet Biol* **130**: 43-53.

Selbmann, L., Zucconi, L., Isola, D., and Onofri, S. (2015) Rock black fungi: excellence in the extremes, from the Antarctic to space. *Curr Genet* **61**: 335-345.

Selbmann, L., de Hoog, G.S., Mazzaglia, A., Friedmann, E.I., and Onofri, S. (2005) Fungi at the edge of life: cryptoendolithic black fungi from Antarctic desert. *Stud Mycol* **51**: 1-32.

Selbmann, L., Grube, M., Onofri, S., Isola, D., and Zucconi, L. (2013) Antarctic epilithic lichens as niches for black meristematic fungi. *Biology (Basel)* **2**: 784-797.

Smith, D.F., and Casadevall, A. (2019) The role of melanin in fungal pathogenesis for animal hosts. *Fungal Physiol Immunopathogenesis*: 1-30.

Spurr, A.R. (1969) A low-viscosity epoxy resin embedding medium for electron microscopy. *J Ultrastruct Res* **26**: 31-43.

Thompson, J.E., Fahnestock, S., Farrall, L., Liao, D.I., Valent, B., and Jordan, D.B. (2000) The second naphthol reductase of fungal melanin biosynthesis in *Magnaporthe grisea*: tetrahydroxynaphthalene reductase. *J Biol Chem* **275**: 34867-34872.

Tippelt, A., and Nett, M. (2021) *Saccharomyces cerevisiae* as host for the recombinant production of polyketides and nonribosomal peptides. *Microb Cell Fact* **20**: 161.

Toledo, A.V., Franco, M.E.E., Lopez, S.M.Y., Troncozo, M.I., Saparrat, M.C.N., and Balatti, P.A. (2017) Melanins in fungi: types, localization and putative biological roles. *Physiol Molecular Plant Pathol* **99**: 2-6.

Tonon, C., Breitenbach, R., Voigt, O., Turci, F., Gorbushina, A.A., and Favero-Longo, S.E. (2020) Hyphal morphology and substrate porosity-rather than melanization-drive penetration of black fungi into carbonate substrates. *J Cult Herit* **48**: 244-253.

Toreno, G., Isola, D., Meloni, P., Carcangiu, G., Selbmann, L., Onofri, S. et al. (2018) Biological colonization on stone monuments: A new low impact cleaning method. *Journal of Cultural Heritage* **30**: 100-109.

Tsai, H.F., Wheeler, M.H., Chang, Y.C., and Kwon-Chung, K.J. (1999) A developmentally regulated gene cluster involved in conidial pigment biosynthesis in *Aspergillus fumigatus*. *J Bacteriol* **181**: 6469-6477.

Tsai, H.F., Fujii, I., Watanabe, A., Wheeler, M.H., Chang, Y.C., Yasuoka, Y. et al. (2001) Pentaketide melanin biosynthesis in *Aspergillus fumigatus* requires chain-length shortening of a heptaketide precursor. *J Biol Chem* **276**: 29292-29298.

Tsuji, G., Kenmochi, Y., Takano, Y., Sweigard, J., Farrall, L., Furusawa, I. et al. (2000) Novel fungal transcriptional activators, Cmr1p of *Colletotrichum lagenarium* and pig1p of *Magnaporthe grisea*, contain Cys2His2 zinc finger and Zn(II)2Cys6 binuclear cluster DNA-binding motifs and regulate transcription of melanin biosynthesis genes in a developmentally specific manner. *Mol Microbiol* **38**: 940-954.

Voigt, O., Knabe, N., Nitsche, S., Erdmann, E.A., Schumacher, J., and Gorbushina, A.A. (2020a) An advanced genetic toolkit for exploring the biology of the rock-inhabiting black fungus *Knufia petricola*. *Sci Rep* **10**: 22021.

Volkmann, M., and Gorbushina, A.A. (2006) A broadly applicable method for extraction and characterization of mycosporines and mycosporine-like amino acids of terrestrial, marine and freshwater origin. *FEMS Microbiol Lett* **255**: 286-295.

Wheeler, M.H., Abramczyk, D., Puckhaber, L.S., Naruse, M., Ebizuka, Y., Fujii, I., and Szaniszlo, P.J. (2008) New biosynthetic step in the melanin pathway of *Wangiella (Exophiala) dermatitidis*: evidence for 2-acetyl-1,3,6,8-tetrahydroxynaphthalene as a novel precursor. *Eukaryot Cell* **7**: 1699-1711.

Winston, F., Dollard, C., and Ricupero-Hovasse, S.L. (1995) Construction of a set of convenient *Saccharomyces cerevisiae* strains that are isogenic to S288C. *Yeast* **11**: 53-55.

Wollenzien, U., De Hoog, G., Krumbein, W., and Uijthof, J. (1997) *Sarcinomyces petricola*, a new microcolonial fungus from marble in the Mediterranean basin. *Antonie van Leeuwenhoek* **71**: 281-288.

3.9 Supplementary materials

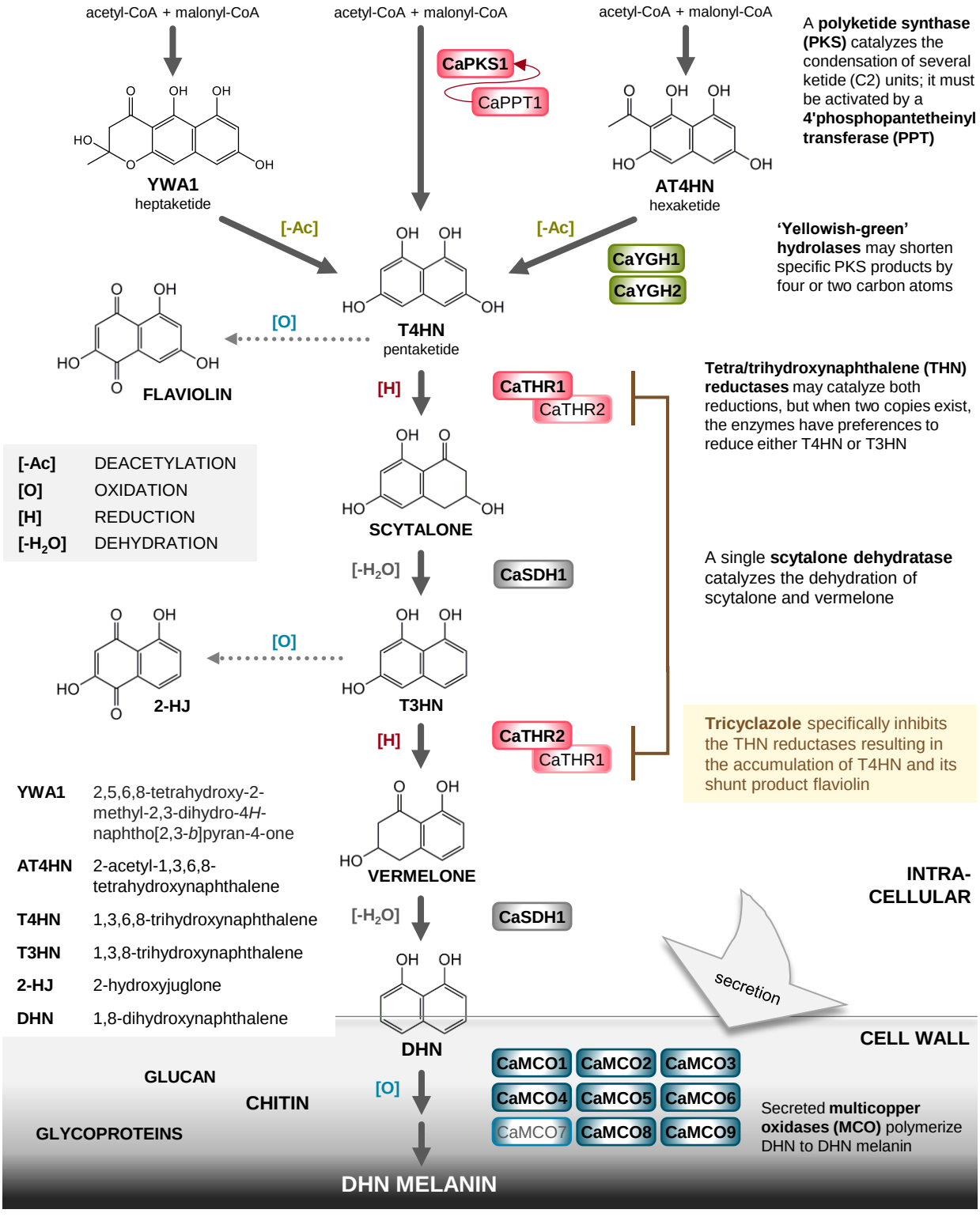

Figure S1. The proposed synthesis pathway of DHN melanin in *C. antarcticus*.

The putative DHN melanogenic genes of *C. antarcticus* were identified in the genome database based to their similarity with the ones described in *A. fumigatus* (**Figure 11A**). It is supposed that the PKS of *C. antarcticus* releases a longer polyketide (yellowish pigment) that is in turn deacetylated by CaYGH1/2 to T4HN. Nine MCO/laccases were identified due to their typical domain structure, for eight MCOs a N-terminal signal peptide for secretion was predicted (bold letters) (**Figure 11B**).

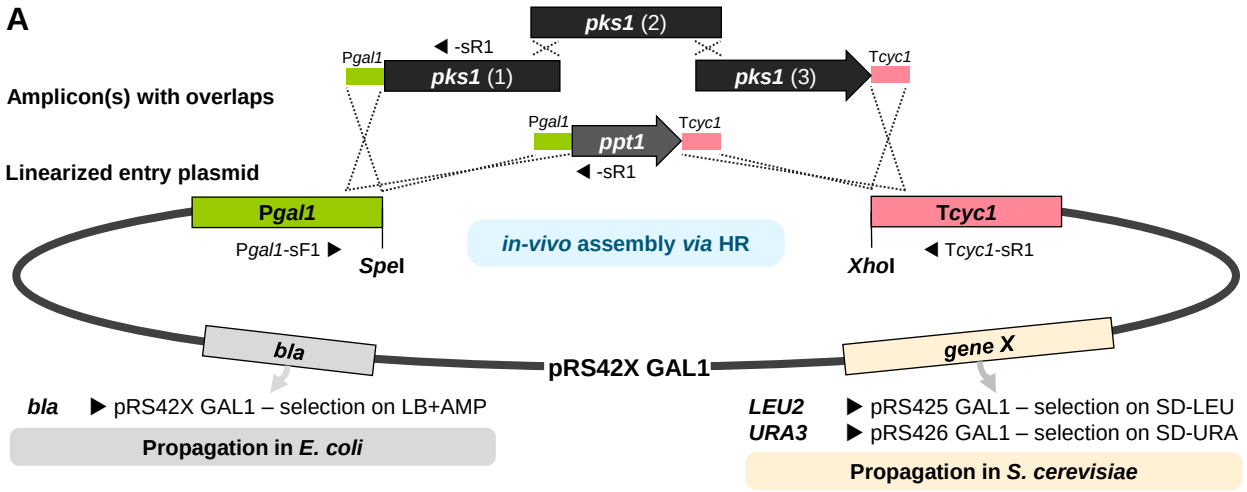

B

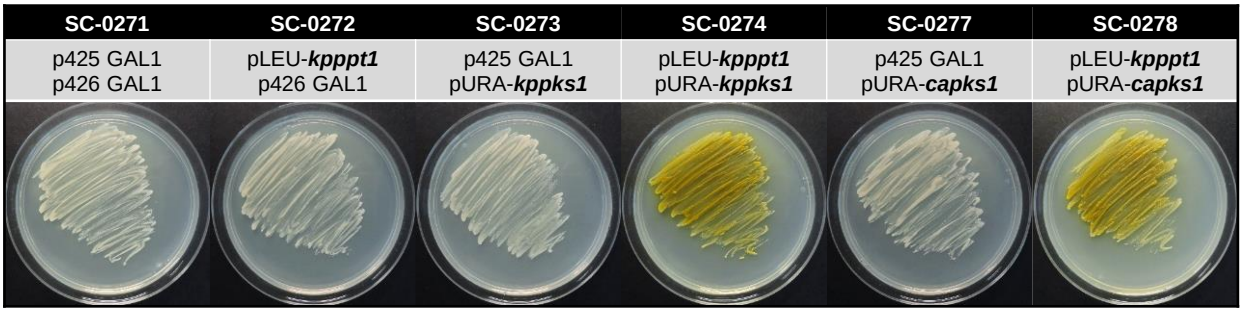

Figure S2. Heterologous expression of *C. antarcticus* and *K. petricola* genes in *S. cerevisiae*.

A. Cloning of the expression vectors. The genes of interest (*goi*) with their stop codons were amplified from genomic DNA as one fragment (*kpppt1*; no intron) or three fragments (*kppks1*, *capks1*; each gene with one intron) using primers for generating 25-bp-long overlaps with P*gal1* and T*cyc1*. Assembly in a *Spe*I+*Xho*I-digested entry plasmid of the pRS42X GAL1 series (Mumberg et al., 1994) was carried out in the LEU and URA-auxotrophic *S. cerevisiae* strain FY834 (**Table S4**). Plasmid DNA from LEU-prototrophic (p425 GAL1 derivatives, selected on SD-LEU) or URA-prototrophic (p426 GAL1 derivatives, selected on SD-URA) colonies was extracted and introduced into *E. coli*. Ampicillin-resistant *E. coli* colonies were screened by PCR for insert-carrying plasmids by combining a primer binding in a regulatory sequence (P*gal1*-sF1) with a primer binding in the insert (*goi*-sR1). The three cloned expression vectors, containing intron-free *kpppt1*, *kppks1* or *capks1*, were sequenced with primers P*gal1*-sF1 and T*cyc1*-sR1 for verification of the sequence. **B. Formation of the yellowish PKS products requires PPT activity (KpPPT1).** *S. cerevisiae* strain FY834 was co-transformed with plasmids containing *LEU2* or *URA3* and selected for LEU and URA prototrophy by using glucose-containing SD-LEU-URA (SD/GLU-LU) medium. Empty plasmids (p425 GAL1 and p426 GAL1) were transformed for mediating prototrophy of the control strains. Prototrophic *S. cerevisiae* colonies containing different combinations of *K. petricola* and *C. antarcticus* genes were streaked onto galactose-containing SD-LEU-URA (SD/GAL-LU) agar for induction of the galactose-responsive promoter (P*gal1*). Pictures were taken after three days of incubation at 30 °C in the dark. See also **Figure 12C**.

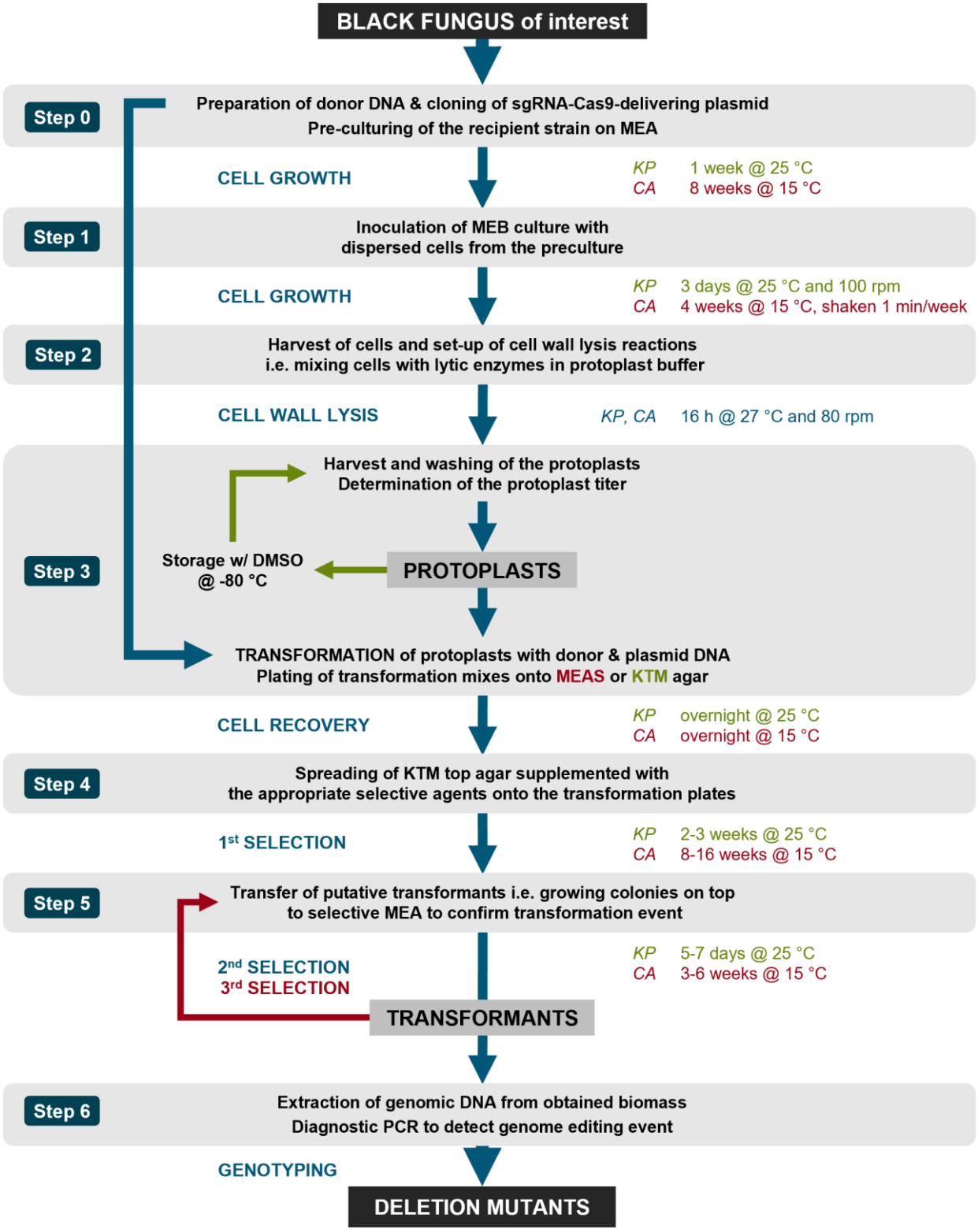

Figure S3. The generation of *C. antarcticus* deletion mutants takes eight to nine months.

Work and time flow of the generation and transformation of protoplasts, and the isolation and genotyping of resistant transformants of *K. petricola* [*KP*, in green] (Noack-Schönmann et al., 2014; Voigt et al., 2020; Erdmann et al., 2022) and *C. antarcticus* [*CA*, in red] (this study). The option to preserve *C. antarcticus* protoplasts with DMSO at -80°C has not been evaluated. Examples are shown: protoplasts and cells (**Figure 13C**), putative transformants on transformation plates and resistance transformants growing on selective medium (**Figure S4B**), and deletion mutants confirmed by diagnostic PCR to lack the gene of interest (**Figure S4C**).

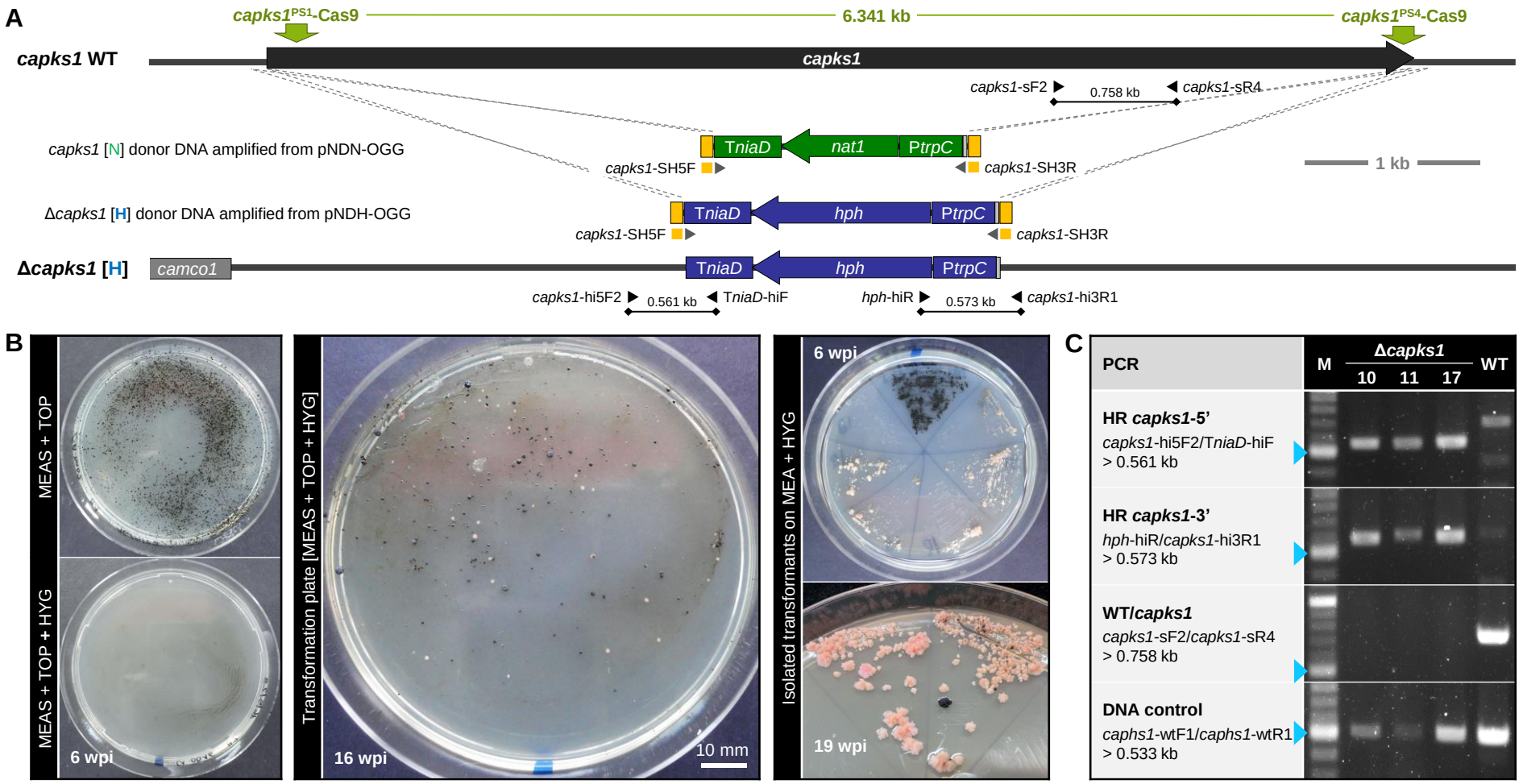

Figure S4. Generation and verification of *C. antarcticus pks1* deletion mutants.

A. Strategy for replacing *capks1* with a resistance cassette. Wild type protoplasts were transformed with the circular sgRNA/Cas9-delivering plasmid pAMA/tRNA-*capks1*^{PS1}-*capks1*^{PS4} and linear donor DNA that was amplified with the primer pair *capks1*-SH5F/*capks1*-SH3R from pNDN-OGG or pNDH-OGG. The primers attached 75-bp-long sequences homologous to the 5'- and 3'-noncoding regions of *capks1* to the resistance cassettes (orange bars). The Cas9 cutting sites are indicated as green arrows. **B. The transformation with donor DNA containing a hygromycin resistance (hygR) cassette yielded hygR transformants with different pigmentation.** Left: for control, protoplasts were transformed without DNA showing that protoplasts regenerates when no hygromycin (25 µg/ml HYG) was added. Middle: transformation plate with black and pinkish colonies. Right: examples of isolated transformants growing on HYG-containing medium. **C. Diagnostic PCR revealed three non-melanised Δ*capks1* mutants.** Homologous recombination (HR) events at 5' and 3' of *capks1* and the absence of *capks1* were detected by using the primer pairs shown. Blue triangles refer to the 0.5-kb-large band of the used DNA ladder (M).

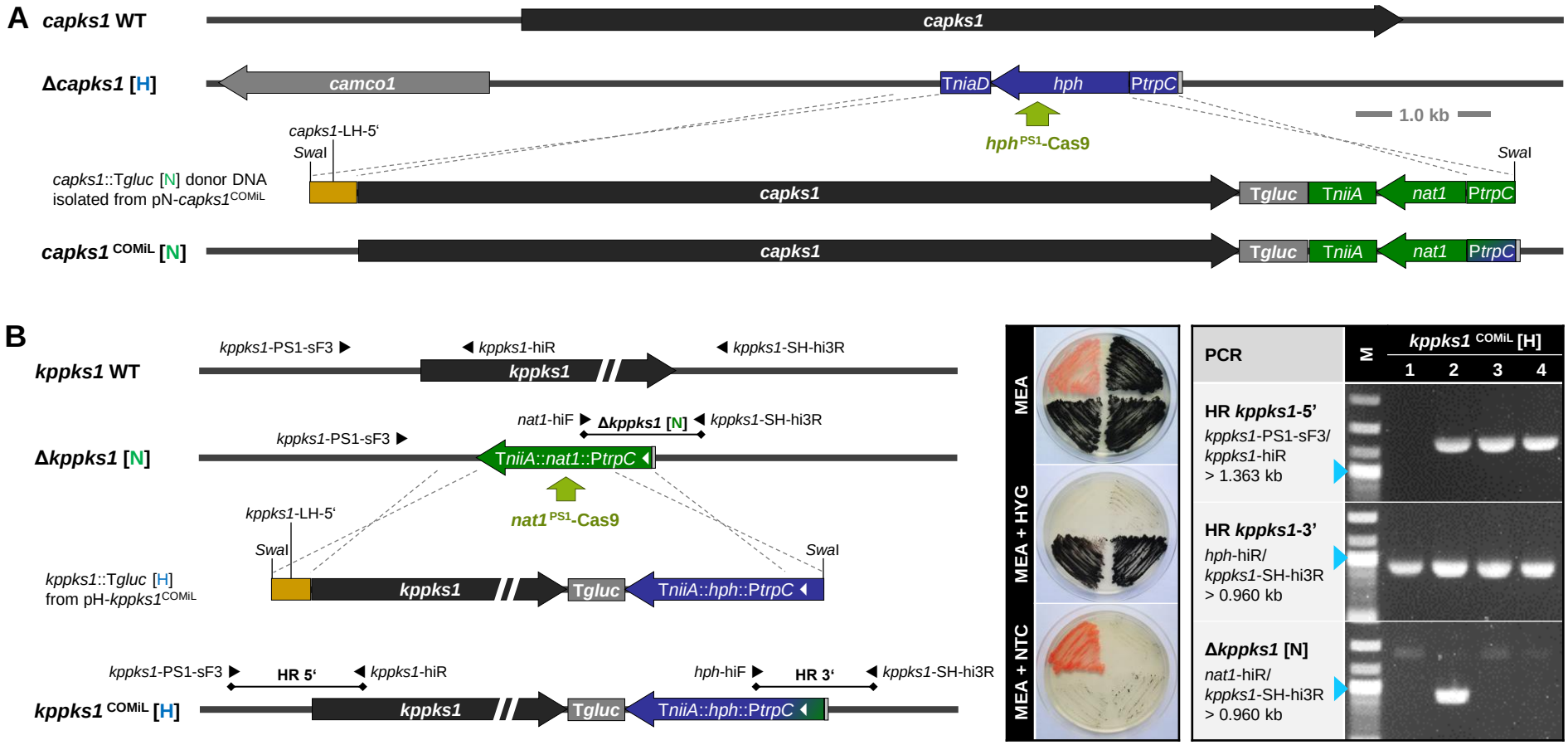

Figure S5. Complementation of deletion mutants by reintroducing the gene into the native locus.

A. Strategy pursued for replacing the hygromycin resistance (hygR) cassette in the Δ*capks1* mutant by a *capks1* expression construct. Protoplasts of Δ*capks1* were transformed with the circular sgRNA/Cas9-delivering plasmid pAMA/tRNA-*hph*^{PS1} and the linear expression construct *capks1*::T*gluc* [N] isolated from pN-*capks1* by digestion with *Swa*I. It was envisaged that the DSB in the hygR cassette would be repaired by homologous recombination via the 5'-noncoding region of *capks1* and P*trpC*, which is present in both resistance cassettes. However, nourseothricin-resistant (natR) transformants could not be isolated. **B. Validation of the strategy in *K. petricola* by complementing the natR Δ*kppks1* mutant.** Left: Δ*kppks1* protoplasts were transformed with pAMA/tRNA-*nat1*^{PS1} for inserting a DSB in *nat1* and the linear *kppks1*::T*gluc* [H] construct as donor DNA. Middle: Obtained hygR transformants [growth on MEA with 25 µg/ml of hygromycin (HYG)] had a black pigmentation and lost the ability to grow on MEA containing 5 µg/ml of nourseothricin (NTC). Wild type A95 (top right), melanin-deficient Δ*kppks1* (top left) and two transformants (T3, T4; bottom) were cultivated for five days. Right: The correct replacement of the natR cassette by the *kppks1* expression construct in transformants *kppks1* ^{COMiL} T3 and T4 was verified by diagnostic PCR (transformants 1 to 4 were tested). Light blue triangles highlight the 1-kb-band of the used DNA ladder (M).

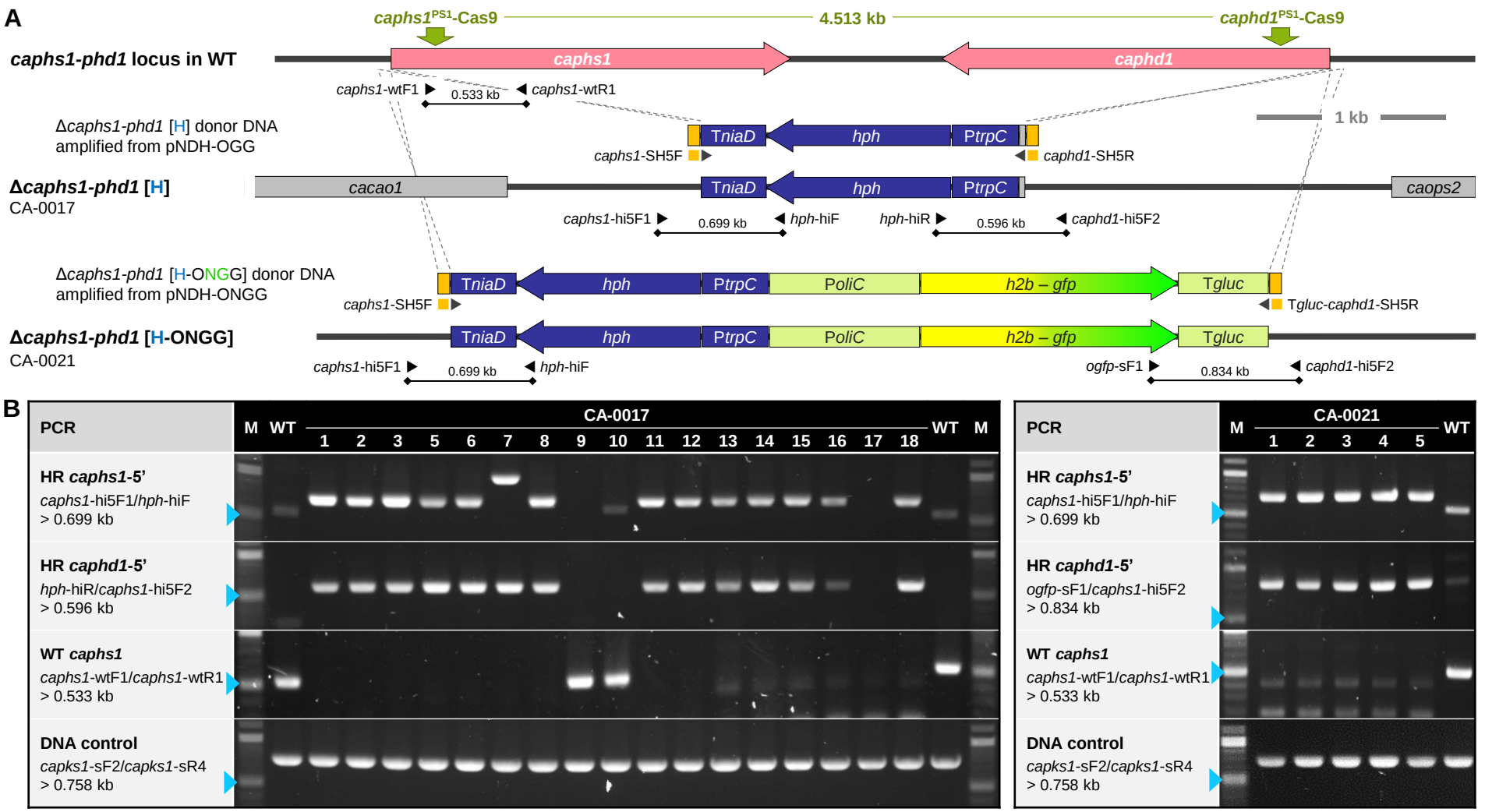

Figure S6. Replacement of the carotenogenic genes in *C. antarcticus*.

A. Strategies for replacing adjacent *caphs1* and *caphd1* in detail. Wild type protoplasts were transformed with the circular pAMA/tRNA-*caphs1*^{PS1}-*caphd1*^{PS1} and linear donor DNA, which was amplified from pNDH-OGG and pNDH-ONGG with the primer pairs *caphs1*-SH5F/*caphd1*-SH5R and *caphs1*-SH5F/ T*gluc*-*caphd1*-SH5R, respectively. Homologous recombination via the 75-bp-long homologous sequences (orange bars) results in the replacement of both genes. **B. Detection of replacement in obtained hygR transformants.** DNA from the hygR transformants was submitted to diagnostic PCR using the primer pairs as indicated. Light blue triangles highlight the 0.5-kb-band of the DNA ladder (M).

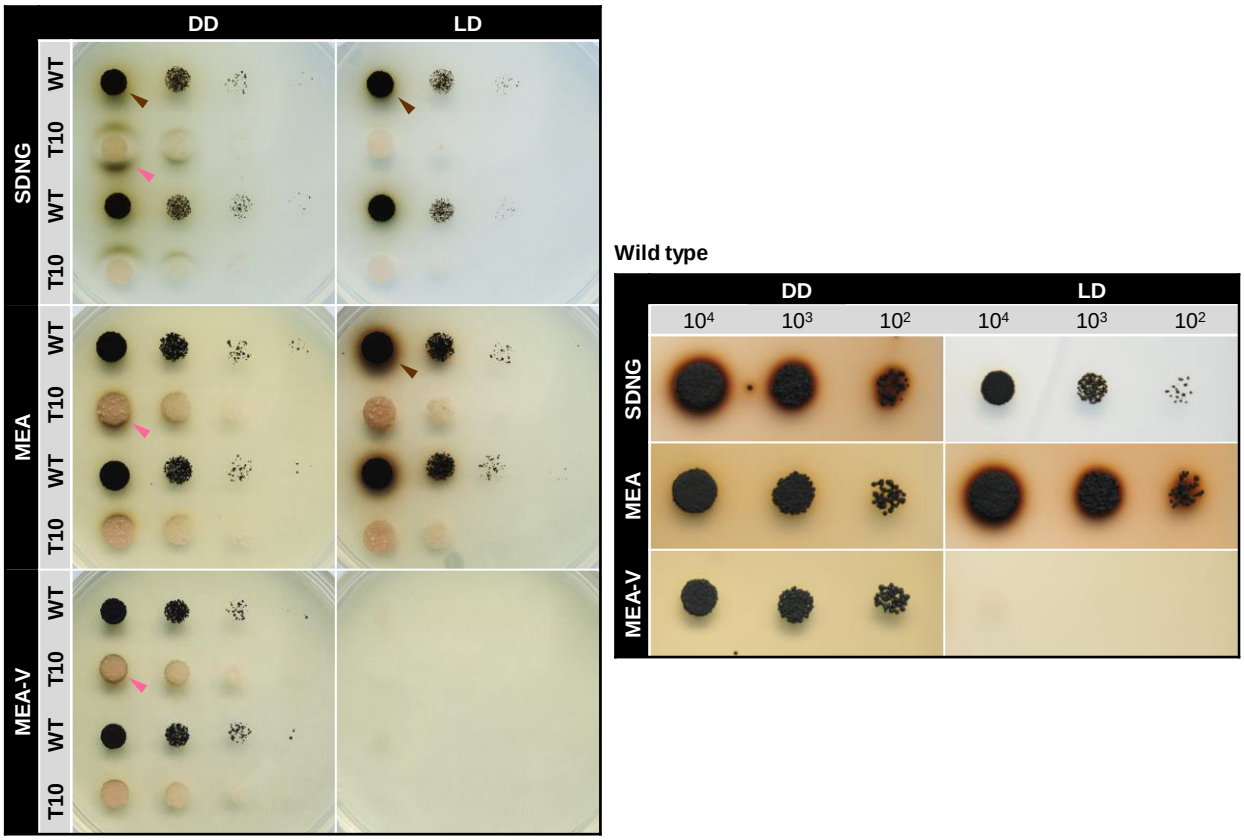

Figure S7. The *C. antarcticus* wild type but not the Δ*capks1* mutant secretes brownish pigments.

On the left: pictures of the *C. antarcticus* cultures shown in **Figure 16** were taken on a white background to demonstrate the secretion of brownish pigments by the wild type, and the uptake and conversion of these pigments by the Δ*capks1* mutant when cultivated under DD conditions in contrast to LD conditions. Brown arrows: secretion of brownish water-soluble metabolites by WT; pink arrows: conversion of the brownish metabolites to black DHN melanin by non-melanised mutant. On the right: pictures of a drop assay in which cell suspensions of the wild type (alone) were spotted on the same media and incubated for three months in the two different light conditions. Note the staining of the media (SDNG in DD and MEA in LD) due to the secretion of the brownish metabolites in the absence of Δ*capks1* colonies.

Table S1. *Cryomyces antarcticus* melanogenic and carotenogenic genes.

Name	Description	JGI protein ID	Size	Note	Location	Possible allelic (secondary) variant
CaPPT1	Phosphopantetheinyl transferase	**Cryan3|30097**	337 aa	primary allele	Scaffold_01: 1742250-1743437	n/a
CaPKS1	Polyketide synthase	**Cryan3|585847**	2165 aa	primary allele	Scaffold_06: 122131-129243	Protein ID **456827** on scaffold_42
CaYGH1	Yellowish-green hydrolase	**Cryan3|833091**	419 aa	primary allele	Scaffold_01: 630851-632345	Protein ID **858952** on scaffold_40
CaYGH2	Yellowish-green hydrolase	**Cryan3|27039**	397 aa	primary allele	Scaffold_01: 1579623-1581597	Protein ID **548851** on scaffold_52
CaTHR1	T4HN reductase	**Cryan3|836228**	270 aa	primary allele	Scaffold_03: 205816-206693	Protein ID **995051** on scaffold_28
CaTHR2	T3HN reductase	**Cryan3|586390**	266 aa	primary allele	Scaffold_06: 147010-148334	Protein ID **1031432** on scaffold_42
CaSDH1	Scytalone dehydratase	**Cryan3|954298**	195 aa	primary allele	Scaffold_33: 504911-505643	Protein ID **543413** on scaffold_51
CaCMR1	Transcription factor	**Cryan3|586214**	964 aa	primary allele	Scaffold_06: 141665-145152	Protein ID **1031431** on scaffold_42
CaFET1	Multicopper oxidase/ferroxidase	**Cryan3|837159**	601 aa	primary allele	Scaffold_04: 520366-522519	Protein ID **710496** on scaffold_9
CaMCO1	Multicopper oxidase/laccase	**Cryan3|586223**	595 aa	primary allele	Scaffold_06: 132368-134973	Protein ID **1068762** on scaffold_42
CaMCO2	Multicopper oxidase/laccase	**Cryan3|839253**	544 aa	primary allele	Scaffold_06: 927319-929072	Protein ID **957745** on scaffold_67
CaMCO3	Multicopper oxidase/laccase	**Cryan3|856845**	644 aa	primary allele	Scaffold_35: 413320-415153	Protein ID **861533** on scaffold_48
CaMCO4	Multicopper oxidase/laccase	**Cryan3|860958**	619 aa	primary allele	Scaffold_46: 313375-315394	Protein ID **1070979** on scaffold_60
CaMCO5	Multicopper oxidase/laccase	**Cryan3|1057704**	563 aa	primary allele	Scaffold_02: 1111648-1113613	Protein ID **956007** on scaffold_45
CaMCO6	Multicopper oxidase/laccase	**Cryan3|452356**	619 aa	primary allele	Scaffold_41: 247514-250025	Protein ID **1115966** on scaffold_45 Protein ID **1034174** on scaffold_148
CaMCO7	Multicopper oxidase/laccase	**Cryan3|453744**	553 aa	primary allele	Scaffold_41: 320863-323412	Protein ID **1115935** on scaffold_45
CaMCO8	Multicopper oxidase/laccase	**Cryan3|846371**	802 aa	primary allele	Scaffold_15: 894719-898717	n/a
CaMCO9	Multicopper oxidase/laccase	**Cryan3|50117**	1007 aa	primary allele	Scaffold_10: 1004053-1008308	n/a
CaPHS1	Phytoene synthase/lycopene cyclase	**Cryan3|1119942**	628 aa	primary allele	Scaffold_55: 156344-158724	Protein ID **1104509** on scaffold_26
CaPHD1	Phytoene desaturase	**Cryan3|1070518**	635 aa	primary allele	Scaffold_55: 153713-155792	Protein ID **273264** on scaffold_26
CaCAO1	Carotenoid oxygenase	**Cryan3|1011935**	738 aa	primary allele	Scaffold_55: 159475-162523	Protein ID **993463** on scaffold_26
CaOPS2	Green light-absorbing microbial opsin	**Cryan3|563816**	322 aa	primary allele	Scaffold_55: 150397-151843	Protein ID **1065685** on scaffold_26

Genes and proteins from *Cryomyces antarcticus* strain CBS 116301 (DOE Joint Genome Institute) are shown. Many of the smaller scaffolds are very similar to larger scaffolds and are predicted to constitute an alternate or secondary haplotype. Thus, 'primary alleles' and 'secondary alleles' gene model tracks are given in the genome portal (https://mycocosm.jgi.doe.gov/mycocosm/home). The primary alleles are listed only for providing a non-redundant set of genes putatively involved in DHN melanin formation.

Table S2. Accession numbers of proteins associated with DHN melanogenesis from other fungi.

	Aspergillus fumigatus **Af293 [Eurotiomycetes]**		***Alternaria alternata*** **ATCC 66981 [Dothideomycetes]**		***Neurospora crassa*** **OR74A [Sordariomycetes]**		***Botrytis cinerea*** **B05.10 [Leotiomycetes]**	
	Name [size]	Locus tag GenBank acc.	Name [size]	Protein ID JGI	Name [size]	Locus tag GenBank acc.	Name [size]	Locus tag GenBank acc.
Phosphopantetheinyl transferase (PPT)	NpgA [359 aa]	Afu2g08590 XP_755193.1	PPT1 [375 aa]	Alalte1|106450	PPT-1 [348 aa]	NCU00581 XP_965721.2	PPT1 [354 aa]	BCIN_06g04100 ATZ50945.1
Polyketide synthase (PKS)	Alb1 [2146 aa]	Afu2g17600 XP_756095.1	PKSA [2161 aa]	Alalte1|111952	PER-1 [2206 aa]	NCU03584 XP_960586.3	PKS12 [2147 aa]	BCIN_02g08770 ATZ47616.1
Polyketide synthase (PKS)	*no hit*	*no hit*	*no hit*	*no hit*	*no hit*	*no hit*	PKS13 [2138 aa]	BCIN_03g08050 ATZ48614.1
Yellowish-green hydrolase (YGH)	Ayg1 [406 aa]	Afu2g17550 XP_756090.1	AYGA [420 aa]	Alalte1|115293	PKH-2 [430 aa]	NCU05821 XP_960081.1	YGH1 [410 aa]	BCIN_02g04360 ATZ47119.1
Yellowish-green hydrolase (YGH)	*no hit*	*no hit*	AYGB [403 aa]	Alalte1|105009	PKH-1 [487 aa]	NCU01903 XP_965534.3	*no hit*	*no hit*
Tetrahydroxynaphthalene reductase (T4HNR)	Arp2 [273 aa]	Afu2g17560 XP_756091.1	BRM3 [268 aa]	Alalte1|112254	PKR-2 [268 aa]	NCU06905 XP_959252.1	BNR2 [266 aa]	BCIN_03g08100 ATZ48619.1
Trihydroxynaphthalene reductase (T3HNR)	*no hit*	*no hit*	BRM2 [267 aa]	Alalte1|111954	PKR-1 [282 aa]	NCU09390 XP_011395293.1	BNR1 [289 aa]	BCIN_04g04800 ATZ49315.1
Scytalone dehydratase (SDH)	Arp1 [168 aa]	Afu2g17580 XP_756093.1	BRM1 [185 aa]	Alalte1|105968	SCY-1 [174 aa]	NCU07823 XP_962944.1	SCD1 [167 aa]	BCIN_03g08110 ATZ48620.1
C2H2-Zn(2)Cys(6) transcription factor	RegA [866 aa]	Afu1g17640 XP_753130.1	CMR1 [1010 aa]	Alalte1|111953	SAH-12 [1241 aa]	NCU02787 XP_963943.3	SMR1 [938 aa]	BCIN_02g08760 ATZ47614.1
Multicopper oxidase/laccase (MCO)	Abr1 [664 aa]	Afu2g17540 XP_756089.2	n/a	n/a	n/a	n/a	n/a	n/a
Multicopper oxidase/laccase (MCO)	Abr2 [587 aa]	Afu2g17530 XP_756088.2	n/a	n/a	n/a	n/a	n/a	n/a
Multicopper oxidase/ferroxidase (FET)	FetC [592 aa]	Afu5g03790 XP_747965.2	FET1 [586 aa]	Alalte1|114711	LCC3 [693 aa]	NCU03498 XP_955835.1	FET1 [615 aa]	BCIN_02g02780 ATZ46936.1
Phytoene synthase/lycopene cyclase (PHS1)	*no hit*	*no hit*	[583 aa]	Alalte1|108710	AL-2 [602 aa]	NCU00585 XP_965725.3	PHS1 [610 aa]	BCIN_01g04560 ATZ45729.1
Phytoene desaturase (PHD1)	*no hit*	*no hit*	[628 aa]	Alalte1|108713	AL-1 [595 aa]	NCU00552 XP_964713.1	PHD1 [602 aa]	BCIN_01g04550 ATZ45728.1
Carotenoid oxygenase (CAO1)	*no hit*	*no hit*	[707 aa]	Alalte1|108711	*no hit*	*no hit*	CAO1 [649 aa]	BCIN_01g04570 ATZ45730.1
Green light-absorbing microbial opsin (OPS2)	*no hit*	*no hit*	[308 aa]	Alalte1|108712	[292 aa]	NCU01735 XP_011393497.1	BOP2 [338 aa]	BCIN_01g04540A TZ45726.1

Table S3. Oligonucleotides used in this study.

Name	Sequence (5'→ 3')	Features (5'→ 3')/binding sites
***Kpppt1*-P*gal1*-F**	aggagaaaaaaccccggattctaga-ATGGCCTACACCACCGGCGATG	*S. cerevisiae* P*gal1* – *kpppt1*
***Kpppt1*-T*cyc1*-R**	taagcgtgacataactaattacatg-TCAGTCGAGACAACAACATTTGCC	*S. cerevisiae* T*cyc1* – *kpppt1*
***Kpppt1*-wtR**	GAGCGAAGTGTGCATGGTGTGTG	*K. petricola ppt1* coding region
***Kppks1*-P*gal1*-F**	aggagaaaaaaccccggattctaga-ATGGAGGAAGTCTACGTGTTCGG	*S. cerevisiae* P*gal1* – *kppks1* start of coding region
***Kppks1*-T*cyc1*-R**	taagcgtgacataactaattacatg-TTAGCCCTGAATGGCTTCACGAATG	*S. cerevisiae* T*cyc1* – *kppks1* end coding region
***Kppks1*-Y1R**	AGCATTTTCAGAGCGTTCATCAACATATATAC	*K. petricola pks1* coding region
***Kppks1*-Y2F**	ggctgtatatatgttgatgaacgctctgaaaatgctc-CAATGAAATGACAAAACTGAGAAATGCAAAG	*K. petricola pks1* coding region deleted for intron
***Kppks1*-wtF2**	GCCGATCTGGCATACACCACCAC	*K. petricola pks1* coding region
***Kppks1*-wtR2**	GTCCGAGACGCCGTTGATGCATG	*K. petricola pks1* coding region
P*gal1*-sF1	GTCGCGTTCCTGAAACGCAGATG	*S. cerevisiae* P*gal1* in p42X GAL1
T*cyc1*-sR1	GGACCTAGACTTCAGGTTGTCTAAC	*S. cerevisiae* T*cyc1* in p42X GAL1
***Capks1*-P*gal1*-F**	aggagaaaaaaccccggattctaga-ATGTCCAACATCGTACTTTTCGGC	*S. cerevisiae* P*gal1* – *capks1* start of coding region
***Capks1*-T*cyc1*-R**	aagcgtgacataactaattacatg-ctatgcggagagaccgagtccctgtctgat gagacggccaagggtttcacc-GTGTTCATCACGCATCATCGTGAAG	*S. cerevisiae* T*cyc1* – *capks1* end of coding region with deleted intron
***Capks1*-sF1**	GGCTGAGGAGACACTCCACTTGG	*C. antarcticus pks1* coding region
***Capks1*-sF2**	GAACACTGAGGCCACTGCTTCCG	*C. antarcticus pks1* coding region
***Capks1*-sF3**	GCCGCTATCCAACTCGCTTGTAC	*C. antarcticus pks1* coding region
***Capks1*-sF4**	GCGAGTATGCTGCTCTTCACGTTG	*C. antarcticus pks1* coding region
***Capks1*-sF5**	GTTGCTTGGTCACCATTGCCCAG	*C. antarcticus pks1* coding region
***Capks1*-sR5**	GTTCCAATACGGTGCAACTTCGTCG	*C. antarcticus pks1* coding region
***Capks1*-sR1**	GTGATTCTTGCGAAGAGCCTCCG	*C. antarcticus pks1* coding region
***Capks1*-sR2**	GTGTTACCACCGGCAGCAGAGAAG	*C. antarcticus pks1* coding region
***Capks1*-sR3**	GTCGGAAGCGTTGACGATGAAGCC	*C. antarcticus pks1* coding region
***Capks1*-sR4**	GAGCGGCACCATCGTATTGTGAG	*C. antarcticus pks1* coding region
pFC334-F1	GGTCATAGCTGTTTCCGCTGA	pFC332/pFC902 and derivatives
pFC334-R1	TGATTCTGCTGTCTCGGCTG	pFC332/pFC902 and derivatives
P*afU3*-sF1	GCTTGAGGTTAGCGCACTCGCTAG	*A. fumigatus* P*U3* in pFC902 and derivatives
P*tef1*-sR1	CGTTCGAGAGCATGATCAGCAC	*A. nidulans* P*tef1* in pFC332 and derivatives

Name	Sequence (5'→ 3')	Features (5'→ 3')/binding sites
***Capks1*-tRNA-PS1F**	gctaccgcgctctcagcgtg-GTTTTAGAGCTAGAAATAGCAAGTTAAAAT	*C. antarcticus pks1*-PS1 – sgRNA in pFC902
***Capks1*-tRNA-PS1R**	cacgctgagagcgcggtagc-TGCATCATCCGTGAATCGAAC	*C. antarcticus pks1*-PS1 – tRNA in pFC902
***Capks1*-tRNA-PS4F**	gccagtgctaacattgtcac-GTTTTAGAGCTAGAAATAGCAAGTTAAAAT	*C. antarcticus pks1*-PS4 – sgRNA in pFC902
***Capks1*-tRNA-PS4R**	gtgacaatgttagcactggc-TGCATCATCCGTGAATCGAAC	*C. antarcticus pks1*-PS4 – tRNA in pFC902
***Capks1*-SH5F**	cactcgctgcatttacgagatctatcgacctataccatatcatctacgaacgatccatcccctaaaataatcaat-GCTAAGCGAGCGGGAGCTATCG	*C. antarcticus pks1*-5' (75 nt) – *B. cinerea* T*niaD*
***Capks1*-SH3R**	agggtaccactccgcagcgtcaccaaggcactgtggaaaaagaagaatcacacatgtatctgtcgagaaggaagt-GAATCGGGAATGCGGCTCCACAG	*C. antarcticus pks1*-3' (75 nt) – *A. nidulans* P*oliC*
***Capks1*-hi5F1**	GATCATCAGTCCACTTCCAGCCCG	*C. antarcticus pks1*-5' non-coding region
***Capks1*-hi5F2**	GGCAGCATAGGAGGCACTGGATAC	*C. antarcticus pks1*-5' non-coding region
***Capks1*-hi3R1**	GCTCCAACCAGATTGCCAATATCG	*C. antarcticus pks1*-3' non-coding region
***Capks1*-hi3R2**	GCCACAGCTGTGATCGATGTAATC	*C. antarcticus pks1*-3' non-coding region
***Caphs1*-tRNA-PS1R**	cggggtagtagagacaaggg-TGCATCATCCGTGAATCGAAC	*C. antarcticus phs1*-PS1 – tRNA in pFC902
***Caphs1*-tRNA-PS1F**	cccttgtctctactaccccg-GTTTTAGAGCTAGAAATAGCAAGTTAAAAT	*C. antarcticus phs1*-PS1 – gRNA in pFC902
***Caphd1*-tRNA-PS1R**	caggtgtatcgctaacattc-TGCATCATCCGTGAATCGAAC	*C. antarcticus phd1*-PS1 – tRNA in pFC902
***Caphd1*-tRNA-PS1F**	gaatgttagcgatacacctg-GTTTTAGAGCTAGAAATAGCAAGTTAAAAT	*C. antarcticus phd1*-PS1 – gRNA in pFC902
***Caphs1*-SH5F**	gctgtccacctccggaagcgctccatcccccgcttctcactctcatggcccggtaacgactactttgacgcgca-GCTAAGCGAGCGGGAGCTATCG	*C. antarcticus phs1*-5' (75 nt) – *B. cinerea* T*niaD*
***Caphd1*-SH5R**	gctcccggcgcacgcagtcggacatcttcacatcaaaccgccgacatgtgattccctcaactcacgtataatgcg-GAATCGGGAATGCGGCTCCACAG	*C. antarcticus phd1*-5' (75 nt) – *A. nidulans* P*oliC*
***Caphs1*-wtF1**	GCTCTGCTGCACTCACTGACCG	*C. antarcticus phs1* coding region
***Caphs1*-wtR1**	GATTGGCAAGAGTGTGTTCGACAGTG	*C. antarcticus phs1* coding region
***Caphs1*-hi5F1**	CTCGACGAGAGTCGTGGCTGCACTG	*C. antarcticus phs1*-5' non-coding region
***Caphs1*-hi5F2**	GTCTGCACTGCTTCTCGCCAACACG	*C. antarcticus phs1*-5' non-coding region
***Caphd1*-hi5F1**	GCCTTCAACCCGTTGTCCTAATGG	*C. antarcticus phd1*-5' non-coding region
***Caphd1*-hi5F2**	GAGTGTACGCCTTTGCCATGCTGAG	*C. antarcticus phd1*-5' non-coding region
T*niaD*-hiF	GGTGCCAGATGTATCAGTGAGTCTG	*B. cinerea* T*niaD*
***Hph*-hiF**	GTCTGGACCGATGGCTGTGTAGAAG	*hph* [hygromycin resistance (hygR, H) cassette]
***Hph*-hiR**	GACAGACGTCGCGGTGAGTTCAG	*hph* [hygromycin resistance (hygR, H) cassette]
***Nat1*-hiF**	CGGCGAGCAGGCGCTCTACATGAGC	*nat1* [nourseothricin resistance (natR, N) cassette]

Name	Sequence (5'→ 3')	Features (5'→ 3')/binding sites
***Nat1*-hiR**	GTACCGGTAAGCCGTGTCGTCGAG	*nat1* [nourseothricin resistance (natR, N) cassette]
***Ogfp*-sF1**	GGTGATGGTCCAGTCTTGCTC	*B. cinerea* optimised *gfp* coding region
***Hph*-tRNA-PS1R**	cgtattgggaatccccgaac-TGCATCATCCGTGAATCGAAC	*hph*-PS1 – tRNA in pFC902
***Hph*-tRNA-PS1F**	gttcggggattcccaatacg-GTTTTAGAGCTAGAAATAGCAAGTTAAAAT	*hph*-PS1 – gRNA scaffold in pFC902
***Nat1*-tRNA-PS1R**	tggtcaggggcgggtccacc-TGCATCATCCGTGAATCGAAC	*nat1*-PS1 – tRNA in pFC902
***Nat1*-tRNA-PS1F**	ggtggacccgcccctgacca-GTTTTAGAGCTAGAAATAGCAAGTTAAAAT	*nat1*-PS1 – gRNA scaffold in pFC902
P*oliC*-pRS426-5F	gccagggttttcccagtcacga-ccgcgg-atttaaat-TGCAGCTGTGGAGCCGCATTCCCG	pRS426-5F – *Sac*II – *Swa*I – *A. nidulans* P*oliC*
T*gluc*-R1	GATCTTGTTGGGGGGAAGGGGTTGTCAAATC	*B. cinerea* T*gluc*
P*trpC*-SS-pRS426-3R	ggataacaatttcacacaggaaaca-atttaaat-actagt-GATATTGAAGGAGCATTTTTTGGGC	pRS426-3R – *Swa*I – *Spe*I – *A. nidulans* P*trpC*
T*niiA*-*Pac*I-T*gluc*-F	caaccccttccccccaacaagat-taattaa-CAGATGCTGCTGGCAAGGTTACATC	*B. cinerea* T*gluc* – *Pac*I – *B. cinerea* T*niiA*
T*gluc*-hiF	CATACGTACATCTGATTTGACAACC	*B. cinerea* T*gluc*
T*gluc*-sR2	CCGCCCTCTTTTGTCTTCCGC	*B. cinerea* T*gluc*
P*oliC*-sF2	GGGAGACGTATTTAGGTGCTAGGG	*A. nidulans* P*oliC*
pRS426-s5F2	GTAGCGGTCACGCTGCGCGTAACC	upstream of cloning site in pRS42X derivatives
pRS426-s3R2	CATTAATGCAGCTGGCACGACAGG	downstream of cloning site in pRS42X derivatives
***Capks1*-pRS426-5F**	gtaacgccagggttttcccagtcacg-atttaaat-GGCAGCATAGGAGGCACTGGATAC	pRS426-5F – *Swa*I – *capks1*-5'
***Capks1*-T*gluc*-R**	taatcatacatcttatctacatacg-CTATGCGGAGAGACCGAGTCCCTG	*B. cinerea* T*gluc* – *capks1*
***Kppks1*-pRS426-5F**	gtaacgccagggttttcccagtcacg-atttaaat-CAGGTCGGTTTCCGAATCTCAATG	pRS426-5F – *Swa*I – *kppks1*-5'
***Kppks1*-COM-5R**	ACACCAGATACAGCCTCACCGTGACCAATGTTGGACTTGA	*K. petricola pks1* coding region
***Kppks1*-T*gluc*-R**	taatcatacatcttatctacatacg-TTAGCCCTGAATGGCTTCACGAATG	*B. cinerea* T*gluc* – *kppks1*
***Kppks1*-PS1-sF3**	GCTGGTAGAGTACGCTATATCCGC	*K. petricola pks1*-5' non-coding region
***Kppks1*-wtF3**	GGCCGACTGAACTACTTCTTCAAG	*K. petricola pks1* coding region
***Kppks1*-hiR**	GCTCCAGCTCTGAAAGCAATGCG	*K. petricola pks1* coding region
***Kppks1*-SH-hi3R**	GAGTTAGATTCGAGACACTCCACCAG	*K. petricola pks1*-3' non-coding region

Lowercase letters – 5' overhangs for cloning or for homologous recombination; uppercase letters – 3' part of the DNA oligonucleotides annealing to template DNA.

Table S4. Plasmids cloned in this study.

Name [ID] (size)	Entry plasmid	Amplicon(s)			Assembly
pLEU-*kpppt1* [pEC0242] (8.572 kb)	**p425 GAL1** (Mumberg et al., 1994) digested w/ *Spe*I + *Xho*I	***kpppt1*** (1.101 kb) primers: *kpppt1*-P*gal1*-F/*kpppt1*-T*cyc1*-R template: *K. petricola* gDNA			*in vivo*
pURA-*kppks1* [pEC0243] (12.897 kb)	**p426 GAL1** (Mumberg et al., 1994) digested w/ *Spe*I + *Xho*I	***kppks1*-Y1** (0.339 kb) primers: *kppks1*-P*gal1*-F/*kppks1*-Y2F template: *K. petricola* gDNA	***kppks1*-Y2** (2.893 kb) primers: *kppks1*-Y1R/*kppks1*-wtR2 template: *K. petricola* gDNA	***kppks1*-Y3** (4.039 kb) primers: *kppks1*-wtF2/*kppks1*-T*cyc1*-R template: *K. petricola* gDNA	*in vivo*
pURA-*capks1* [pEC0390] (12.846 kb)	**p426 GAL1** (Mumberg et al., 1994) digested w/ *Spe*I + *Xho*I	***capks1*-1** (2.418 kb) primers: *capks1*-P*gal1*-F/*capks1*-sR2 template: *C. antarcticus* gDNA	***capks1*-2** (2.461 kb) primers: *capks1*-sF1/*capks1*-sR3 template: *C. antarcticus* gDNA	***capks1*-3** (2.068 kb) primers: *capks1*-sF2/*capks1*-T*cyc1*-R template: *C. antarcticus* gDNA	*in vivo*
pAMA/tRNA-*capks1*^{PS1}-*capks1*^{PS4} [pEC0256] (16.670 kb)	**pFC332** (Nødvig et al., 2015) digested with *Pac*I	***capks1*^{PS1} tRNA** (0.589 kb) primers: pFC334-F1/ *capks1*-tRNA-PS1R template: pFC902 (Nødvig et al., 2018)	***capks1*^{PS1}/*capks1*^{PS4} tRNA** (0.191 kb) primers: *capks1*-tRNA-PS1F/ *capks1*-tRNA-PS4R template: pFC902 (Nødvig et al., 2018)	***capks1*^{PS4} tRNA** (0.427 kb) primers: *capks1*-tRNA-PS4F/ pFC334-R1 template: pFC902 (Nødvig et al., 2018)	*in vitro*
pAMA/tRNA-*caphs1*^{PS1}-*caphd1*^{PS1} [pEC0448] (16.670 kb)	**pFC332** (Nødvig et al., 2015) digested with *Pac*I	***caphs1*^{PS1} tRNA** (0.589 kb) primers: pFC334-F1/ *caphs1*-tRNA-PS1R template: pFC902 (Nødvig et al., 2018)	***caphs1*^{PS1}/*caphd1*^{PS1} tRNA** (0.191 kb) primers: *caphs1*-tRNA-PS1F/ *caphd1*-tRNA-PS1R template: pFC902 (Nødvig et al., 2018)	***caphd1*^{PS1} tRNA** (0.427 kb) primers: *caphd1*-tRNA-PS1F/ pFC334-R1 template: pFC902 (Nødvig et al., 2018)	*in vitro*
pAMA/tRNA-*hph*^{PS1} [pEC0461] (16.499 kb)	**pFC332** (Nødvig et al., 2015) digested with *Pac*I	***hph*^{PS1} tRNA-A** (0.589 kb) primers: pFC334-F1/*hph*-tRNA-PS1R template: pFC902 (Nødvig et al., 2018)		***hph*^{PS1} tRNA-B** (0.427 kb) primers: *hph*-tRNA-PS1F/pFC334-R1 template: pFC902 (Nødvig et al., 2018)	*in vitro*
pAMA/tRNA-*nat1*^{PS1} [pEC0462] (16.499 kb)	**pFC332** (Nødvig et al., 2015) digested with *Pac*I	***nat1*^{PS1} tRNA-A** (0.589 kb) primers: pFC334-F1/*nat1*-tRNA-PS1R template: pFC902 (Nødvig et al., 2018)		***nat1*^{PS1} tRNA-B** (0.427 kb) primers: *nat1*-tRNA-PS1F/pFC334-R1 template: pFC902 (Nødvig et al., 2018)	*in vitro*
pH-OCG [pEC0459] (9.655 kb)	**pRS426$^{\Delta NcoI}$** (Schumacher, 2012) digested w/ *EcoR*I + *Xho*I	**P*oliC*::*mch*::T*gluc*** (2.152 kb) primers: P*oliC*-pRS426-5F/T*gluc*-R1 template: pIGR1S-OCG [pEC0407] (unpublished)		**P*trpC*::*hph*::T*niiiA*** (2.071 kb) primers: P*trpC*-SS-pRS426-3R/T*niiA*-*Pac*I-T*gluc*-F template: pNAH-GGG [pEC0046] (Erdmann et al., 2022)	*in vivo*
pN-OCG [pEC0460] (9.190 kb)	**pRS426$^{\Delta NcoI}$** (Schumacher, 2012) digested w/ *EcoR*I + *Xho*I	**P*oliC*::*mch*::T*gluc*** (2.152 kb) primers: P*oliC*-pRS426-5F/T*gluc*-R1 template: pIGR1S-OCG [pEC0407] (unpublished)		**P*trpC*::*nat1*::T*niiiA*** (1.598 kb) primers: P*trpC*-SS-pRS426-3R/T*niiA*-*Pac*I-T*gluc*-F template: pNAN-GGG [pEC0120] (Erdmann et al., 2022)	*in vivo*
pN-*capks1*-COMIL [pEC0466] (14.477 kb)	**pN-OCG** [pEC0459] (this study) digested w/ *Sac*II + *Not*I	***capks1*-5'::*capks1*** (6.918 kb) primers: c*apks1*-pRS426-5F/*capks1*-T*gluc*-R template: *C. antarcticus* gDNA			*in vivo*
pH-*kppks1*-COMIL [pEC0478] (14.975 kb)	**pH-OCG** [pEC0460] (this study) digested w/ *Sac*II + *Not*I	***kppks1* [1]** (2.562 kb) primers: *kppks1*-pRS426-5F/*kppks1*-COM-5R template: *K. petricola* gDNA		***kppks1* [2]** (4.995 kb) primers: *kppks1*-wtF3/*kppks1*-T*gluc*-R template: *K. petricola* gDNA	*in vivo*

Table S5. Transformations of *C. antarcticus* and *K. petricola* carried out in this study.

Strain (alias)	BAM ID	Entry	Donor DNA	CRISPR/Cas9 plasmid	Attempts	Results
Δ***capks1*** **[N]**	**CA-0001**	*C. antarcticus* **WT:515**	**[(T*niaD*::*nat1*::P*trpC*)]** $^{\Delta capks1}$ (1.473 kb) primers: *capks1*-SH5F/*capks1*-SH3R template: pNDN-OGG (Schumacher, 2012)	**pAMA/tRNA-*capks1*^{PS1}-*capks1*^{PS4}** [pEC0256] (this study)	Five	White colonies on transformation plates from one experiment, no growth on MEA+NTC after transfer
Δ***capks1*** **[H]**	**CA-0002**	*C. antarcticus* **WT:515**	**[(T*niaD*::*hph*::P*trpC*)]** $^{\Delta capks1}$ (1.941 kb) primers: *capks1*-SH5F/*capks1*-SH3R template: pNDH-OGG (Schumacher, 2012)	**pAMA/tRNA-*capks1*^{PS1}-*capks1*^{PS4}** [pEC0256] (this study)	Five	White/pinkish colonies in different numbers in four out of five attempts, grew on MEA+HYG after transfer
Δ*capks1*:: ***capks1*** **[N]**	**CA-0011**	*C. antarcticus* **Δ*pks1* [H]**	**[(*capks1*-5'::*capks1*::T*gluc*)–(T*niiA*::*nat1*::P*trpC*)]** $^{\Delta capks1}$ (8.967 kb) isolated with *Swa*I from pN-*capks1*-COMiL [pEC0466] (this study)	**pAMA/tRNA-*hph*^{PS1}** [pEC0461] (this study)	Five	No colonies on transformation plates
Δ*capks1*/ Δ*caphs1-phd1* [H/N]	**CA-0012**	*C. antarcticus* **Δ*pks1* [H]**	**[(T*niaD*::*nat1*::P*trpC*)]** $^{\Delta caphs1\text{-}phd1}$ (1.473 kb) primers: *caphs1*-SH5F/*caphd1*-SH5R template: pNDN-OGG (Schumacher, 2012)	**pAMA/tRNA-*caphs1*^{PS1}-*caphd1*^{PS1}** [pEC0448] (this study)	Four	No colonies on transformation plates
Δ*caphs1-phd1* [H]	**CA-0017**	*C. antarcticus* **WT:515**	**[(T*niaD*::*hph*::P*trpC*)]** $^{\Delta capks1}$ (1.941 kb) primers: *caphs1*-SH5F/*caphd1*-SH5R template: pNDH-OGG (Schumacher, 2012)	**pAMA/tRNA-*caphs1*^{PS1}-*caphd1*^{PS1}** [pEC0448] (this study)	Three	Black colonies on transformation plates from two out of three attempts, grew on MEA+HYG after transfer
Δ*caphs1-phd1* [H-ONGG] Alias: H2B-GFP	**CA-0021**	*C. antarcticus* **WT:515**	**[(T*niaD*::*hph*::P*trpC*)–(P*oliC*::*h2b-gfp*::T*gluc*)]** $^{\Delta caphs1\text{-}phd1}$ (4.700 kb) primers: *caphs1*-SH5F/T*gluc-caphd1*-SH5R template: pNDH-ONGG (Erdmann et al.)	**pAMA/tRNA-*caphs1*^{PS1}-*caphd1*^{PS1}** [pEC0448] (this study)	Two	Black colonies on transformation plates from one experiment, grew on MEA+HYG after transfer
Δ*kppks1*:: ***kppks1*** **[H] Alias: Δ*kppks1*^{COMiL}**	**KP-0505**	*K. petricola* **Δ*pks1* [N]**	**[(*kppks1-5'::kppks1*::T*gluc*)–(T*niiA*::*hph*::P*trpC*)]** $^{\Delta kppks1}$ (9.525 kb) primers: *kppks1*-pRS426-5F/P*trpC*-SS-pRS426-3R; template: pH-*kppks1*^{COMiL} [pEC0478] (this study)	**pAMA/tRNA-*nat1*^{PS1}** [pEC0462] (this study)	One	Black colonies (restored melanin synthesis) on transformation plates, grew on MEA+HYG after transfer

Chapter 4

1,8-dihydroxynaphthalene (DHN) melanin plays a different role in protection against UV-B in the black fungi *Knufia petricola* and *Cryomyces antarcticus*

4.1 Abstract

Black fungi inhabiting rock surfaces endure a spectrum of abiotic stresses, primarily harmful UV radiation. Their ability to tolerate even extreme conditions is attributed to the convergent evolution of common traits, including thick and highly melanised cell walls. However, studies on fungal melanins have not proved univocal results on the photoprotective functions of these pigments. Here, we investigate whether black fungi only utilise DHN melanin or can employ alternative mechanisms to counter UV-induced biological damage. Survival thresholds and tolerance strategies of two fungal representatives, *Knufia petricola* and *Cryomyces antarcticus*, were compared exposing the respective wild types and non-pigmented mutants (Δ*pks1*, Δ*phs1*, Δ*pks1*/Δ*phs1*) to UV-B radiation. *C. antarcticus* could tolerate higher UV-B doses yet was sensitive to white light, while *K. petricola* had the opposite trend. DHN melanin was effective in providing UV-B protection in *C. antarcticus*, yet the same pigment or even carotenoids proved ineffective in *K. petricola*. Both fungi showed a comprehensive photosensory system and demonstrated functional DNA repair photolyases through photoreactivation. Our findings revealed that adaptations to UV-damage avoidance or repair strategies correlate to the ecological niche of each fungus, and even though similar photoresponses occur in black fungi, they may not be equally functional.

4.2 Introduction

Solar radiation represents a universal driver for life, with a spectrum spanning from ultraviolet (UV) to infrared. The UV fraction is subdivided in three categories: UV-C (200–280 nm), UV-B (280–315 nm) and UV-A (315–400 nm). The Earth's atmosphere absorbs the most harmful UV wavelengths (<290 nm), preventing them from interacting with the biosphere; however, the incoming UV-B and UV-A fractions still cause significant biological effects. Exposure to UV-B radiation can induce various chemical alterations in organisms, most notably helix-distorting damages in the DNA (Jones and Baxter, 2017). These damages occur from the formation of cyclobutane pyrimidine dimers (CPDs) and pyrimidine-pyrimidone (6-4) photoproducts (6-4 PPs) formed by adjacent pyrimidine residues on the same strand. Both CPDs and 6-4 PPs are highly cytotoxic and mutagenic. Single (SSBs) and double strand breaks (DSBs) in the DNA may also occur (Banaś et al., 2020). UV-A radiation further leads to the accumulation of reactive oxygen species (ROS), which can damage the DNA and proteins and trigger the oxidation of lipids (Kebbi et al., 2020). Once organisms can cope with the deleterious effects of sunlight, they can use it as source of energy in terms of photosynthesis or heat production and/or as signal to regulate their metabolism, development and behaviour, and to run a circadian clock to anticipate daily upcoming changes (Seemann, 1979; Dunlap, 1999).

Many organisms including fungi synthesise metabolites that may function as the first line of defence against UV radiation by mitigating the consequences of habitual exposure to intense UV (Vanhaelewyn et al., 2020). These metabolites are deemed to prevent damages to the DNA and other macromolecules before they occur. Notably, the accumulation of non-photosynthetic pigments such as the brown to black melanins and/or orange to reddish carotenoids has long been linked to photoprotection (Wong et al., 2019). Melanins constitute a heterogenous group of macromolecules derived from the oxidative polymerisation of different phenolic precursors (Cordero and Casadevall, 2020). Despite the challenges in studying the multifunctional potential of melanins, their broad-spectrum absorption, especially in the UV range, along with antioxidant properties, support their protective role against UV radiation. Carotenoids are tetraterpenoids functioning as antioxidants, mitigating UV-induced damages primarily by ROS quenching (Gao and Garcia-Pichel, 2011). The second line of defence against harmful UV encompasses the enzymatic detoxification of ROS and the repair of damaged molecules. UV-induced lesions and breaks in the DNA need to be repaired before replication occurs to ensure that the genetic information remains intact. CPDs and 6-4 PPs are cleaved by specialised enzymes known as photolyases for reconstituting the original base pairing, a light-dependent process called

photorepair or photoreactivation (Banaś et al., 2020). Similar or other damages such as oxidised purines, SSBs and DSBs are repaired independent of light (dark repair) e.g., via nucleotide excision repair (NER), base excision repair (BER), non-homologous end-joining (NHEJ), or homologous recombination (HR) (Strzałka et al., 2020).

Many fungi produce the black 1,8-dihydroxynaphthalene (DHN) melanin that derives from the extracellular polymerisation of DHN. The biosynthetic routes slightly differ as the polyketide synthase (PKS) as the key enzyme may release 1,3,6,8-tetrahydroxynaphthalene (T4HN) directly or an intermediate that is deacetylated to T4HN by a separate enzyme. Filamentous Ascomycetes such as *Botrytis cinerea,* the causal agent of grey mould diseases in plants, produce DHN melanin in a spatial-temporal manner. The vegetative mycelia are non-pigmented but become pigmented in response to light and temperature stress. Further, the conidia and the sclerotia serving as dispersal and resting structures are melanised (Schumacher, 2016). In contrast, the vegetative cells of so-called black fungi, commonly found in various habitats exposed to high solar irradiance e.g., on rock surfaces in cold and hot deserts, are always melanised (Liu et al., 2021). Despite being phylogenetically distant, these fungi share morpho-physiological traits including continuous melanisation, slow growth and simple life cycles as convergent adaptation to abiotic factors in extreme environments (Gueidan et al., 2008; Gueidan et al., 2011). Similarly, different carotenoids leading to an orange, pinkish or reddish pigmentation dependent on their proportions, are produced by several Ascomycetes in a spatial-temporal manner or constitutively (Chen et al., 2014; Avalos et al., 2017; Flieger et al., 2018). Like bacteria and plants, most fungi use photoreactivation to cope with UV-induced DNA damage. The number of photolyases differs in Ascomycetes (Schumacher and Gorbushina, 2020). The relevance of photoreactivation is evident in *Pseudogymnoascus destructans* causing the white-nose syndrome of bats. The fungus lost the photolyase and consequently became extremely sensitive to UV Palmer (Palmer et al., 2018).

Due to their worldwide distribution in different sunlight-flooded extreme environments, black fungi are thought to employ diverse protective mechanisms to mitigate and repair UV-induced damages (Cortesão et al., 2020; Seekles et al., 2021; Campana et al., 2022). Although previous studies have provided valuable insights into the survival strategies of black fungi, detailed studies employing deletion mutants for deciphering the importance of DHN melanin and DNA repair systems are lacking for such a diverse group.

The aim of this study was to compare, for the first time, two black fungi from different lineages and their non-melanised (Δ*pks1*) mutants and to test them in the same experimental set-up to investigate the role of protective pigments and photoreactivation in surviving UV stress. *Knufia petricola* (Eurotiomycetes), colonising exposed rocks and man-made structures

(Gorbushina et al., 2008), has become as a model to explore the physiology and lifestyle of rock-inhabiting fungi due to its moderate growth rates and efficient tools for genetic engineering (Nai et al., 2013; Voigt et al., 2020; Erdmann et al., 2022) (Erdmann et al., under review). *Cryomyces antarcticus* (Dothideomycetes), a cryptoendolithic fungus (Selbmann et al. 2005), is known to withstand many extreme conditions including UV and ionising radiation and is thus used as test organism in astrobiological research on the limits of life (Selbmann et al., 2018; Onofri et al., 2020; Pacelli et al., 2021). The first *C. antarcticus* deletion mutants were recently generated by adopting protocols from *K. petricola* (Catanzaro et al., in press).

4.3 Materials and methods

4.3.1 Fungal strains and cultivation

C. antarcticus and *K. petricola* wild-type (WT) and mutant strains listed in **Table 5** were cultivated on malt extract agars, i.e. on MEA [2.0 % malt extract (Carl Roth GmbH + Co. KG), 0.1 % peptone from casein (Carl Roth GmbH + Co. KG), 2.0 % D-glucose, 2.0 % kobe agar (AppliChem GmbH)], or MEAV [3.0 % malt extract (Carl Roth GmbH + Co. KG), 1.5 % bacteriological agar (AppliChem GmbH)], on SDNG as synthetic-defined medium [0.17 % Difco Yeast Nitrogen Base without Amino Acids and Ammonium Sulfate (BD Biosciences), 0.3 % $NaNO_3$, 2.0 % D-glucose, 2.0 % kobe agar], and on water agar [2.0 % kobe agar]. Biomass from eight-week-old *C. antarcticus* and one-week-old *K. petricola* MEA cultures was homogenised in 1 x phosphate-buffered saline [PBS: 137 mM NaCl, 2.7 mM KCl, 10 mM Na_2HPO_4, 1.8 mM KH_2PO_4, pH 7.4] using glass beads and a Retsch mixer mill (10 min at 30 Hz). 20 ml of MEB [2.0 % malt extract, 0.1 % peptone from casein, 2.0 % D-glucose] were inoculated with 200 µl of cell suspensions and incubated in the dark on a rotary shaker at 100 rpm (*K. petricola*) or shaken 1 min/week (*C. antarcticus*). Agar cultures were incubated either in constant darkness (DD) or under a 12 h white light (400–700 nm)/12 h dark cycle (LD), with *C. antarcticus* strains at 15 °C (Philips F32T8/TL741 cool white, light intensity: 118 µmol photons/m^2/s) and *K. petricola* strains at 25 °C (OSRAM DULUX L cool white, light intensity: 116 µmol photons/m^2/s).

Table 5. Fungal strains used in this study.

Strain name	Genotype	Reference
***C. antarcticus* MNA-CCFEE 515**	WT	Selbmann et al. (2005)
Δ*capks1* [CA-0002; T10, T17]	MNA-CCFEE 515, Δ*pks1* [(T*niaD*::*hph*::P*trpC*)]	Catanzaro et al. (in press)
***K. petricola* A95 (CBS 123.872)**	WT	Voigt et al. (2020)
Δ*kppks1* [KP-0037; T3]	A95, Δ*pks1* [(T*niaD*::*hph*::P*trpC*)]	Voigt et al. (2020)
Δ*kpphs1* [KP-0054; T3]	A95, Δ*phs1* [(T*niaD*::*nat1*::P*trpC*)]	Voigt et al. (2020)
Δ*kppks1*/Δ*kpphs1* [KP-0083; T4]	A95, Δ*pks1* [(T*niaD*::*nat1*::P*trpC*)], Δ*phs1* [(T*niaD*::*hph*::P*trpC*)]	Voigt et al. (2020)

4.3.2 UV-B survival assessment

Biomass harvested from four-week-old *C. antarcticus* or three-day-old *K. petricola* liquid cultures was homogenised in a stainless-steel beaker with seven stainless-steel beads using a Retsch mixer mill (2.5 min at 30 Hz). Cell suspensions were washed with Milli-Q water and centrifuged at 3000 × g for 5 min. Titres of colony-forming units (CFU) were determined using a Thoma cell counting chamber and adjusted with 1 x PBS to 2.5×10^3 CFU/ml for plating and 1×10^8 CFU/ml for dropping. For survival assays, 200 µl of cell suspensions (~5.0×10^2 CFU) were evenly distributed with ten glass beads (3-5 mm) on agar. For drop assays, serial dilutions down to 1×10^3 CFU/ml were prepared, and 10 µl (1×10^6 to 1×10^1 CFU) were dropped on agar. Inoculated Petri dishes without lids were exposed to medium wavelength ultraviolet (UV-B, 312 nm) in a Bio-Link BLX crosslinker (VILBER). A range of preset UV-B doses from 0.1 up to 2.3 J/m^2 was delivered at varying exposure times, calculating an irradiance of approx. 3400 µW/cm^2. Irradiated Petri dishes were covered with lids and either immediately wrapped in aluminium foil and incubated in DD or exposed to LD to allow photoreactivation. Survival rates (%) were determined for each tested strain and UV-B dose by calculating the average number of colonies on irradiated replicates compared to that on control replicates, with colony counts performed after eight (for *C. antarcticus* strains) and one (for *K. petricola* strains) weeks of incubation in DD. Survival assays included a minimum of three biological replicates per strain tested and were performed at three independent times ($n \geq 9$). Lethal dose values, defined as the radiation dose required to inactivate 50 % (LD_{50}), 75 % (LD_{25}), or 90 % (LD_{10}) of the microbial population, were estimated for the WT strains from its dose-response curve.

4.3.3 Standard molecular methods

Genomic DNA from *K. petricola* strains was extracted as described previously (Voigt et al., 2020). DNA and the 1 kb Plus DNA Ladder (New England Biolabs, NEB), mixed with Midori Green Direct (Biozym Scientific GmbH), were separated in 1 % agarose gels in 0.5 % tris-acetate-EDTA (TAE) buffer in a Mupid exU gel electrophoresis chamber and visualised with a ChemiDoc XRS+ Imager equipped with Image Lab 6.0.1 (Bio-Rad Laboratories Inc.). Regions of interest were amplified with the Q5 High-Fidelity DNA Polymerase (New England Biolabs, NEB) and primers listed in **Table S6**. For GenBank accession see **Table S7**. Amplicons were purified with the Monarch PCR & DNA Cleanup Kit (NEB) and sequenced with appropriate primers at Eurofins Genomics.

4.3.4 Bioinformatics analyses

C. antarcticus nucleotide and protein sequences of putative photoreceptors and light-responsive transcription factors listed in **Table S8** were extracted from the *C. antarcticus* CBS 116301 v3.0 database (https://mycocosm.jgi.doe.gov/Cryan3) at the Joint Genome Institute. Muscle alignments for calculating amino acid identities in percent and phylogenetic trees were generated using Geneious Prime 2023.2.1 (Biomatters Ltd.). Conserved protein domains were identified by InterPro (https://www.ebi.ac.uk/interpro) (Paysan-Lafosse et al., 2023). Sanger sequencing reads were mapped onto the respective gene locus using SnapGene v. 4.0.8 (GSL Biotech LLC).

4.4 Results

4.4.1 K. petricola *grows faster than* C. antarcticus *even at 15 °C and in light-dark cycles*

C. antarcticus strain MNA-CCFEE 515 (*Ca* WT:515) was isolated from Antarctic sandstone at Linnaeus Terrace (McMurdo Dry Valleys, Southern Victoria Land) and is cultivated in darkness at 15 °C, which allows for optimum growth rates (Selbmann et al., 2005). *K. petricola* strain A95 (*Kp* WT:A95) was isolated from a marble monument in Athens (Greece) (Gorbushina et al., 2008) and is routinely incubated at 25 °C in the dark.

To compare the growth phenotypes of the two wild types under different nutrient and light conditions, cell suspensions were dropped onto solidified media and incubated at 15 °C either in complete darkness (DD) or in 12 h light/12 h dark cycles (LD). The media were: (1) MEA, a nutrient-rich medium with glucose and peptone as carbon and nitrogen sources routinely used for the cultivation of *K. petricola*; (2) MEAV, an alternative MEA lacking glucose and peptone used for the cultivation of Antarctic fungi (Pacelli et al., 2020); (3) SDNG, a synthetic medium containing vitamins, trace elements, nitrate and glucose used for transformant selection; and (4) WA, a minimalist medium lacking all nutrients (**Figure 18**, **Table 5**). After eight weeks under DD conditions, both strains exhibited growth on all substrates with the typical compact colonies of rock-inhabiting fungi, with the highest biomass produced on MEA. Notably, *Kp* WT:A95 was able to thrive at the low temperature of 15 °C and maintained a faster growth rate than *Ca* WT:515 on all nutrient-containing media and independently of light conditions. However, both fungi showed equally slow growth on WA. *Ca* WT:515 showed instead altered growth rates, especially on MEAV, depending on the light condition. The colonies of *Ca* WT:515 secreted dark metabolites in nutrient-containing media. Growth rates of *Ca* WT:515, but not of *Kp* WT:A95, were reduced in the presence of light (118 µmol photons/m^2/s).

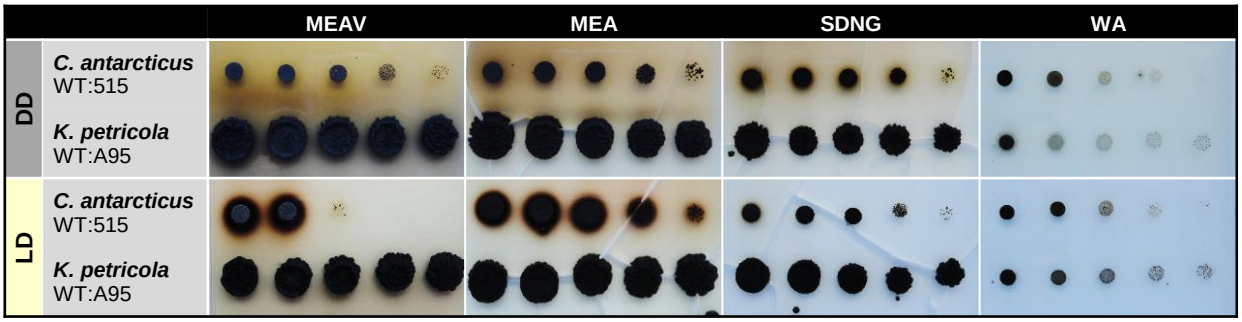

Figure 18. Growth and pigmentation of *C. antarcticus* and *K. petricola* under different conditions.
Four different solid media were inoculated with cell suspensions (10^6, 10^5, 10^4, 10^3, 10^2 CFU per droplet) from wild type strains of *C. antarcticus* MNA-CCFEE 515 (*Ca* WT:515) and *K. petricola* A95 (*Kp* WT:A95) and incubated for eight weeks at 15 °C, either in constant darkness (DD) or 12 h light/12 h darkness (LD).

4.4.2 C. antarcticus *can tolerate higher UV-B doses than* K. petricola

To assess the impact of UV-B radiation on the viability of both *C. antarcticus* and *K. petricola* wild types, MEA plates were inoculated with approx. 500 colony forming units (CFU) to ensure a uniform cell distribution and prevent multilayer shielding effects. The inoculated plates were exposed to incremental doses of UV-B radiation, ranging from 0.1 to 2.3 J/cm^2 for *Ca* WT:515 and from 0.1 to 1.5 J/cm^2 for *Kp* WT:A95. Following irradiation, the plates were kept in dark at

the optimal growth temperature for each strain. The results were plotted as dose-response curves, revealing different survival capacities of the two fungi to UV-B irradiation (**Figure 19A**).

Ca WT:515 exhibited a gradual decline in colony numbers, with 75.3 ± 11.2% survival at 0.3 J/cm^2 and decreasing to 55.8 ± 5.8 % at 0.5 J/cm^2. Its dose-responses showed a consistent growth ability up to 1.3 J/cm^2, with 11.4 ± 3.6 % survival; beyond that, *Ca* WT:515 survival rates fell below 10 %. In contrast, *Kp* WT:A95 sustained colony growth only at low UV-B doses (88.3 ± 10.2 % at 0.2 J/cm^2), with survival rates declining to 56.9 ± 5.8 % at 0.3 J/cm^2 and dropping to 10.3 ± 4.3% at 0.5 J/cm^2. Further increases in radiation dosage resulted in an extremely low growth (< 5%). By maintaining significantly higher LD_{10} value, *C. antarcticus* demonstrated higher tolerance to UV-B irradiation than *K. petricola* (**Figure 19B**).

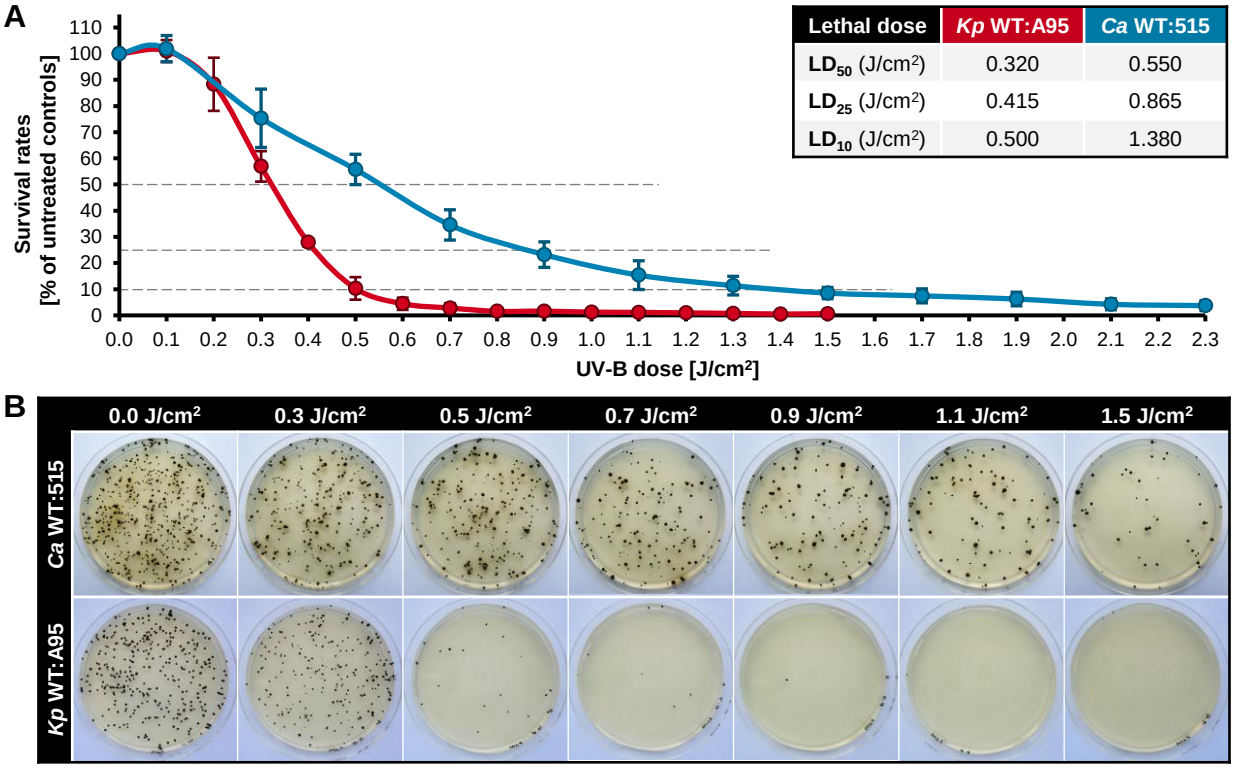

Figure 19. *C. antarcticus* cells survive higher doses of UV-B irradiation than *K. petricola* cells.

Approx. 5 x 10^2 CFU were spread onto MEA (at least three plates per strain and UV-B dose as technical replicates), treated with the indicated UV-B doses (312 nm), and incubated in constant darkness for eight weeks at 15 °C (*Ca* WT:515) or one week at 25 °C (*Kp* WT:A95). **A. UV-B response curves of *C. antarcticus* and *K. petricola*** wild types. Relative mean values and standard deviations of survival rates (colonies on treated plates/colonies on untreated plates) were calculated from three (*Ca* WT:515) and four (*Kp* WT:A95) biological replicates. **B. Pictures of representative plates are shown.**

4.4.3 *DHN melanin significantly contributes to UV-B tolerance of* C. antarcticus

After evaluating the survival thresholds of *C. antarcticus* wild type, a first UV-B survival assay was performed using the melanised *Ca* WT:515 and two independent Δ*capks1* mutant strains (T10 and T17) lacking the ability to synthesise DHN melanin (Δ*capks1* T10, T17). Survival rates were determined for each strain at UV-B doses of 0.1, 0.3, 0.5, and 0.7 J/cm^2 (**Figure 20A**). As both mutants yielded similar results, *Ca* WT:515 and Δ*capks1* T10 were used for the three additional experiments to obtain four biological replicates.

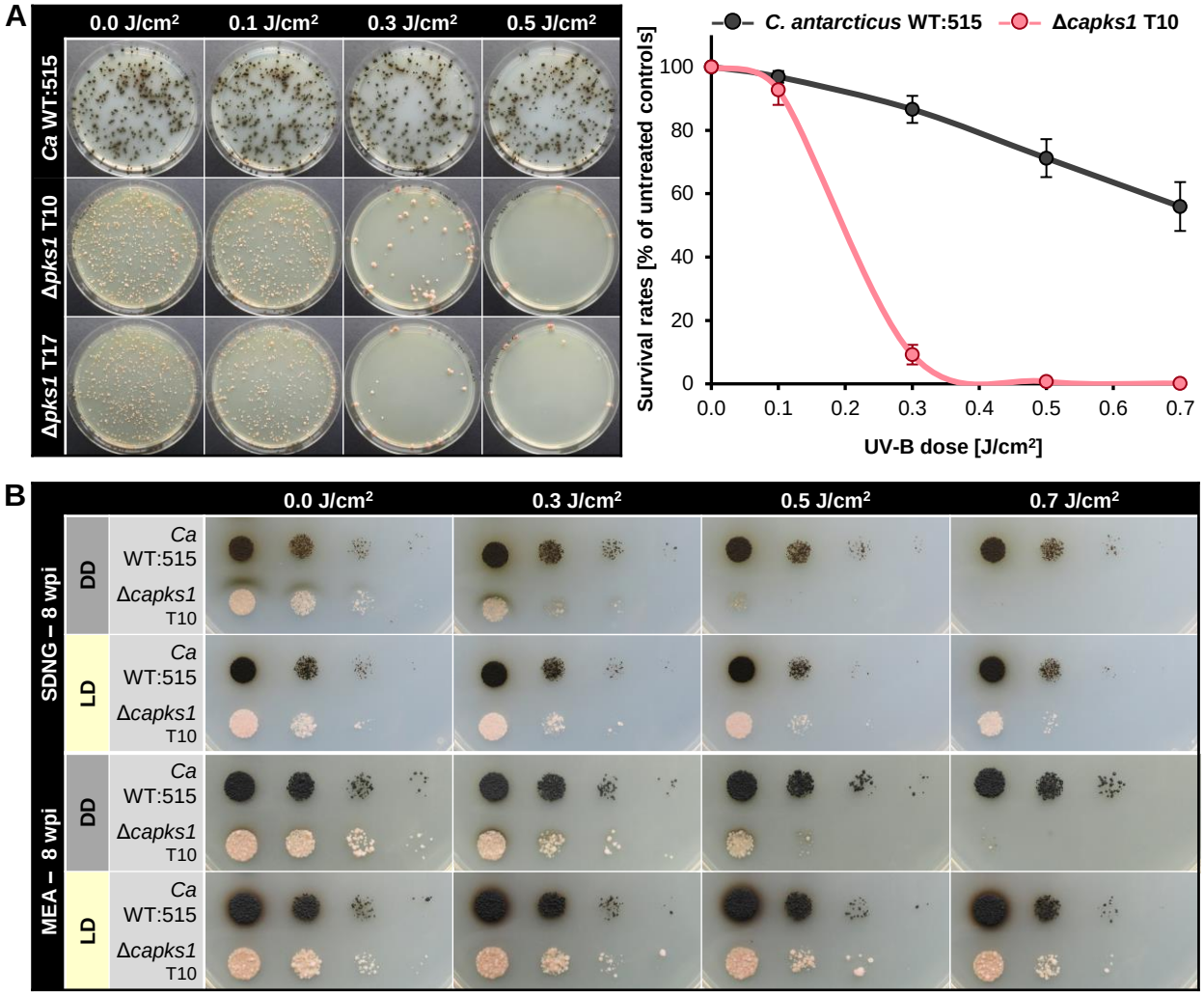

Figure 20. DHN melanin protects *C. antarcticus* cells from UV-B irradiation.

A. The non-melanised *C. antarcticus* Δ*pks1* mutant is hypersensitive to UV-B. Cells (5 x 10^2 CFUs on MEA, four plates per strain and UV dose) of the *C. antarcticus* wild type (*Ca* WT:515) and two Δ*capks1* mutants (T10, T17) were exposed to the indicated UV-B doses (312 nm) and incubated at 15 °C in DD. On the left: representative pictures were taken after 15 weeks. On the right: relative survival rates of the wild type and Δ*capks1* T10 mutant were calculated from four biological replicates. Colonies were counted after eight weeks of incubation. **B. White light upon UV-B exposure increases the survival rate of Δ*capks1* but not that of the wild type.** Cells (10^4-10^1 CFUs) of the wild type (*Ca* WT:515) and the Δ*capks1* mutant (T10) were dropped onto MEA and synthetic SDNG agar and exposed to the UV-B. Pictures were taken after eight weeks of incubation at 15 °C in DD or LD.

Ca WT:515 showed a similar trend to the previous response experiment, displaying gradual reduction of survival rates to 86.6 ± 4.3% and 55.9 ± 7.7 % at doses of 0.3 and 0.7 J/cm^2, respectively. Instead, Δ*capks1* showed a steep decline in CFU growth from 0.3 J/cm^2, resulting in a ten-fold decrease of survival rate to 9.2 ± 3.1 %. In sum, the higher sensitivity of the non-melanized Δ*capks1* compared to the melanized *Ca* WT:515 demonstrated that DHN melanin as a key role in *C. antarcticus* for protection against UV-B irradiation.

4.4.4 Neither DHN melanin nor carotenoids are involved in UV-B tolerance of K. petricola

A comparative survival assay was performed for *K. petricola* as well, including the melanised *Kp* WT:A95 and three mutants lacking either DHN melanin (Δ*kppks1*), carotenoids (Δ*kpphs1*), or both (Δ*kppks1*/Δ*kpphs1*). UV-B dose-response curves were drawn at 0.2 to 0.5 J/cm^2 for each strain (**Figure 21A**). While *Kp* WT:A95 maintained consistent survival rates, all three mutants exhibited similar dose-responses to the wild type. At 0.3 J/cm^2, where *Kp* WT:A95 showed nearly halved survival of 56.6 ± 6.9 %, Δ*kppks1*, Δ*kpphs1*, and Δ*kppks1*/Δ*kpphs1* showed comparable survival rates with 54.4 ± 16.9 %, 48.8 ± 12.6 %, and 59.2 ± 21.5%, respectively. Notably, all pigment-deficient strains demonstrated equal sensitivity to UV-B irradiation, matching the survival thresholds of the wild-type strain. This suggests that the absence of either melanin or carotenoid or both pigments had no significant impact on their sensitivity to UV-B radiation.

4.4.5 Light mediates photorepair of UV-B damaged DNA and in both species

Since photolyases are light-driven enzymes, the total photoreactivation capacity of an organism can be elucidated by exposing UV-B-treated cells to white light. In this regard, two solidified media (MEA and SDNG) were inoculated with cell suspensions (10^4 to 10^1 CFU per drop) of *C. antarcticus* or *K. petricola* strains, irradiated with different doses of UV-B and then incubated in LD to allow photoreactivation and in DD as a control. UV-treated cells developed colonies in light as the untreated controls.

In the case of *C. antarcticus*, the wild type showed slight reduction in colony density under DD conditions, while Δ*capks1* presented evident decrease from the dose of 0.5 J/cm^2, confirming the negative trend observed in the survival assay (**Figure 20B**). Under LD conditions, *Ca* WT:515 showed no significant variations in its growth ability, while Δ*capks1* exhibited best growing capacity in all radiation conditions. Eventually, the non-melanised mutant produced comparable biomass to that of the wild type even at the highest dose (0.7 J/cm^2) when incubated in LD.

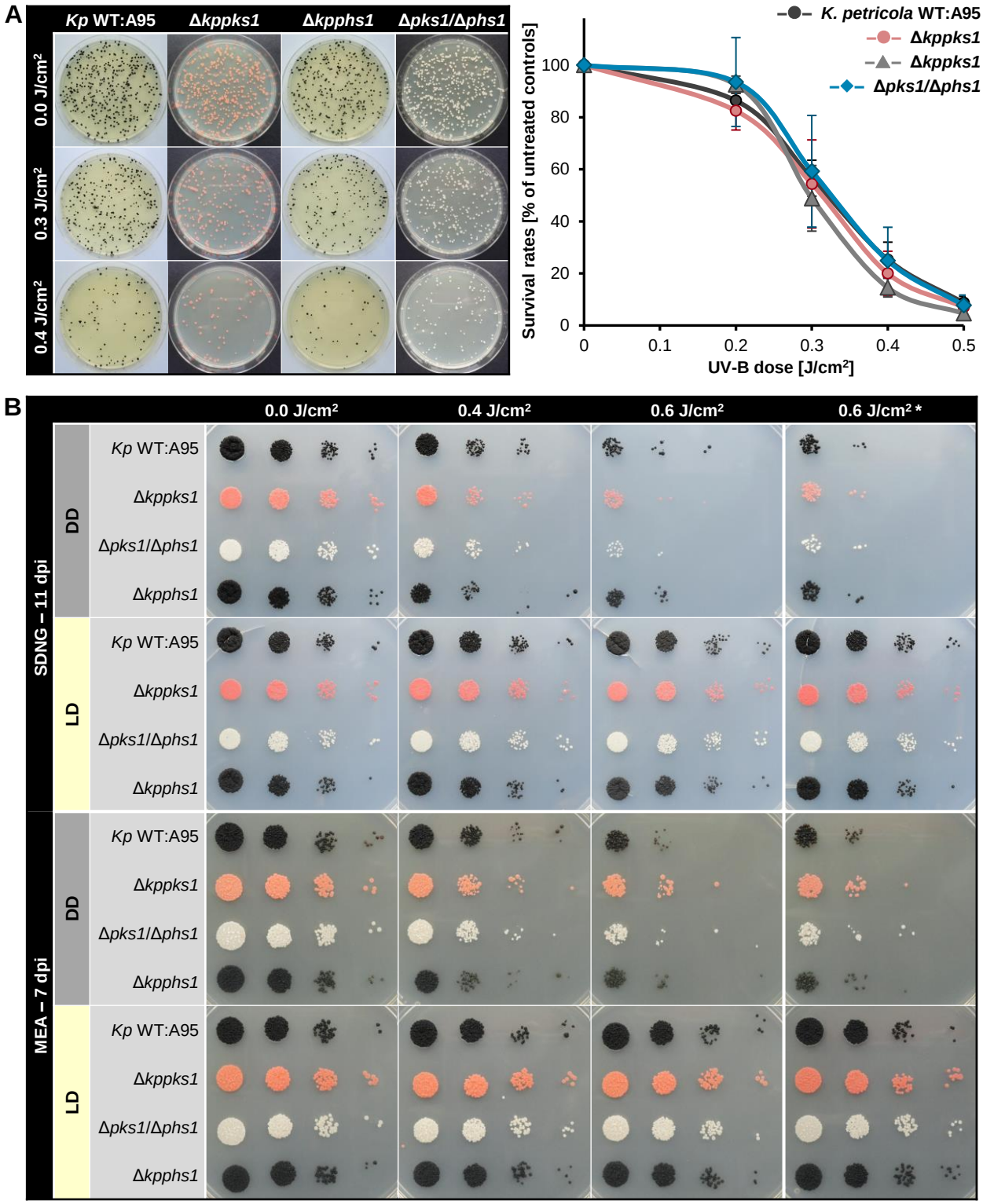

Figure 21. Neither DHN melanin nor carotenoids protect *K. petricola* cells from UV-B irradiation.

A. Pigment-deficient mutants of *K. petricola* are sensitive to UV-B as the wild type. Cells (5 x 10^2 CFUs per MEA plate, four plates per strain and UV-B dose as technical replicates) of the *K. petricola* wild type (*Kp* WT:A95) and three pigment-deficient mutant strains (Δ*kppks1*, Δ*kpphs1*, and Δ*kppks1*/Δ*kpphs1*) were exposed to the UV-B doses shown and incubated for one week at 25 °C in DD. Relative survival rates were calculated from four biological replicates. Representative plates are shown on the left. **B. White light upon UV-B fully restores survival of all *K. petricola* strains indicating efficient photoreactivation.** Cells (10^4-10^1 CFUs) of the four *K. petricola* strains on MEA or SDNG agar were exposed to UV-B. Plates on the left (0, 0.4 and 0.6 J/cm^2) were incubated at constant temperature (25 °C) in DD or 12 h light-dark cycles (LD) in a climate chamber. Plates on the right labelled with an asterisk were incubated under ambient temperature and sunlight/dark daily cycles (window board in summer).

As for *K. petricola* strains, plates inoculated with the wild type and pigment-deficient mutants were exposed either to 116 µmol photons/m^2/s at 25 °C in a climate chamber or to sunlight daily cycles and ambient temperature on a window board (minimum of three-hour exposure to summer sunlight before sunset) (**Figure 21B**). The latter was included as an additional white light control for the LD conditions. Under DD conditions, decreasing survival trends remained consistent among the wild type and the three non-pigmented mutants, with an evident reduction of the colony density at the dose of 0.6 J/cm². In both LD setups, white light efficiently mediated photoreactivation in the four *K. petricola* strains, as growth was rescued by light on both media, exhibiting comparable biomass to the untreated controls even after exposure to the highest dose (0.6 J/cm^2).

4.4.6 UV-B exposure generated non-melanised mutants of K. petricola *only*

The treatment of fungal cells with UV-B followed by incubation in darkness resulted in *K. petricola* colonies showing an altered pigmentation (**Figure 22**). However, among all test plates of *C. antarcticus* no such colonies were spotted. Obtained mutants from *Kp* WT:A95 formed pink to dark pink colonies (WT-UV001 to -UV004) or showed severely reduced growth accompanied by the secretion of brownish pigments (WT-UV005). Mutants derived from the carotenoid-deficient Δ*kpphs1* mutant exhibited a light to dark grey pigmentation (Δ*phs1*-UV001 and -UV002). The mutants showing reduced melanisation were isolated, their DNA extracted and used for the amplification of the *kppks1* coding region. Sequencing of amplicons revealed point mutations, all non-silent, in WT-UV001 ($^{G}576^{D}$ in β-ketoacyltransferase domain), WT-UV002 ($^{L}294^{P}$ in between the N-terminal starter unit:ACP transcylase domain), Δ*phs1*-UV002 ($^{H}1320^{Y}$ in the dehydratase domain), and a deletion/mutation affecting 5 aa in the C-terminal thioesterase domain in Δ*phs1*-UV001. However, no mutations in *kppks1* were identified for WT-UV003 and WT-UV004. Thus, *kpppt1* encoding the 4'-phosphopantetheinyl transferase required for the posttranslational modification of KpPKS1 when expressed in *Saccharomyces cerevisiae* (Catanzaro et al., in press) was amplified. Sequencing identified non-silent point mutations i.e., $^{Y}247^{D}$ in WT-UV003 and a premature stop codon in WT-UV004 resulting in a protein lacking the last 58 aa. The producibility of mutants with altered pigmentation from *Kp* WT:A95 in contrast to *Ca* WT:515 is in line with the higher sensitivity to UV-B which reflects a higher mutation rate of *K. petricola*.

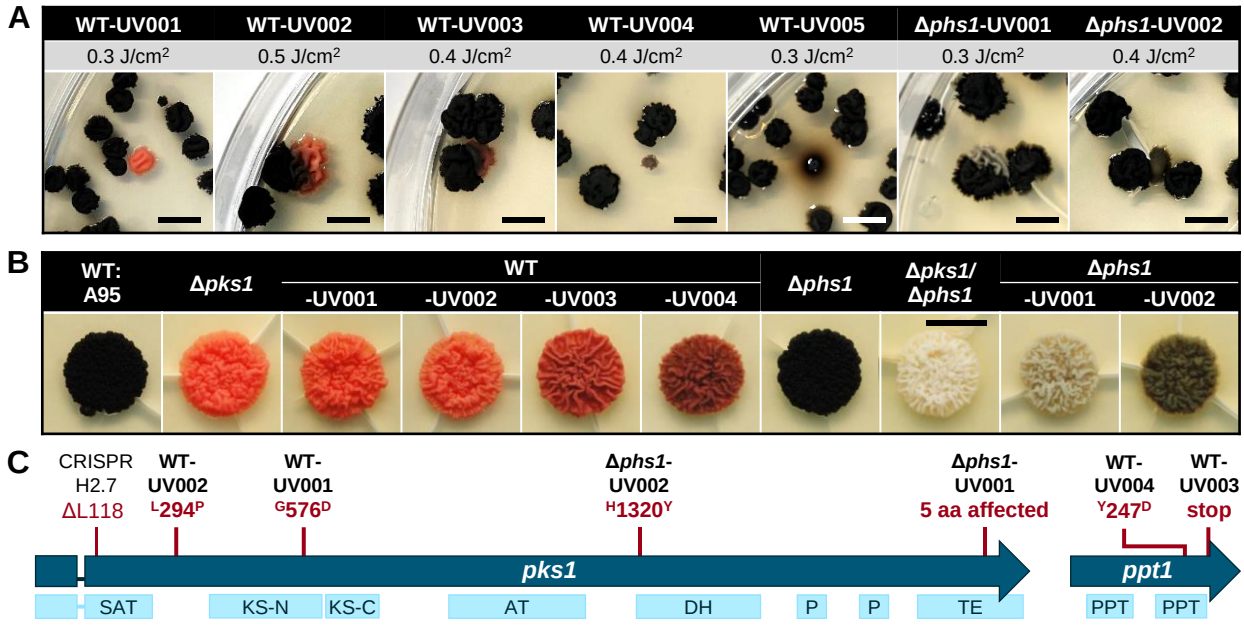

Figure 22. Exposure of *K. petricola* to UV-B resulted in mutants with altered melanisation.

A. Differentially pigmented colonies derived from treatment of wild type and carotenoid-deficient cells with UV-B. Plates from the experiments shown in **Figure 21A** (UV-B doses are shown above) were photographed after two months of incubation at 25 °C. Cells from colonies with altered pigmentation were transferred to MEA. Scale bars – 5 mm. **B. The isolated UV mutants likely produce different amounts of DHN melanin.** Cell suspensions of the indicated strains were dropped onto MEA and cultivated for twelve days at 25 °C in darkness. Scale bar – 1 cm. **C. Sequencing revealed non-silent mutations in *kppks1* and *kpppt1*.** The coding regions of *kppks1* and *kpppt1* were amplified and sequenced. The identified mutations were mapped to the genes. The conserved proteins domains are shown below: SAT – starter unit: ACP transacylase [PF16073], KS – β-ketoacyl synthase [PF00109, PF02801], AT – acyl transferase [PF00698], DH – dehydratase [PF14765], P – phosphopantetheine attachment site [PF00550], TE – thioesterase [PF00975], PPT – 4'-phosphopantetheinyl transferase [IPR037143]. The 3-bp-long (ΔL118) deletion in the CRISPR mutants H2.7 was identified in a previous study (Voigt et al., 2020).

4.4.7 The genome of C. antarcticus *encodes ten putative photoreceptors*

Photolyases mediating photoreactivation belong to the group of photoreceptors (PR) which use chromophores bound to conserved domains to absorb specific wavelengths. This trigger primary changes in the chromophore-binding domain, inducing conformational alterations in proteins and modulating their activities. Fungi can sense the light spectrum through four PR families: cryptochrome/photolyase family proteins (CPFs), light, oxygen and voltage domain-containing proteins (LOVs), microbial opsins (OPSs), and phytochromes (PHYs) (Yu and Fischer, 2019). CPFs contain two conserved domains, the N-terminal PHR and the C-terminal FAD domain, for binding the chromophores methyltetrahydrofolate and flavin adenine dinucleotide (FAD). They can but not have to exhibit photoreactivation activity, as they can just function in light-dependent signalling. Twelve genes encoding PRs, and with this the highest number of PRs in Ascomycetes, have been recently identified in the genome of *K. petricola* (Schumacher and Gorbushina, 2020).

Here, the sequences of the *K. petricola* proteins were used as queries in BlastP analyses to identify PR-encoding genes in genome of *C. antarcticus* (**Table 6**, **Table S8**). In total, ten PRs for sensing UV-A/blue light (three CPFs), blue light (four LOVs), green light (two OPSs) and the red/far-red ratio (one PHY) were identified. From the three CPFs, Cryan3|1036121 as a DASH cryptochrome may not exhibit photolyase activity, while Cryan3|982802 and Cryan3|999807 are putative CPD or 4-6 PP photolyase (**Figure 23**). Taken together, based on the presence of genes encoding PRs, GATA-type transcription factors of the White Collar complex (WCC) and the clock oscillator frequency (FRQ), *C. antarcticus* like *K. petricola* may sense the entire spectrum of white light to regulate cell physiology and entrain a circadian clock. Three and two CPFs may contribute to the observed light-dependent UV survival (photoreactivation) of *K. petricola* and *C. antarcticus*, respectively.

Table 6. Proteins of *K. petricola* and *C. antarcticus* putatively involved light sensing and signalling.

Description	*Kp* proteins	*Ca* proteins	aa identity
CPF protein: DASH cryptochrome; UV-blue	**KpCPF1** (607 aa)	**Cryan3|1036121** (650 aa)	**53 %**
CPF protein: CPD photolyase; UV-blue	**KpCPF2** (648 aa)	**Cryan3|982802** (644 aa)	**50 %**
CPF protein: CPD photolyase; UV-blue	**KpCPF3** (539 aa)	no hit	n/a
CPF protein: (6-4) photolyase; UV-blue	**KpCPF4** (718 aa)	**Cryan3|999807** (643 aa)	**50 %**
LOV protein: GATA-type transcription factor; blue	**KpWCL1** (1,069 aa)	**Cryan3|1059543** (1,033 aa)	**47 %**
LOV protein: unknown function; blue	**KpLOV2** (1,224 aa)	no hit	n/a
LOV protein: unknown function; blue	no hit	**Cryan3|845159** (626 aa)	n/a
LOV protein: unknown function; blue	**KpLOV3** (749 aa)	**Cryan3|1085497** (595 aa)	**35 %**
LOV protein: regulator of G protein; blue	**KpLOV4** (549 aa)	**Cryan3|1018934** (503 aa)	**33 %**
Microbial opsin; green	**KpOPS1** (298 aa)	**Cryan3|1097610** (328 aa)	**52 %**
Microbial opsin; green	**KpOPS2** (306 aa)	**Cryan3|563816** (322 aa)	**56 %**
Microbial opsin; green	**KpOPS3** (282 aa)	no hit	n/a
Phytochrome (histidine kinase); red/far-red	**KpPHY1** (1,519 aa)	**Cryan3|43883** (1,466 aa)	**53 %**
GATA-type transcription factor	**KpWCL2** (517 aa)	**Cryan3|443880** (491 aa)	**51 %**
GATA-type transcription factor	**KpLTF1** (466 aa)	**Cryan3|1024422** (1,158 aa)	**17 %**
Fungal circadian oscillator Frequency	**KpFRQ1** (957 aa)	**Cryan3|447692** (769 aa)	**23 %**

Putative photoreceptors of *K. petricola* were described previously (Schumacher and Gorbushina, 2020). Those of *C. antarcticus* were identified in the database of annotated proteins of *C. antarcticus* CBS 116301 at the Joint Genome Institute (Home - *Cryomyces antarcticus* CBS 116301 v3.0 (doe.gov)) by BlastP analyses using the *K. petricola* protein sequences as queries. Abbreviations: CPF – cryptochrome photolyase family; DASH – *Drosophila*, *Arabidopsis*, *Synechocystis*, *Homo*; CPD – cyclobutane pyrimidine dimer; (6-4) – pyrimidine-pyrimidone adduct [(6-4) photoproduct]; LOV – light-oxygen-voltage domain.

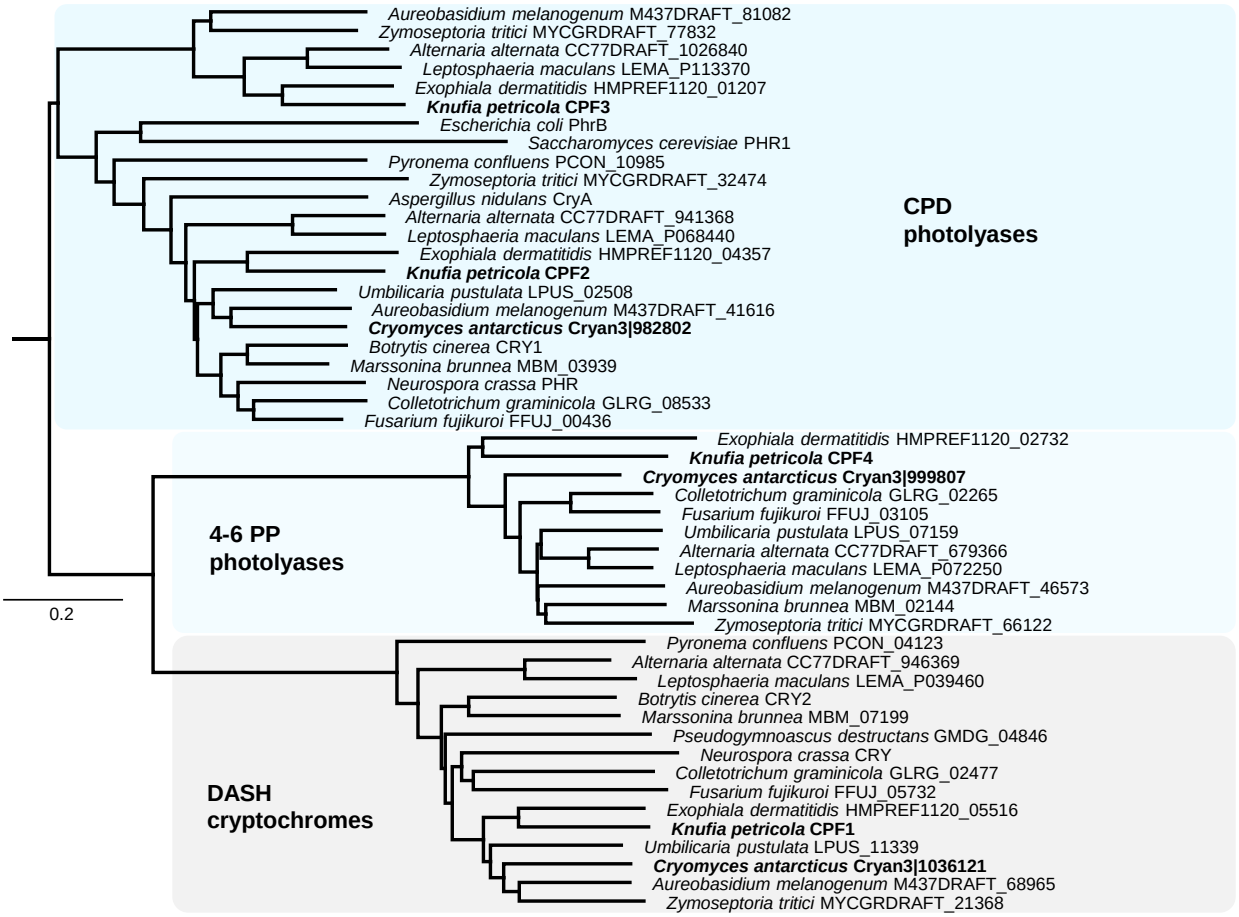

Figure 23. *C. antarcticus* and *K. petricola* have members of the three classes of CPFs.

The phylogenetic tree was generated with protein sequences extracted from GenBank and running Muscle 5.1 and Geneious Tree Builder using default settings (Geneious Prime).

4.5 Discussion and conclusions

K. petricola and *C. antarcticus* are two representatives of black fungi living in lithic communities with distinct habitat distribution. *K. petricola* is mainly found in association with subaerial biofilms from Mediterranean regions (De Leo et al., 2022), actively promoting biogenic weathering of carbonate and silicate surfaces (Tonon et al., 2021). Recently, this species has also been reported from Antarctic rocks (Selbmann et al., 2021). Conversely, *C. antarcticus* has a limited distribution across Antarctica within porous sandstone rocks alongside cryptoendolithic lichen communities (Selbmann et al., 2015). The cryptoendolithic lifestyle, among other lithic niches (Golubic et al., 1981), offers more stable conditions for microbial inhabitants, such as protection from abiotic stresses found at the rock surface (Chan et al., 2012), improving the survival prospects of life in extreme environments (Onofri et al., 2007). Interestingly, both fungi

have adapted this lifestyle in Antarctic rocks, but with different preferences for sunlight exposure: while *K. petricola* mainly prefers southern, shade-exposed rock communities, *C. antarcticus* indifferently inhabits both southern and northern (sun-exposed) rock communities (Selbmann et al., 2021). The distinct rock colonisation is strictly influenced by the high levels of UV radiation in Antarctica due to the local ozone depletion (Coleine et al., 2022).

For this study, we conducted a preliminary investigation on nutrient and light adaptations of the respective fungal wild types, revealing significantly different responses between the two species. Firstly, *Kp* WT:A95 maintained growth even under lower temperatures, which suggests, in combination with the recent species findings in Antarctica (Selbmann et al., 2021), a more psychrotolerant nature than previously thought. Indeed, temperature thresholds have yet to be defined for this strain, and few previous growth attempts at low temperatures may sustain a deeper investigation (Favero-Longo et al., 2011; Flieger et al., 2018). In contrast, *Ca* WT:515 showed release of dark metabolites in rich media, which consist of DHN melanin intermediates susceptible to photooxidation (Catanzaro et al., in press). The extracellular diffusion of these metabolites was similarly reported from another polyextremotolerant black fungus associated with biological soil crusts, *Exophiala viscosa* (Chaetothyriales) in response to extra nitrogen sources (Carr et al., 2023). Since fungi living in oligotrophic and extreme environments have adapted a slow grow to spare energy for other survival cellular mechanisms, including the production of stress protectant compounds like melanins (Gostinčar et al., 2022), it is not clear why some species discard such expensive products. Possibly, the production of extracellular melanin is driven by high nutrient availability (e.g., no dark diffusion by *Ca* WT:515 in WA), and the apparently cost-inefficient response might instead confer broader ecological benefits, such as protective services or alternative carbon sources, to the entire microbial community (Carr et al., 2023).

K. petricola and *C. antarcticus* expressed also distinct photoresponses when exposed to the broad spectrum of sunlight, i.e., white light and ultraviolet radiation. While *Kp* WT:A95 exhibits full viability under white light yet low tolerance to UV-B radiation (LD_{10} = 0.50 J/cm^2), *Ca* WT:515 shows an inverse trend, with growth inhibition to white light confirmed by previous observations (Catanzaro et al., in press) and high tolerance to UV-B instead (LD_{10} = 1.38 J/cm^2). The overall irradiation using first white and then UV-B light provides evidence of variability to the light stressor among members of the black fungal group. Indeed, sunlight has emerged as a significant factor influencing the biology of these fungi, as revealed by the substantial portion of gene expression regulated by the broad light spectrum as in *K. petricola* (Schumacher and Gorbushina, 2020), as well as their biodiversity and ecological distribution, especially within cryptoendolithic communities (Coleine et al., 2018). Even white light can be a source of biological

stress by inducing oxidative damages, and black fungi are thought to act as protective filters by shielding the microbial community from excessive irradiation and mitigating photooxidative damage with their melanin content (Nienow et al., 1988). However, we suppose that excessive light may induce ROS production in *Ca* WT:515 as seen in other Ascomycetes (Fuller et al., 2015). Adding antioxidants in the culture medium as done for *Botrytis cinerea* (Canessa et al., 2013) could easily help identifying the photooxidative stress observed in *C. antarcticus*. It is noteworthy to say that this light effect is equally expressed by the DHN melanin-deficient mutant in following experiments (**Figure 20**), confirming previous observations on the inherent sensitive nature of *C. antarcticus* to light, but raising questions concerning its photoprotection potential within cryptoendolithic communities.

To assess UV-B survival thresholds and minimise biases arising from cross-protection, the UV irradiation was performed using metabolic-active single cells. As UV-B is a non-ionising radiation with limited penetration ability (Qi et al., 2003), the UV tolerance can be indirectly increased by various biological mechanisms, such as shifting to an anhydrobiotic state (Wong et al., 2019) or irradiation shielding by cell multilayers (e.g. colonies). Differences between *K. petricola* and *C. antarcticus* may be due to differences in cell wall organisation or melanin structure. Although both species have multilayered, melanised cell walls (Breitenbach et al., 2022; Catanzaro et al., in press), *C. antarcticus* could have adapted thicker ones due to permanent exposure to extreme conditions. Moreover, while both species synthesise melanin through the DHN pathway (Voigt et al., 2020; Catanzaro et al., in press), final composition may differ as the melanin polymer can be associated with proteins/carbohydrates (Wong et al., 2019).

To evaluate the functionality of protective fungal pigments, mutant strains lacking either DHN melanin, carotenoids, or both pigments were included in the UV-B irradiation. While DHN melanin significantly improved the survival of *C. antarcticus*, no pigment showed protective effect in *K. petricola*. This denotes that the presence of DHN melanin alone might not be sufficient for UV protection for some fungi. Indeed, melanins are generally ascribed protective functions after a multitude of stress factors, but studies on melanogenic fungi have often yield contradictory results (Berthelot et al., 2020; Gaber et al., 2020; Vasileiou and Summerer, 2020). Solano (2016) has explored the cryptic nature of melanin, suggesting that the pigment switch from a photoprotective to a photodamaging agent when the input energy from UV light exceeds a threshold and the output energy cannot be scattered or safely dissipated as heat, leading to ROS generation that cause DNA damage. In the case of carotenoids, their synthesis did not provide any significant UV protection to *K. petricola*. Although the fungus constitutively produces carotenoids composed by torulene, didehydrolycopene, and lycopene (Gorbushina et al., 2008;

Flieger et al., 2018), photoprotective functions of carotenoids in fungi are still poorly understood (Avalos and Carmen Limón, 2015). However, carotenoids may still convey key functions in photoresponses as they appear to be upregulated in *K. petricola* in response to white light.

Given the identification of a shared set of putative repair photolyases between *K. petricola* and *C. antarcticus*, we checked the functionality of additional UV defence mechanisms through photoreactivation after UV-B irradiation. Interaction between photolyases and DNA strands is facilitated by a positive charge on the surface of the binding enzymatic substrate., but UV-A/blue light is an indispensable energy resource in the process for catalysing the repair of CPDs and 6-4 PPs. Light-driven expression of photolyases and consequent DNA photodamage repair was observed in both species. However, while the UV-sensitive *K. petricola* was able to regain full growth ability in all strains, the overall recovery of *C. antarcticus* was not as efficient as in *K. petricola*, since both the UV-tolerant wild type and UV-sensitive Δ*capks1* mutant were unable to match the growth of control cultures, possibly due to the conflicting photosensitive nature.

As an additional observation from the UV-B survival assays, the contrasting occurrence of random mutations reported for *K. petricola* and none for *C. antarcticus* confirms previous findings regarding the distinct UV tolerance adaptations employed by each fungus. While *K. petricola* relies primarily on DNA repair systems to manage photodamage, *C. antarcticus* employs alternative strategies, such as melanin-mediated quenching, to mitigate photodamage and reduce the burden on the DNA repair machinery. However, the repair of UV-induced CPD and 6-4 PP damage can be effectively driven in fungi by photoreactivation, while the same photodamages can be prominently repaired by nucleotide excision repair (NER) in the absence of light . Indirect UV-induced DNA damage such as SSBs or DSBs is exclusively repaired by other light-independent mechanisms (Strzałka et al., 2020). Dark repair mechanisms have not been ever observed in these two fungal species . However, our findings suggest that *K. petricola* may repair photodamage via NER events when photoreactivation is not available, but the fungus is more prone to mutation. Furthermore, we show that *C. antarcticus* can also use photoreactivation as the backup repair mechanism for photodamage.

This study provides the first evidence on the adaption variability of two black fungi to white and UV solar radiation. Against UV stress, the adoption of either damage avoidance or repair strategy by these fungi appear to be linked to differentiation of the species niche. For instance, *K. petricola* shows remarkable versatility in colonising rocks under stressful conditions, resulting in a wide distribution across temperate and desert habitats. Its primary defence against UV-induced damage lies in the light-driven repair mechanism, taking advantage of the consistent availability of UV-A/blue light in the Mediterranean area. However, when faced with permanent

stress such as in the harsh Antarctic drylands with increased UV-B irradiation due to the ozone depletion, *K. petricola* may adopt the avoidance strategy of associating with lithic communities less exposed to solar radiation . Although not the most successful black fungus under the extremes, the ecological plasticity of *K. petricola* makes this a polyextremotolerant generalist species, as also demonstrated by its capacity to grow at 15° C. Conversely, *C. antarcticus* is specialised to live only in the harsh Antarctic environment. Its extremotolerant nature to UV possibly stems from the occurrence of multiple survival strategies, mainly damage avoidance through a cryptoendolithic lifestyle and the accumulation of DHN melanin in the cell wall. In addition, photorepair mechanisms of photodamage may be used as backup strategies, as the species occurs independently in both sun- and shade-exposed Antarctic lithic communities .

4.6 Acknowledgements

I thank Romy Breitenbach for carrying pilot experiments on UV-B exposure in *K. petricola*, Eileen Erdmann for discussion, and Jenny Straßner for technical support. The Italian National Program of Antarctic Research (PNRA) and the Italian National Antarctic Museum 'Felice Ippolito' (MNA) are acknowledged for funding the collection of Antarctic samples MNA-CCFEE. This work was supported financially by internal funds of the BAM and the grant of the Italian Space Agency (ASI), Life in Space – ASI N. 2019-3-U.0.

4.7 References

Avalos, J., and Carmen Limón, M. (2015) Biological roles of fungal carotenoids. *Curr Genet* **61**: 309-324.

Avalos, J., Nordzieke, S., Parra, O., Pardo-Medina, J., and Limon, M.C. (2017) Carotenoid production by filamentous fungi and yeasts. In *Biotechnology of yeasts and filamentous fungi*. Sibirny, A.A. (ed). Cham: Springer, pp. 225-279.

Banaś, A.K., Zgłobicki, P., Kowalska, E., Bażant, A., Dziga, D., and Strzałka, W. (2020) All you need is light. Photorepair of UV-induced pyrimidine dimers. *Genes* **11**: 1304.

Berthelot, C., Zegeye, A., Gaber, D.A., Chalot, M., Franken, P., Kovács, G.M. et al. (2020) Unravelling the role of melanin in Cd and Zn tolerance and accumulation of three dark septate endophytic species. *Microorganisms* **8**.

Breitenbach, R., Gerrits, R., Dementyeva, P., Knabe, N., Schumacher, J., Feldmann, I. et al. (2022) The role of extracellular polymeric substances of fungal biofilms in mineral attachment and weathering. *NPJ Mater Degrad* **6**: 42.

Campana, R., Fanelli, F., and Sisti, M. (2022) Role of melanin in the black yeast fungi *Aureobasidium pullulans* and *Zalaria obscura* in promoting tolerance to environmental stresses and to antimicrobial compounds. *Fungal Biol* **126**: 817-825.

Canessa, P., Schumacher, J., Hevia, M.A., Tudzynski, P., and Larrondo, L.F. (2013) Assessing the effects of light on differentiation and virulence of the plant pathogen *Botrytis cinerea*: characterization of the *White Collar* Complex. *PLoS One* **8**: e84223.

Carr, E.C., Barton, Q., Grambo, S., Sullivan, M., Renfro, C.M., Kuo, A. et al. (2023) Characterization of a novel polyextremotolerant fungus, *Exophiala viscosa*, with insights into its melanin regulation and ecological niche. *G3: Genes Genomes Genet* **13**.

Catanzaro, I., Gerrits, R., Feldmann, I., Gorbushina, A.A., Onofri, S., and Schumacher, J. (in press) Deletion of the polyketide synthase-encoding gene *pks1* prevents melanization in the extremophilic fungus *Cryomyces antarcticus*. *IUBMB Life*.

Chan, Y., Lacap, D.C., Lau, M.C.Y., Ha, K.Y., Warren-Rhodes, K.A., Cockell, C.S. et al. (2012) Hypolithic microbial communities: between a rock and a hard place. *Environ Microbiol* **14**: 2272-2282.

Chen, Z., Martinez, D.A., Gujja, S., Sykes, S.M., Zeng, Q., Szaniszlo, P.J. et al. (2014) Comparative genomic and transcriptomic analysis of *Wangiella dermatitidis*, a major cause of phaeohyphomycosis and a model black yeast human pathogen. *G3: Genes Genomes Genet* **4**: 561-578.

Coleine, C., Selbmann, L., Singh, B.K., and Delgado-Baquerizo, M. (2022) The poly-extreme tolerant black yeasts are prevalent under high ultraviolet light and climatic seasonality across soils of global biomes. *Environ Microbiol* **24**: 1988-1999.

Coleine, C., Zucconi, L., Onofri, S., Pombubpa, N., Stajich, J.E., and Selbmann, L. (2018) Sun exposure shapes functional grouping of fungi in cryptoendolithic Antarctic communities. *Life* **8**: 19.

Cordero, R.J.B., and Casadevall, A. (2020) Melanin. *Curr Biol* **30**: R142-R143.

Cortesão, M., de Haas, A., Unterbusch, R., Fujimori, A., Schutze, T., Meyer, V., and Moeller, R. (2020) *Aspergillus niger* spores are highly resistant to space radiation. *Front Microbiol* **11**: 560.

De Leo, F., Marchetta, A., and Urzì, C. (2022) Black fungi on stone-built heritage: Current knowledge and future outlook. *Appl Sci* **12**: 3969.

Dunlap, J.C. (1999) Molecular bases for circadian clocks. *Cell* **96**: 271-290.

Erdmann, E.A., Nitsche, S., Gorbushina, A.A., and Schumacher, J. (2022) Genetic engineering of the rock inhabitant *Knufia petricola* provides insight into the biology of extremotolerant black fungi. *Front Fungal Biol* **3**: 862429.

Favero-Longo, S.E., Gazzano, C., Girlanda, M., Castelli, D., Tretiach, M., Baiocchi, C., and Piervittori, R. (2011) Physical and chemical deterioration of silicate and carbonate rocks by meristematic microcolonial fungi and endolithic lichens (Chaetothyriomycetidae). *Geomicrobiol J* **28**: 732-744.

Flieger, K., Knabe, N., and Toepel, J. (2018) Development of an improved carotenoid extraction method to characterize the carotenoid composition under oxidative stress and cold temperature in the rock inhabiting fungus *Knufia petricola* A95. *J Fungi* **4**.

Fuller, K.K., Loros, J.J., and Dunlap, J.C. (2015) Fungal photobiology: visible light as a signal for stress, space and time. *Curr Genet* **61**: 275-288.

Gaber, D.A., Berthelot, C., Camehl, I., Kovács, G.M., Blaudez, D., and Franken, P. (2020) Salt stress tolerance of dark septate endophytes is independent of melanin accumulation. *Front Microbiol* **11**: 562931.

Gao, Q., and Garcia-Pichel, F. (2011) Microbial ultraviolet sunscreens. *Nat Rev Microbiol* **9**: 791-802.

Golubic, S., Friedmann, E.I., and Schneider, J. (1981) The lithobiontic ecological niche, with special reference to microorganisms. *J Sediment Res* **51**: 475-478.

Gorbushina, A.A., Kotlova, E.R., and Sherstneva, O.A. (2008) Cellular responses of microcolonial rock fungi to long-term desiccation and subsequent rehydration. *Stud Mycol* **61**: 91-97.

Gostinčar, C., Zalar, P., and Gunde-Cimerman, N. (2022) No need for speed: slow development of fungi in extreme environments. *Fungal Biol Rev* **39**: 1-14.

Gueidan, C., Ruibal, C., de Hoog, G.S., and Schneider, H. (2011) Rock-inhabiting fungi originated during periods of dry climate in the late Devonian and middle Triassic. *Fungal Biol* **115**: 987-996.

Gueidan, C., Villasenor, C.R., de Hoog, G.S., Gorbushina, A.A., Untereiner, W.A., and Lutzoni, F. (2008) A rock-inhabiting ancestor for mutualistic and pathogen-rich fungal lineages. *Stud Mycol* **61**: 111-119.

Jones, D.L., and Baxter, B.K. (2017) DNA repair and photoprotection: mechanisms of overcoming environmental ultraviolet radiation exposure in halophilic Archaea. *Front Microbiol* **8**.

Kebbi, Y., Muhammad, A.I., Sant'Ana, A.S., do Prado-Silva, L., Liu, D., and Ding, T. (2020) Recent advances on the application of UV-LED technology for microbial inactivation: Progress and mechanism. *Rev Food Sci Food Saf* **19**: 3501-3527.

Liu, B., Fu, R., Wu, B., Liu, X., and Xiang, M. (2021) Rock-inhabiting fungi: terminology, diversity, evolution and adaptation mechanisms. *Mycology* **13**: 1-31.

Nai, C., Wong, H.Y., Pannenbecker, A., Broughton, W.J., Benoit, I., de Vries, R.P. et al. (2013) Nutritional physiology of a rock-inhabiting, model microcolonial fungus from an ancestral lineage of the Chaetothyriales (Ascomycetes). *Fungal Genet Biol* **56**: 54-66.

Nienow, J.A., McKay, C.P., and Friedmann, E.I. (1988) The cryptoendolithic microbial environment in the Ross Desert of Antarctica: light in the Photosynthetically Active Region. *Microb Ecol* **16**: 271-289.

Onofri, S., Pacelli, C., Selbmann, L., and Zucconi, L. (2020) The amazing journey of *Cryomyces antarcticus* from Antarctica to space. In *Extremophiles as astrobiological models*. Seckbach, J., and Stan-Lotter, H. (eds): Scrivener Publishing LLC, pp. 237-254.

Onofri, S., Zucconi, L., Selbmann, L., de Hoog, S., de los Ríos, A., Ruisi, S., and Grube, M. (2007) Fungal associations at the cold edge of life. In *Algae and cyanobacteria in extreme environments*. Seckbach, J. (ed). Dordrecht: Springer, pp. 735-757.

Pacelli, C., Cassaro, A., Aureli, L., Moeller, R., Fujimori, A., and Onofri, S. (2020) The responses of the black fungus *Cryomyces antarcticus* to high doses of accelerated helium ions radiation within Martian regolith simulants and their relevance for Mars. *Life* **10**: 130.

Pacelli, C., Cassaro, A., Siong, L.M., Aureli, L., Moeller, R., Fujimori, A. et al. (2021) Insights into the survival capabilities of *Cryomyces antarcticus* hydrated colonies after exposure to Fe particle radiation. *J Fungi* **7**: 495.

Palmer, J.M., Drees, K.P., Foster, J.T., and Lindner, D.L. (2018) Extreme sensitivity to ultraviolet light in the fungal pathogen causing white-nose syndrome of bats. *Nat Commun* **9**: 35.

Paysan-Lafosse, T., Blum, M., Chuguransky, S., Grego, T., Pinto, B.L., Salazar, Gustavo A. et al. (2023) InterPro in 2022. *Nucleic Acids Res* **51**: D418-D427.

Qi, Y., Bai, S., Vogelmann, T., and Heisler, G. (2003) *Penetration of UV-A, UV-B, blue, and red light into leaf tissues of pecan measured by a fiber optic microprobe system*: SPIE.

Schumacher, J. (2016) DHN melanin biosynthesis in the plant pathogenic fungus *Botrytis cinerea* is based on two developmentally regulated key enzyme (PKS)-encoding genes. *Mol Microbiol* **99**: 729-748.

Schumacher, J., and Gorbushina, A.A. (2020) Light sensing in plant- and rock-associated black fungi. *Fungal Biol* **124**: 407-417.

Seekles, S.J., Teunisse, P.P.P., Punt, M., van den Brule, T., Dijksterhuis, J., Houbraken, J. et al. (2021) Preservation stress resistance of melanin deficient conidia from *Paecilomyces variotii* and *Penicillium roqueforti* mutants generated via CRISPR/Cas9 genome editing. *Fungal Biol Biotechnol* **8**: 4.

Seemann, J. (1979) The biological effects of light. In *Agrometeorology*. Berlin, Heidelberg: Springer Berlin Heidelberg, pp. 17-21.

Selbmann, L., Zucconi, L., Isola, D., and Onofri, S. (2015) Rock black fungi: excellence in the extremes, from the Antarctic to space. *Curr Genet* **61**: 335-345.

Selbmann, L., de Hoog, G.S., Mazzaglia, A., Friedmann, E.I., and Onofri, S. (2005) Fungi at the edge of life: cryptoendolithic black fungi from Antarctic desert. *Stud Mycol* **51**: 1-32.

Selbmann, L., Stoppiello, G.A., Onofri, S., Stajich, J.E., and Coleine, C. (2021) Culture-dependent and amplicon sequencing approaches reveal diversity and distribution of black fungi in Antarctic cryptoendolithic communities. *J Fungi* **7**: 213.

Selbmann, L., Pacelli, C., Zucconi, L., Dadachova, E., Moeller, R., de Vera, J.P., and Onofri, S. (2018) Resistance of an Antarctic cryptoendolithic black fungus to radiation gives new insights of astrobiological relevance. *Fungal Biol* **122**: 546-554.

Solano, F. (2016) Photoprotection versus photodamage: updating an old but still unsolved controversy about melanin. *Polym Int* **65**: 1276-1287.

Strzałka, W., Zgłobicki, P., Kowalska, E., Bażant, A., Dziga, D., and Banaś, A.K. (2020) The dark side of UV-induced DNA lesion repair. *Genes* **11**: 1450.

Tonon, C., Breitenbach, R., Voigt, O., Turci, F., Gorbushina, A.A., and Favero-Longo, S.E. (2021) Hyphal morphology and substrate porosity-rather than melanization-drive penetration of black fungi into carbonate substrates. *J Cult Herit* **48**: 244-253.

Vanhaelewyn, L., Van Der Straeten, D., De Coninck, B., and Vandenbussche, F. (2020) Ultraviolet radiation from a plant perspective: the plant-microorganism context. *Front Plant Sci* **11**.

Vasileiou, T., and Summerer, L. (2020) A biomimetic approach to shielding from ionizing radiation: the case of melanized fungi. *PLoS One* **15**: e0229921.

Voigt, O., Knabe, N., Nitsche, S., Erdmann, E.A., Schumacher, J., and Gorbushina, A.A. (2020) An advanced genetic toolkit for exploring the biology of the rock-inhabiting black fungus *Knufia petricola*. *Sci Rep* **10**: 22021.

Wong, H.J., Mohamad-Fauzi, N., Rizman-Idid, M., Convey, P., and Alias, S.A. (2019) Protective mechanisms and responses of micro-fungi towards ultraviolet-induced cellular damage. *Polar Sci* **20**: 19-34.

Yu, Z., and Fischer, R. (2019) Light sensing and responses in fungi. *Nat Rev Microbiol* **17**: 25-36.

4.8 Supplementary materials

Table S6. Oligonucleotides used in this study.

Name	Sequence (5'← 3')	Binding site
***kppks1*-SH-hi5F**	GGTTGTCGGCAGTGATACGACAAG	Upstream of *kppks1* (–1.283 to 1.259 kb)
***kppks1*-PS1sF1**	CTACGTGTTCGGTGACCAAA	In *kppks1* (+0.011 to 0.031 kb)
***kppks1*-PS1sR2**	GTTGCGCGAACGGTGCTTACC	In *kppks1* (+0.277 to 0.298 kb)
***kppks1*-sF1**	GCTCTGAGAGAAGTCATCCTCGAG	In *kppks1* (+0.928 to 0.952 kb)
***kppks1*-wtF3**	GGCCGACTGAACTACTTCTTCAAG	In *kppks1* (+1.606 to 1.630 kb)
***kppks1*-wtF2**	GCCGATCTGGCATACACCACCAC	In *kppks1* (+2.587 to 2.610 kb)
***kppks1*-wtR2**	GTCCGAGACGCCGTTGATGCATG	In *kppks1* (+3.200 to 3.223 kb)
***kppks1*-sF3**	GTCCAGCTCTACCATCAGCGAATC	In *kppks1* (+3.519 to 3.543 kb)
***kppks1*-com3F**	TGAGAACGGTGAGGCCGATAAGGTGAGCAGAAAGATGGCA	In *kppks1* (+4.830 to 4.420 kb)
***kppks1*-sF4**	GACACAGTAGAGTCCGGCATCAC	In *kppks1* (+5.341 to 5.364 kb)
***kppks1*-hi3R3**	GCGCCGTCTATAACCTTTGCAATAG	Downstream of *kppks1* (+6.858 to 6.883 kb)
***kppks1*-SH-hi3R**	GAGTTAGATTCGAGACACTCCACCAG	Downstream of *kppks1* (+7.112 to 7.138 kb)
***kpppt1*-hi5F**	GTCAAGCATTCTTGGCTCCGCG	Upstream of *kpppt1* (–0.337 to 0.315 kb)
***kpppt1*-hi3R**	GCCATCGATGTGGCCTCTAAGTG	Downstream of *kpppt1* (+1.365 to 1.388 kb)

Open reading frames: *kppks1* – 6.601 kb (one intron of 52 bp), *kpppt1* – 1.101 kb (no introns).

Table S7. GenBank accessions of *K. petricola* genes and proteins.

Name	Description	Gene	Protein
KpPKS1	Polyketide synthase, non-reducing	MT859418.1	**QOE76777.1**
KpPPT1	4'-phosphopantetheinyl transferase, sfp-type	PP374627.1	**WWL91116.1**
KpCPF1	Cryptochrome photolyase family (CPF) protein	PP449068.1	**WWZ17649.1**
KpCPF2	Cryptochrome photolyase family (CPF) protein	PP449069.1	**WWZ17650.1**
KpCPF3	Cryptochrome photolyase family (CPF) protein	PP449070.1	**WWZ17651.1**
KpCPF4	Cryptochrome photolyase family (CPF) protein	PP449071.1	**WWZ17652.1**
KpWCL1 (LOV1)	GATA-type transcription factor, white collar 1 ortholog	OM802157.1	**WAK13571.1**
KpWCL2	GATA-type transcription factor, white collar 2 ortholog	OM802158.1	**WAK13572.1**
KpLTF1	GATA-type transcription factor, NsdD/SUB-1/LTF1 ortholog	PP340519.1	**WWA97541.1**
KpLOV2	Light-oxygen-voltage (LOV) domain-containing protein	PP449072.1	**WWZ17653.1**
KpLOV3	Light-oxygen-voltage (LOV) domain-containing protein	PP449073.1	**WWZ17654.1**
KpLOV4	Light-oxygen-voltage (LOV) domain-containing protein	PP449074.1	**WWZ17655.1**
KpOPS1	Microbial opsin, transmembrane	PP449075.1	**WWZ17656.1**
KpOPS2	Microbial opsin, transmembrane	MT859420.1	**QOE76782.1**
KpOPS3	Microbial opsin, transmembrane	PP449076.1	**WWZ17657.1**
KpPHY1	Phytochrome (histidine kinase)	PP449077.1	**WWZ17658.1**
KpFRQ1	Frequency, circadian oscillator	PP449078.1	**WWZ17659.1**

Table S8. Photoreceptors and transcription factors of *Cryomyces antarcticus* putatively involved in light sensing and signaling.

Description	JGI protein ID	Size	Note	Location	Possible allelic (secondary) variant
Cryptochrome photolyase family (CPF) protein	**Cryan3|1036121**	650 aa	primary allele	Scaffold_05: 884944-887172	Protein ID **1026569** on scaffold_12
Cryptochrome photolyase family (CPF) protein	**Cryan3|982802**	644 aa	primary allele	Scaffold_15: 693824-696484	Protein ID **1019225** on scaffold_85 Protein ID **1022842** on scaffold_245
Cryptochrome photolyase family (CPF) protein	**Cryan3|999807**	643 aa	primary allele	Scaffold_34: 357838-360355	Protein ID **1009500** on scaffold_50
GATA-type transcription factor, WC-1 ortholog (LOV)	**Cryan3|1059543**	1,033 aa	primary allele	Scaffold_06: 520269-523711	Protein ID **610509** on scaffold_62
GATA-type transcription factor, WC-2 ortholog	**Cryan3|443880**	491 aa	primary allele	Scaffold_40: 196268-198212	Protein ID **954205** on scaffold_33
GATA-type transcription factor, SUB-1 ortholog	**Cryan3|1024422**	1,158 aa	primary allele	Scaffold_04: 974657-980346	Protein ID **1025956** on scaffold_9
Light-oxygen-voltage (LOV) domain-containing protein	**Cryan3|845159**	626 aa	primary allele	Scaffold_13: 553202-555279	Protein ID **861104** on scaffold_47
Light-oxygen-voltage (LOV) domain-containing protein	**Cryan3|1085497**	595 aa	primary allele	Scaffold_58: 102874-105477	n/a
Light-oxygen-voltage (LOV) domain-containing protein	**Cryan3|1018934**	503 aa	primary allele	Scaffold_83: 13743-15804	n/a
Microbial opsin (OPS)	**Cryan3|1097610**	328 aa	primary allele	Scaffold_18: 492625-494599	Protein ID **572511** on scaffold_56
Microbial opsin (*ops2* linked with carotenogenic genes)	**Cryan3|563816**	322 aa	primary allele	Scaffold_55: 150397-151843	Protein ID **1065685** on scaffold_26
Phytochrome (histidine kinase)	**Cryan3|43883**	1,466 aa	primary allele	Scaffold_10: 531591-536313	Protein ID **352654** on scaffold_32
Frequency, circadian oscillator	**Cryan3|447692**	769 aa	primary allele	Scaffold_40: 477880-480470	Protein ID **9934** on scaffold_1

Genes and proteins from *Cryomyces antarcticus* strain CBS 116301 (DOE Joint Genome Institute) are shown. Many of the smaller scaffolds are very similar to larger scaffolds and are predicted to constitute an alternate or secondary haplotype. Thus, 'primary alleles' and 'secondary alleles' gene model tracks are given in the genome portal (https://mycocosm.jgi.doe.gov/mycocosm/home). The primary alleles are listed only for providing a non-redundant set of genes.
WC-1 and WC-2 (*white collar*) and SUB-1 (*submerged protoperithecia*) are the names of the transcription factors from *Neurospora crassa* where they were first described.

Chapter 5

Conclusions

Microcolonial black fungi are a widespread group of Ascomycetes specialised in polyextremotolerance. Their remarkable ability to withstand a wide range of abiotic stresses, including various forms of radiation, makes them valuable eukaryotic subjects for exploring the limits of life in an astrobiological context. Previous studies have shed light on the genetic and ecological adaptations of this group, revealing a polyphyletic composition of rock-dwelling fungi characterised by the convergent evolution of common morpho-physiological traits. Notably, melanin production is one of the most evident traits in these fungi and has been generally associated with providing cellular protection against environmental stresses. However, the heterogeneous and amorphous molecular structure of these pigments poses analytical challenges, and there is no clear consensus on their biological functions in fungi. In this context, the disposal of a model system that reflects the adaptive mechanisms of polyextremotolerant organisms would facilitate comparative analysis of experimental findings among members of this extremely diverse group.

Using fungal melanins as a *fil rouge*, this study explores the utility of polyextremotolerant black fungi in various areas of astrobiology, confirming these organisms as good candidate models. Specifically, the first part of this thesis involved evaluating the application of black fungi in current efforts to search for life beyond Earth. Although this search is inherently challenging, it can be addressed through a systematic investigative approach. From the study of planetary analogues on Earth – and their respective inhabitants – to the exposure of biological samples to real space conditions, space missions aimed at searching for signs of putative life in extraterrestrial environments can only benefit from a multi-step investigative approach that allows such complex scientific challenges to be simplified. To support this space research framework, we evaluated the detection potential of fungal biomolecules such as DNA and melanin pigments from the astrobiologically relevant black fungus *C. antarcticus*, as suitable biogenic traces to search for in a Mars scenario (**Chapter 2**). Our findings indicated that melanins possess the highest molecular

stability and detectability, and it could be effectively used as candidate biosignatures in the Martian environment.

After assessing the functionality of fungal melanins as biosignatures, the second part of this thesis explored the use of black fungi in understanding life's adaptations to extreme environmental conditions. In order to study distinct adaptive traits and eventually propose astrobiological references for further experimental studies, reliable and efficient engineering tools were first required to be implemented for these non-amenable organisms (**Chapter 3**). Using the black model *K. petricola* A95 for the optimisation of CRISPR/Cas9-mediated gene editing techniques and transformation protocols, we were able to generate deletion mutants of *C. antarcticus* lacking DHN-melanin or carotenoid pigments by knocking out key encoding genes (Δ*capks1*, Δ*caphs1/caphd1*). Despite working with extremophiles can be methodologically difficult (e.g., slow growth rates), this study proved the feasibility of genetic manipulation of recalcitrant black fungi, paving the way for further applications of these polyextremotolerant organisms in astrobiological as well as in biotechnological areas.

Finally, a first comparative study was conducted between *C. antarcticus* and *K. petricola* to explore ultraviolet (UV) tolerance strategies among black rock-inhabiting fungi (**Chapter 4**). Although both species constitutively produce melanised cell walls and show comprehensive photosensory systems, they actually exhibited different adaptive responses to harmful UV radiation. Confirming the high survival threshold to UV-B radiation of previous studies, *C. antarcticus* demonstrated the primary use of DHN-melanin as a protective compound to avoid UV-induced damage. However, DNA photorepair mechanisms were also functional. In contrast, *K. petricola* was more sensitive to UV-B radiation, resulting in a high occurrence of non-silent mutations. Neither DHN-melanin nor carotenoids could enhance its UV tolerance; instead, this fungus could rely on the efficient repair of UV-induced DNA damage by photoreactivation. These findings suggest that DHN-melanin does not universally serve as a UV-B protective compound in black fungi, and alternative strategies such as DNA photorepair systems can be functional against the same environmental stress. Eventually, the variability of adopting either a damage avoidance or repair strategy in these two black rock-inhabiting fungi may be linked to differentiation of the species niche.

Altogether, this thesis illustrates the extensive use of microcolonial black fungi across astrobiological research. Additionally, the introduction of the model *K. petricola*, originally implemented for studying biofilm formation and lithic lifestyles of rock-dwelling fungi, provided evidence of possible different responses against the same environmental stress within this polyphyletic group. Further astrobiological investigations on black fungi are encouraged to

comprehensively characterise their polyextremotolerant nature and responses to a wider spectrum of environmental stresses, including ionising radiation, yet employing a methodological approach with similar reference systems. Indeed, further investigations into the genetic and functional traits adapted by this unique fungal group are essential to gain a deeper understanding of the actual limits of life. From an astrobiological perspective, this will improve our search for analogous life forms beyond Earth, as it is likely that potential life forms on other planetary bodies have evolved survival strategies for harsh environments similar to those evolved by extremophiles on Earth. In addition, the recent availability of melanin-deficient mutants of *C. antarcticus* opens interesting possibilities to deepen the study of the role of melanin in cell protection, especially in this exceptionally stress-resilient fungus, which has even demonstrated the ability to survive in real space and simulated Martian conditions for 1.5 year of exposure on the International Space Station.

Acknowledgements

My doctoral career began in 2020, when the pandemic was a huge part of our lives and routines were filled with instability and insecurities. Starting a PhD with all these premises may not have been the smartest decision ever, but I am glad of the person it has pushed me to become today. As my senior colleague Alessia once told me, 'A doctorate is more of a life journey than just an academic path'. I have found this to be true later, when dealing with a rich 'biodiversity' of hurdles, inconveniences and complex circumstances, for which one is hardly prepared in advance. It may sound like a cliché, but I truly believe that this is not solely thanks to myself: if I can feel proud of what I have accomplished and the young researcher I have outgrown, it is undeniably thanks to all those who believed in me and helped me face, in their own ways, this personal challenge. Some of them have been there from the very beginning, while others arrived along the way, and some sadly departed before seeing the end of it. But I am truly grateful to each and every one of them, so let me express it here in my own words.

First, I would like to thank Prof. Silvano Onofri, for believing in me when I applied for this opportunity and for supporting my work even after his retirement. I am grateful to Prof. Laura Zucconi as well for her unwavering support, especially during the final stage of my student career. I am also grateful to Prof. Anna A. Gorbushina for hosting me in Berlin and for her longstanding support of a scientific collaboration that has been dear to me. A special mention goes to Dr. Julia Schumacher for being the best mentor I could ever wished for on this difficult journey.
Alongside the PhD supervisors and host advisors, I would like to thank Prof. Cene Gostinčar, Dr. Rosa Santomartino, Dr. Rosa de la Torre Noetzel and all the anonymous referees who generously dedicated their time and expertise to evaluate this work.

No PhD student can fully enjoy the ups and downs of their academic life without sharing them with friends and fellow colleagues. Therefore, a first thank you to my senior colleagues and peers at the University of Tuscia – Caterina, Daniela, Fabiana, Federica, Alessia, Lorenzo, Federico, Antonio, Patrick, and Brunella – for providing me with a roof over my head when I needed it most, jokes to lighten moments of hard work, and even shared moments of deep reflection. A big shout out to my 'science mum' Fabiana, who patiently guided me through every doubt I had, and to my fellow mate Patrick for sharing the joys and stresses of our adventures abroad.
In this regard, I am deeply thankful to my colleagues at the BAM Institute, including Jenny, Ruben, Chiara, Khaled, Eileen, Abolfazl, Antonia, and Robert, who made me feel always

welcome and made my days in the lab and at conferences better with many laughs. A special thank you to Jenny, Chiara, and Eileen for their precious support – both technical and emotional.
Thank you also to my flatmate Niklas and the new friends Ivo, Jakob, Sarah, Markus, Beatriz, Elena, and Alessia (with Emma) for filling my time in Germany with so many wonderful memories and bonds that I will always cherish.

Last but not least, I want to express my gratitude to my old friends and loved ones, who have always been there for me even when I was far away from home. Thank you to Davide, Valerio, Giulio, Paolo, Stefania, Diego, Serena, Arianna, Letizia, Marco, Giacomo, Laura, and Amina for appreciating my bright side of never-ending sarcasm and complaints. To my old classmates Daniele, Viviana, Matteo, Riccardo, Guendalina, Gabriele as well as Eleonora, Irene, Cecilia, Francesca, Daniel for their long-distance but never dormant friendship. A big thank you to Arianna, Lilli, and Roberta, who braved the cold and gloomy German weather to visit me in Berlin. Thanks to Riccardo and Yukai for sharing the PhD life experience, and to Elisa and Anna, because without our shared love of BTS and Korean dramas, these years would have been infinitely longer and (J-)hopeless.
But most of all, I would like to thank my mother Alessandra, my partner Antonio, and my uncle Sandro, because without their unconditional love I would not have made it this far. Thank you for being my greatest supporters and anchor points in times of greatest loss.
One last dedication in loving memory of my grandmother Rosa, who enjoyed watching me grow towards my childhood dream of becoming a scientist, and of my old friend Serena and her dear Hesam, with whom I shared precious moments when we were students and wish we could have continued to share our paths as young researchers today. I miss you all deeply.

The PhD journey has been an extraordinary adventure, with the opportunity to appreciate the natural and human heritage that sustains the world of research. Mostly, I have enjoyed the kindness of many researchers and professors who have shared their thoughts in pursuing such a scientific career, because they have helped me to be less anxious about my future life choices. Now that this long chapter of student life has finally come to an end, I am eager to see where the next chapter will take me.